Progress Report

Georgia Tech Project A-5858

DISTRIBUTION STATEMENT A
Approved for Public Release
Distribution Unlimited

Information-Based Multisensor Detection

Sponsored by:

Office of Naval Research
ONR Grant Number N00014-99-1-0084

Attention: **Dr. Rabinder N. Madan**
Program Officer
ONR 313
800 North Quincy Street
Arlington, Virginia 22217-5660

Period covered by Progress Report : October 1, 1998 through September 30, 1999

1 OVERVIEW OF PROGRAM

This program addresses the Navy need for extended firm track range for low altitude cruise missiles through the integration of multiple sensors. Track-Before-Declare (TBD) techniques that utilize signal features are proposed for the synergistic integration of an Electronically Scanned Array (ESA) radar with other sensors for the detection of weak targets. A comparison of the performances of a notional multisensor system with that of a federated system of sensors is planned. More specifically, the integration of an ESA radar and Infrared Search and Track (IRST) sensor for a shipboard combat system was proposed. The computer simulation models of the radars and IRST sensor will include the effects of many issues such as finite sensor resolution, limitations on the sensor resources, atmospheric refraction, sensor pointing errors, sea-surface induced multipath, nonhomogeneous clutter, sea clutter, etc. that are omitted in most of the legacy simulations. The computer simulation models will be utilized to develop tracking benchmark problems for broad distribution. These benchmark problems will serve to educate the research community on many of the "real-world" problems that are faced in actual tracking systems and the integration of multiple sensors.

The technical objectives of the project include the following:

- Development and demonstration through computer simulation of algorithms that provide enhanced detection of weak targets through the integration of multiple sensors. More specifically, Track-Before-Declare (TBD) techniques that utilize signal features are proposed for the synergistic integration of an Electronically Scanned Array (ESA) radar with others sensors for the detection of weak targets. The integration of the ESA radar with the Infrared (IR) sensor are to be considered. The detection performance of a notional multisensor system will be compared with that of the federated system of sensors.

- Development and demonstration through computer simulation of efficient radar resource allocation techniques that maximizes the information procured by the multisensor suite, while accommodating remote cues and/or warnings and adapting to changes in the characteristics of the targets of interest, weather conditions, etc. The waveforms and revisit times of the ESA will be selected to maximize the information procured by the multisensor system. The detection performance of a notional multisensor system with the new resource allocation techniques will be compared to that of the multisensor system with conventional resource allocation and that of the federated system of sensors.

This report summaries the progress and accomplishments made during October 1, 1998 and September 30, 1999, which is the first year of a three year program. Section 2 gives a summary of the progress toward the objectives of the project, while Section 3 summarizes future plans. Section 4 lists the papers that have been published or submitted for publication, and Section 5 summarizes related activities that were supported as part of this project.

2 PROJECT ACCOMPLISHMENT FOR FIRST YEAR

The two primary accomplishments for the first year of this program were the development of a phased array radar model with search and track management functions for multiple targets as well as the development of a sea-clutter model with moving target indictor (MTI) waveform designs.

The development of the radar model for this project was to involve the addition of a horizon search function to an existing computer simulation of a phased array radar that was developed by the Naval Surface Warfare Center, Dahlgren Division (NSWCDD). After further consideration, the structure of the NSWCDD computer simulation was determined to be inappropriate for the

inclusion of a horizon search function. The following list gives some of the reasons that the NSWCDD simulation was determined to be inappropriate.

- The existing simulation allows for the simultaneous tracking of at most two targets, while the horizon search function will need to allow for the tracking of many targets.
- The existing simulation requires that the number of targets at the beginning of a Monte Carlo experiment (or run) be the same as the number at the end of an experiment.
- The existing simulation does not include the infrastructure for starting false tracks, while false tracks are key to performance assessment of a horizon search function.
- The existing simulation includes only one array, while most shipboard phased array radars have multiple arrays to search the horizon.
- The existing simulation includes no method for the introduction of new targets after the scenario starts or the reacquisition of lost targets, while the purpose of the horizon search is to detect new targets and put them into track.
- The existing simulation does not include a model for sea clutter, while sea clutter is a major issue for horizon search.

These issues and the associated structure of the simulation program precluded its use without a major rewrite of the simulation. Thus, a new computer simulation with an alternative structure was developed for this project. The new radar model is an event-driven simulation with search, track, and dual track test modes as discussed in Appendix A. The search mode is a pseudo-search that is included to allow for automatic acquisition of new targets or reacquisition of targets that have been lost. In the pseudo-search mode, search dwells and the resulting detections are generated near targets and persistent clutter. This pseudo-search is readily extendable to accomplish a full search for the horizon as discussed in Appendix A. In the track mode, a track dwell and the resulting detections are generated for the specified target and used for tracking that target. The dual track mode is included to eliminate redundant or dual tracks. Appendix A gives an overview of the phased array radar model.

As the problem of realistically modeling sea backscatter is itself a difficult research problem, the modeling effort is proceeding in stages with the goal of balancing realism with implementability. The model will be a purely statistical model that captures the phenomenology that is most relevant to the detection and tracking process. Thus, the problem initially is to generate a stream

of random numbers that have a given non-Rayleigh amplitude fluctuation and that have the proper correlation properties. During this first year, a model was developed and coded for K-distributed sea clutter without any spatial or temporal correlation. Appendix B gives an overview of the calculation of the average RCS and spectral distribution of the sea clutter, while Appendix C describes the generation of the random variables for the K-distributed sea clutter.

3 PLANS FOR FUTURE EFFORTS

Future efforts will include the development of an algorithm for an automatic track formation in the presence of sea clutter. The algorithm will be a TBD technique such as the Interacting Multiple Model Probabilistic Data Association Filter (IMMPDAF) or the Intelligent PDAF (IPDAF) algorithm. The automatic track formation technique will be added to the radar simulation for the horizon search function so that studies of the effectiveness of TBD techniques for extending the firm track range can be accomplished. The inclusion of spatial and temporal correlation into the clutter model and atmospheric refraction will be considered. The development of information-based radar resource allocation for the horizon search function will also be considered. The upgrade of an existing IRST model to include the detection of new targets via TBD techniques will be pursed for the development and assessment of multisensor TBD techniques.

4 PUBLICATIONS

The following four papers have been accomplished through funding from this grant. Copies of the papers are included in Enclosures 1 though 4.

1. W. D. Blair and M. Brandt-Pearce, "Monopulse DOA Estimation for Two Unresolved Rayleigh Targets," submitted to the *IEEE Transactions on Aerospace and Electronic Systems* on December 10, 1998 and accepted for publication after minor revisions.

2. W. D. Blair, "NNJPDA for Possibly Merged Monopulse Measurements," *Proc. of the 31st Southeastern Symposium on Systems Theory,* Auburn, AL, March 21-23, 1999.

3. W. D. Blair and M. Brandt-Pearce, "NNJPDA for Tracking Closely-Spaced Rayleigh Targets With Possibly Merged Measurements," *in Signal and Data Processing for Small Targets 1999,* Oliver Drummond, Editor, Proceedings of SPIE Vol. 3809, pp. 396-404 (1999).

4. W. Wong and W. D. Blair, "Steady-State Tracking With LFM Waveforms," submitted to the *IEEE Transactions on Aerospace and Electronic Systems* on September 15, 1999.

5 RELATED ACTIVITIES

The follow related activities have been supported at the request of the Office of Naval Research.

1. Hosted the 2nd ONR/GTRI Workshop on Target Tracking and Sensor Fusion, June 22-23, 1999, at the Cobb Research Facility of the Georgia Tech Research Institute. The workshop included approximately 35 attendees and 23 technical presentations.

2. Assisted NSWCDD personnel with corrections to their multipath model for the phased array radar simulation for ONR/NSWC Tracking Benchmark IV.

3. Assisted GTRI personnel with the modeling of sea-surface induced multipath into the PESM simulation for ONR/NSWC Tracking Benchmark IV.

4. Supported meetings with Northrup-Grumman on multisensor integration for the E2-C.

5. Supported meetings at NSWCDD and ONR for planning of projects for airborne and shipboard multisensor integration.

Respectfully,

William D. Blair

William Dale Blair, Senior Research Engineer
Project Director

Appendix A

Overview of Phased Array Radar Simulation Model

The radar model is an event-driven simulation with search, track, and dual track test modes as shown in Figure 1. The search mode is a pseudo-search that is included to allow for automatic acquisition of new targets or reacquisition of targets that have been lost. In the pseudo-search mode, search dwells and the resulting detections are generated near targets and persistent clutter. This pseudo-search is readily extendable to accomplish a full search for the horizon as discussed below. In the track mode, a track dwell and the resulting detections are generated for the specified target and used for tracking that target. The dual track mode is included to eliminate redundant or dual tracks.

The phased array radar model is currently configured as an notional Shipboard S-Band Phased Array Radar that operates at 3.4 to 4.0 GHz with four arrays that provide 360 degrees of azimuthal coverage and 70 degrees of elevation coverage. The four arrays are tilted to 15 degrees in elevation and located at 0, 90, 180, and 270 degrees relative to the ship's heading. Linear motion of the platform is included as well as roll, pitch, and yaw. Each array has uniform illumination across the array and each element has cosine illumination. As shown by Figure 2, the 3 dB beamwidth of the radar varies from 1.7 degrees at a broadside angle of 0 to 3.5 degrees at of broadside angle of 60 degrees. The radar model includes single pulse and 3-pulse moving target indicator (MTI) waveforms. The single pulse waveforms include four subpulses at distinct frequencies, while the MTI waveforms include two subpulses at distinct frequencies. Five, single-pulse waveforms that differ by 3 dB in energy for a total difference of 15 dB are included with waveform #1 denoting the highest energy. Each subpulse is bi-phase coded with a bandwidth of 15 MHz to give a range resolution of 10 m for each range cell. Two MTI waveforms have been designed for inclusion in the simulation.

The first action of the pseudo-search mode is to identify the targets that are in the search space that is specified by the function call. Each call to the search mode includes a search of the horizon and a fraction of the above horizon search region for each array. The search space is discretized into beam pointing angles and range intervals. The beam positions overlap resulting in a cluster of beams that may contain the target. The detection signals are generated for all of the range cells in beam angles and range intervals that include targets or persistent clutter tracks. For a full search of the horizon, the range intervals are defined to extend from the minimum detection range to the maximum detection range and detection signals are generated for all

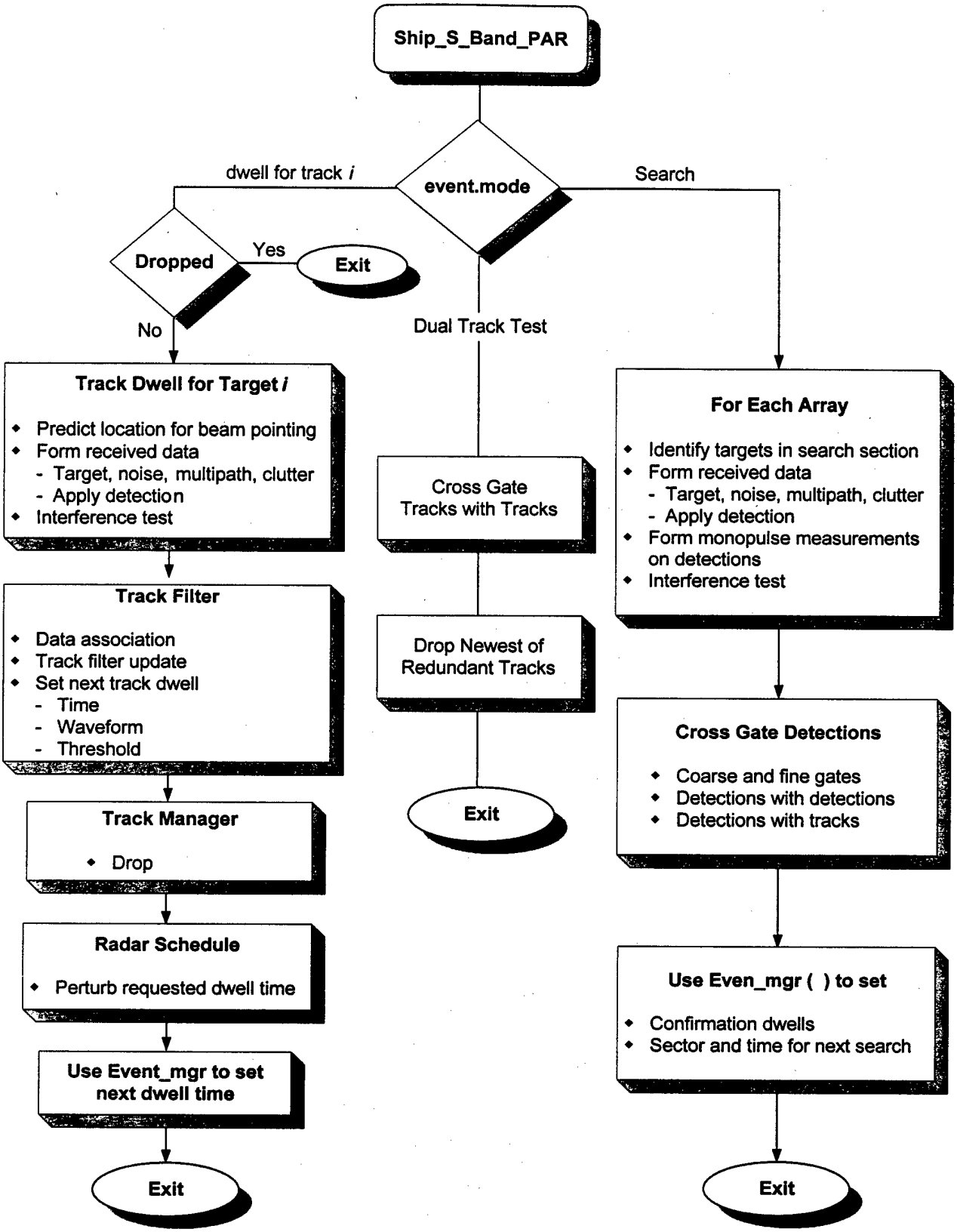

Figure 1. Function Flow of Shipboard S-Band Phased Array Radar Model

azimuth beaming pointing angles. Sensitivity time control (STC) is included in the search dwells to prevent the detection of very small objects at short ranges. The energy from clutter, targets, multipath, etc., and the receiver noise are included in each range cell. The subpulse energies are integrated noncoherently and an SNR threshold is applied to each range cell for detection. Monopulse measurements and an interference test for the detection of unresolved objects are computed for each detection. The measurements are then transformed from sine space at the array to a shipboard reference coordinate frame. The current model allows for biases in the location and orientation of each array.

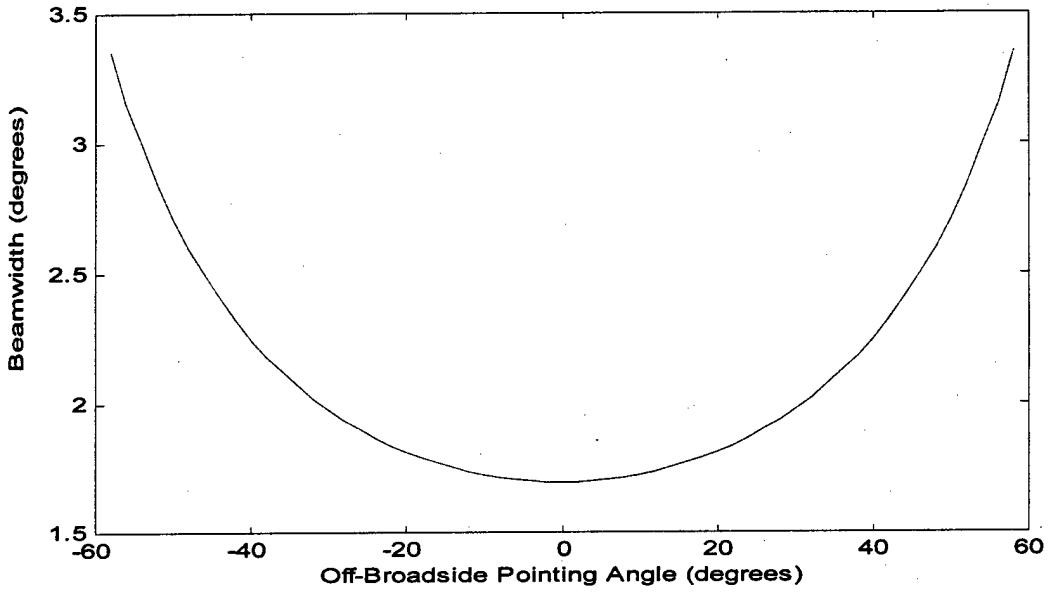

Figure 2. 3 dB Beamwidth Versus Off-broadside Angle

The second action of the search mode is cross gating that is required to prevent the initiation of new tracks on targets that are already under track. The cross gating is performed by first applying a course range and angle gates of 5 km and 2 degrees and then applying a chi-square test. The detections obtained in this search call are cross gated with each other to eliminate adjacent beam detections on a common target. The detections that remain are then cross gated with the tracks. Detections that do not correlate to any existing track are then assigned a track number and a confirmation dwell is scheduled for the track mode. If an error occurs in the cross gating so that a detection that should have been correlated with an existing track, a dual or redundant track is more than likely to be formed. Confirmation dwells are scheduled 0.1 s after the search mode. The final action of the search mode involves calling the event manager to schedule the time and

sector for the next search and the confirmation dwells for the detections that did not correlate with existing tracks.

The first action of the track mode is to exit if the specified track has been dropped by the dual track mode. The first action for an active track is to predict the position of the target at the current time and generate the detection signals for all of the range cells in beam and range window. The energy from clutter, targets, multipath, etc., and the receiver noise are included in each range cell. The subpulse energies are integrated noncoherently and an SNR threshold that is specified by the tracking function is applied to each range cell for detection. Monopulse measurements and an interference test for the detection of unresolved objects are computed for each detection. The measurements are then transformed from sine space at the array to a shipboard reference coordinate frame. The current model allows for biases in the location and orientation of each array. The second action for an active track is the track filtering and data association. A nearly constant velocity Kalman filter is used for the first five measurements and then an IMM estimator with two nearly constant velocity models is initialized. The measurement-to-track data association is accomplished by picking the measurement with the range that is closest to that of the predicted range of the specified target and standard gating to verify the validity of the measurement. The fact that a measurement might actually belong to a target near the target specified in the function call is not considered at this time. If a misassociation occurs between to targets, a track swap or track loss is likely. A five sample median estimator is used to select the waveform so that a desired SNR for tracking is maintained. The sample period and waveform are scheduled for transition-to-track and missed measurements. If a valid detection occurs in the confirmation dwell, transition-to-track is initiated. Otherwise, the track initiated with the search detection is dropped. The transition to track is accomplished by a set of scheduled revisit periods {*e.g.*, 0.1, 0.1, 0.1, 0.1,0.25, 0.25, 0.5, 0.5, 1.0, 1.0, 1.5, 1.5, 2.0 s}, where the revisit periods are set at 2 s until a missed detection occurs. After a missed detection occurs, the revisit period is set to 0.1 s. Adaptive revisit time and waveform and revisit time scheduling for measurements with interference will be addressed later. The time update portion of the track filters includes platform motion. Tracks are dropped after five consecutive missed detections. The request dwell times are then perturbed by a positive uniform random number so that measurements are not received at the exact time requested by the track filter. The final action for an active track is a call to the event manager to schedule the time for the next track dwell on the target specified in the function call.

In the dual track test, the tracks are cross gated with each other. The dual track test is performed every 5 s and if two tracks correlate on two consecutive test, the newer track is dropped.

Two PRF's are needed for the radar model. The two primary issues in PRF selection are maximum unambiguous range and the position of the Doppler nulls. Since this model is to be representative of operational systems, the PRF is limited to a maximum of 1 KHz, implying a maximum unambiguous range of about 150 Km. With this constraint, the PRF pair was selected to minimize the impact of Doppler nulls on the detection performance.

Assuming an unstaggered PRF, an MTI filter has Doppler nulls at integer multiples of the PRF. For a radar operating at wavelength λ, the Doppler frequency f_d of a target with radial velocity v is given by

$$f_d = \frac{2v}{\lambda}$$

The resulting MTI response for a 3.5 GHz radar using a 1 KHz PRF is shown in Figure 3, where deep nulls appear periodically at multiples of 42.8 m/s. The selection of the two different PRFs was made to achieve a response that minimizes the number of deep nulls.

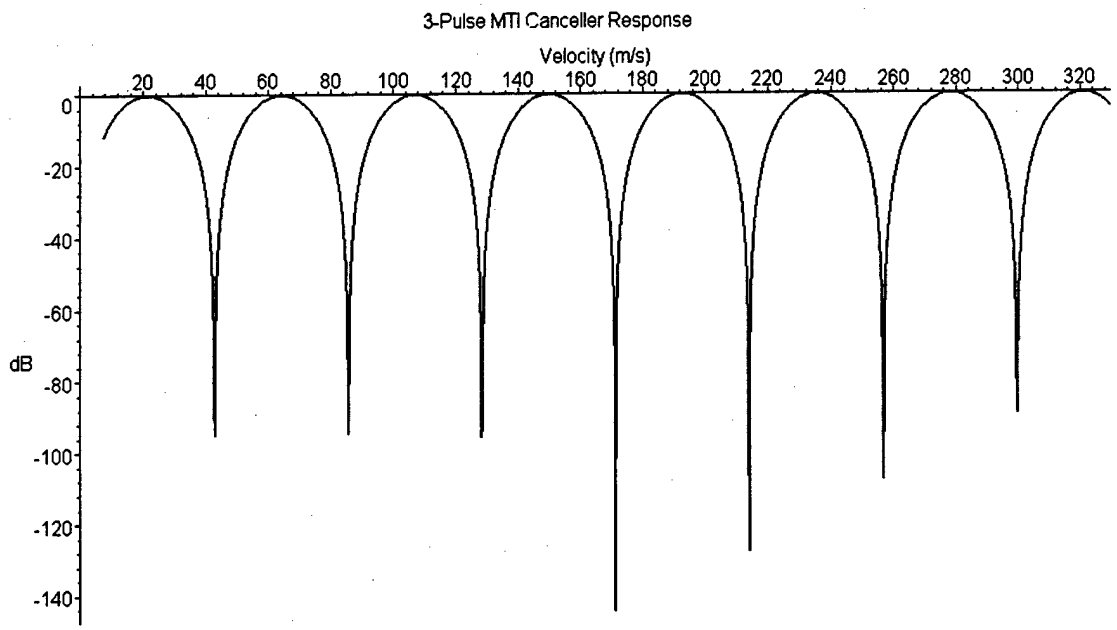

Figure 3 MTI Response for 3-Pulse Canceler

Several performance indices were considered. For example, minimizing the ratio of the region below –10dB to the regions above –3dB was considered. Ultimately, the integral of the area under the composite MTI function was maximized (note that all optimization performance

indices considered produced different PRF pairs, but their composite responses were substantially similar). Let *PRF1* and *PRF2* be such that

$$\{PRF1, PRF2\} = \arg\max\left\{\int_0^{331} \max[MTI(PRF1, v), MTI(PRF2, v)]dv\right\}$$

where *MTI()* is the MTI filter response defined in Appendix B, and the limits of integration were (somewhat arbitrarily) taken over the 0 to 1 Mach interval. Using this criteria, a two dimensional optimization procedure was developed to find *PRF1* and *PRF2* for PRF values near, but below, 1 KHz. The optimal pair was found to be {977, 891}, and their composite response is shown in Figure 4. As can be seen the number of deep nulls (<20dB) is reduced from seven to two, and these two nulls are actually only –34 dB and –22 dB instead of $-\infty$.

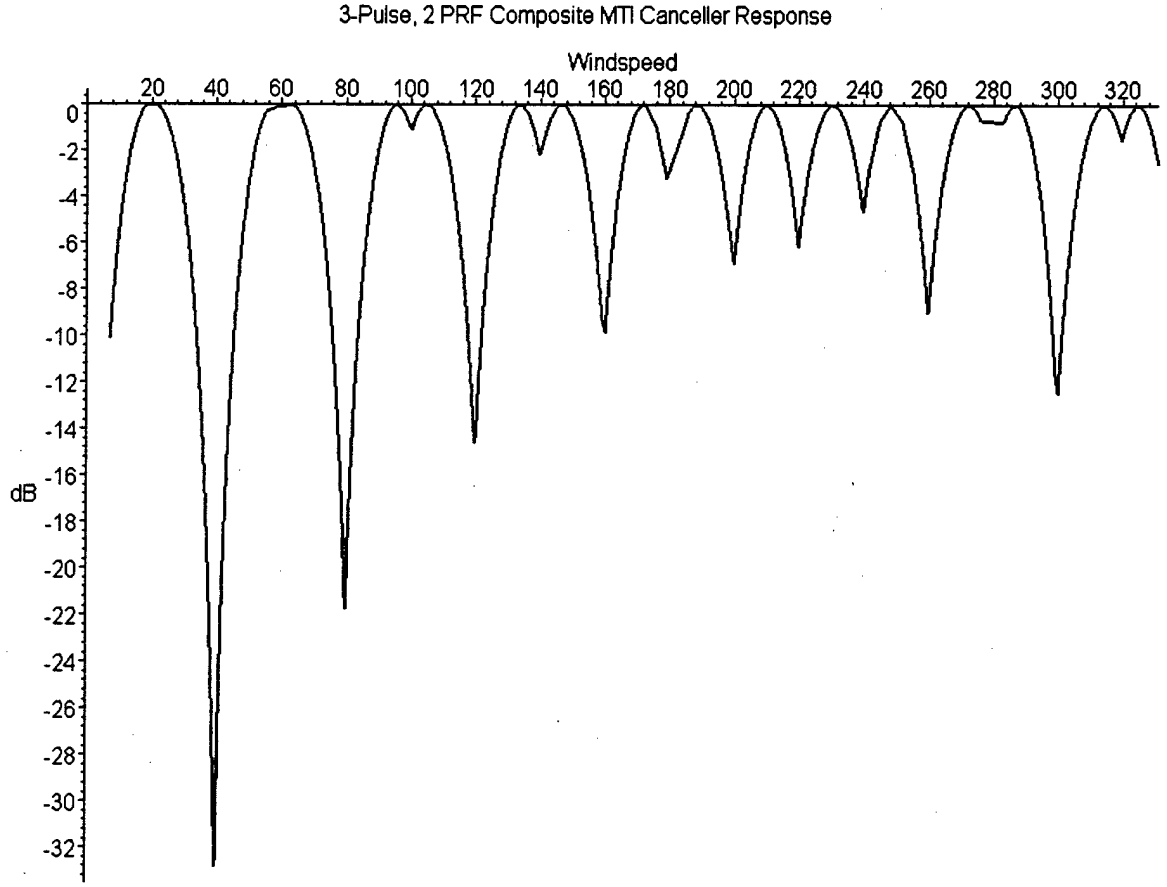

Figure 4 Two-PRF Composite MTI response

Appendix B

Average Sea Clutter RCS Modeling for Shipboard MSI

Prepared by:
Philip D. West, October 1999

1 INTRODUCTION

This appendix documents the equations, tables and concepts used in the development of the sea clutter model. We consider five primary facets of the problem:

- Scenario Geometry
- Average clutter RCS
- Statistical Sample generation
- Clutter Doppler Signature
- MTI Improvement Factor

Scenario geometry deals with the angles and distances between the sea surface and the radar antenna. The primary quantities of interest in the geometry problem are the *depression angle, grazing angle,* and *clutter patch* size. After these parameters have been determined, a table of reference RCS values, indexed by radar frequency, is used to generate a reference clutter *radar cross section (RCS)* for a particular reference condition. Next, analytical interpolation and correction/adjustment factors are applied to compensate for differing sea states, polarizations, grazing angles, and frequency. After all of these computations have been made, a statistical model can be used to generate random samples to represent clutter returns for each range cell of interest. Of course, our primary interest is not on clutter phenomenology, but rather on its impact on radar detection and tracking performance. It is realized that all modern radar systems will use some type of moving target indicator (MTI) or Doppler processing circuitry to remove or separate low velocity targets from the targets of interest. In the final two sections, we first present the Doppler (frequency domain) signature of sea clutter, and then present a closed-form methodology for computing the expected clutter output power from an MTI filter using this clutter model.

2 GEOMETRY

We employ the standard clutter geometry scenario used in many texts [see, e.g. 1] as shown in Figure 1. In this figure, the radar antenna is located at some height H_R meters above the sea surface illuminating a patch of clutter at range R. The Depression Angle of the clutter with respect to the radar is θ_d and the Grazing Angle is θ_g. The grazing angle and depression angle may be computed as:

$$\theta_g = \sin^{-1}\left(\frac{2a_eH_R + H_R^2 - R^2}{2a_eR}\right)$$

$$\theta_d = \sin^{-1}\left(\frac{2a_eH_R + H_R^2 + R^2}{2R(a_e + H_R)}\right) \quad (1)$$

where a_e is the effective radius of the earth.

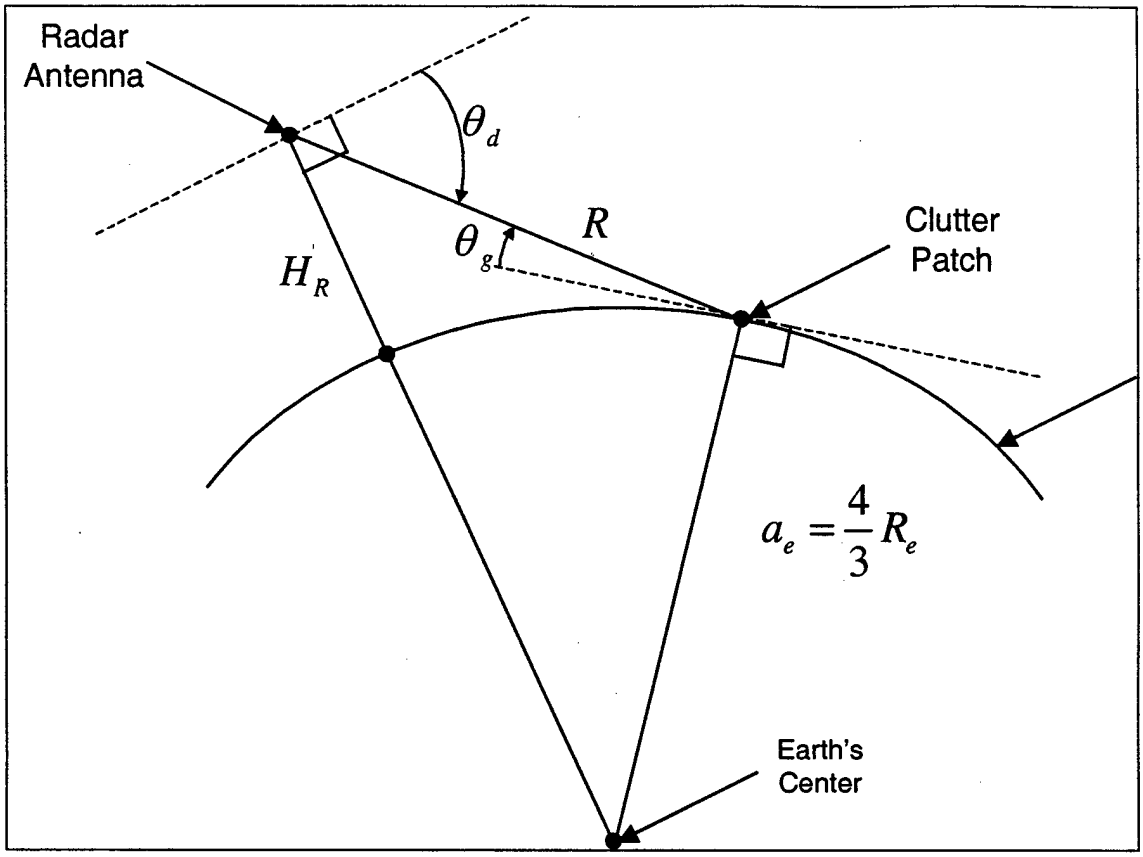

Figure 1. Clutter Geometry

Next,we seek to compute the physical area on the sea surface that will be illuminated by the radar beam. For range-gated radars with range resolution ΔR and beamwidth *BW*, the area will be defined by a strip with width equal to the radar's range resolution and width proportional to the radar azimuthal beamwidth. Specifically:

$$A = R \cdot \Delta R \sin(BW) / \cos(\theta_g) \approx R \cdot \Delta R \cdot BW \quad (2)$$

3 MEAN CLUTTER RCS

In this section, we follow the development advocated in the APL report "Clutter Models for Shipboard Radar Applications: 0.5 to 70 GHz" [2]. Computing the mean sea clutter RCS, σ_0, is a multistep procedure involving first computing the nominal mean clutter RCS as a function of frequency and area and then computing and applying corrections for:

- Wind Speed (effectively sea state) and Direction ***(S)***
- Polarization ***(P)***
- Grazing Angle (Ψ)
- Look Direction ***(D)***

3.1 Fundamental Equation

The fundamental sea clutter RCS equation is:

$$\sigma_0 = \sigma_{ref} + K_\Psi + K_S + K_P + K_D \tag{3}$$

where σ_{ref} is the reference RCS corresponding to $S = 5, \Psi = 0.1°, P = V,$ and $D = 0°,$ and K_Ψ, K_S, K_P and K_D are the corrections for grazing angle, windspeed, polarization and wind direction, respectively. We now consider each term individually. To obtain the RCS in a given resolution cell, the mean clutter RCS (equation(3)) is simply multiplied by the area given by equation (2):

$$\sigma = \sigma_0 \, A \tag{4}$$

3.1.1 Reference RCS

This value, σ_{ref}, is obtained from a table assuming sea state 5, vertical polarization, look direction = 0 (directly upwind) and grazing angle = 0.1°. The values as a function of frequency are:

Table 1 Reference RCS values by Frequency

F (GHz)	0.5	1.25	3.0	5.6	9.3	17.0	35.0	70.0
dBsm	-72.0	-63.0	-54.0	-47.0	-41.0	-38.0	-37.0	-36.0

Interpolation between the tabulated values is done linearly with respect to log(frequency).

3.1.2 Grazing Angle Adjustment

We first define the *transitional grazing angle* as

$$\Psi_t = \mathrm{Sin}^{-1}(0.066\lambda / \sigma_S) \tag{5}$$

where σ_S is the RMS wave height (see Section 3.1.5). With this, the grazing angle adjustment can be partitioned into six regions with different functional adjustments:

for $\Psi_t > \Psi_r = 0.1^\circ$

$$K_\Psi = \begin{cases} 0 & \Psi < \Psi_r \\ 20\log(\Psi/\Psi_r) & \Psi_r < \Psi < \Psi_t \\ 20\log(\Psi_t/\Psi_r) + 10\log(\Psi/\Psi_t) & \Psi_t < \Psi < 30^\circ \end{cases} \tag{6}$$

for $\Psi_t < \Psi_r$

$$K_\Psi = \begin{cases} 0 & \Psi \le \Psi_r \\ 10\log(\Psi/\Psi_r) & \Psi > \Psi_r \end{cases}$$

3.1.3 Polarization Adjustment

For vertical polarization, Kp is 0. Horizontal polarization adjustment is a function of wave height and frequency. Specifically if the polarization is Horizontal:

$$K_p = \begin{cases} 1.7\ln(h_a + 0.015) - 3.8\ln(\lambda) - 2.5\ln\left(\frac{\Psi}{57.3} + 0.0001\right) - 22.2 & f < 3\,GHz \\ 1.1\ln(h_a + 0.015) - 1.1\ln(\lambda) - 1.3\ln\left(\frac{\Psi}{57.3} + 0.0001\right) - 9.7 & 3GHz \le f < 10GHz \\ 1.4\ln(h_a) - 3.4\ln(\lambda) - 1.3\ln\left(\frac{\Psi}{57.3}\right) - 18.6 & f \ge 10Ghz \end{cases} \tag{7}$$

where h_a is the *average* wave height in meters (see section 3.1.5).

3.1.4 Wind Direction Adjustment

The wind direction adjustment, K_d, is a function of the radar look angle with respect to the wind, Θ.

$$K_d = \left(2 + 1.7\log\frac{0.1}{\lambda}\right)(\cos(\Theta) - 1) \tag{8}$$

Figure 2 shows this cosinusoidal variation of sea clutter RCS with look angle for measured data.

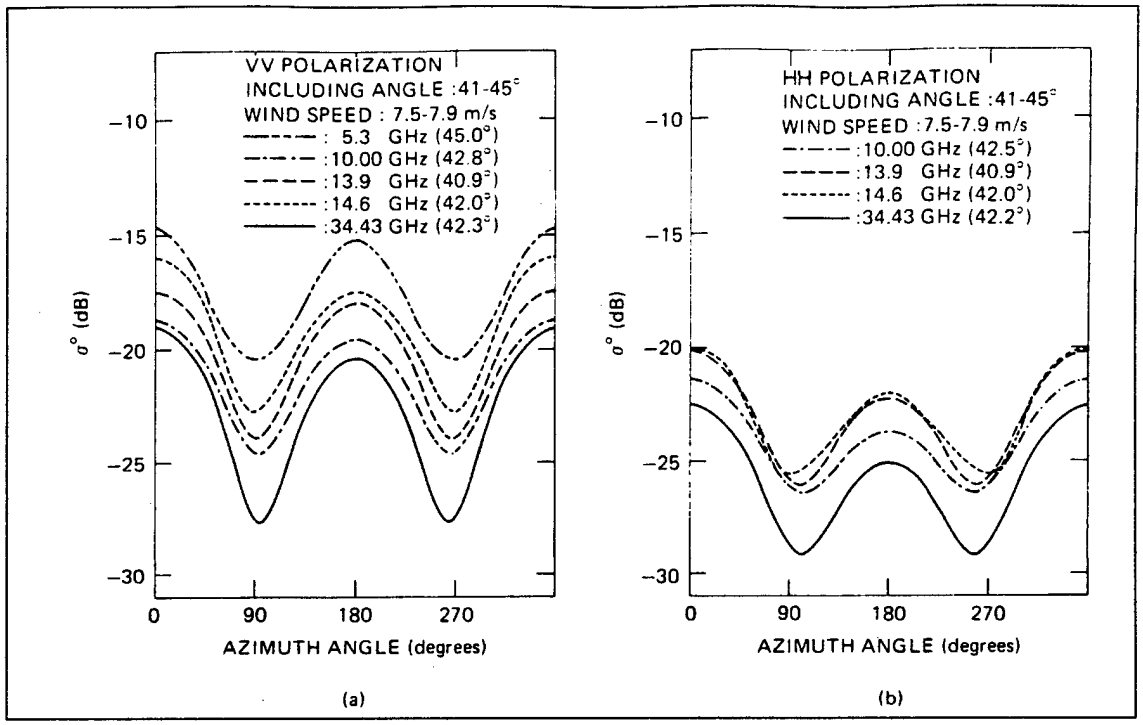

Figure 2. Clutter RCS as a function of look angle w.r.t. wind (from Skolnik pp 13.16)

3.1.5 Sea State Adjustment

The sea state adjustment is:

$$K_S = 5(S-5) \tag{9}$$

where S is the sea state. For blue-water scenarios, wind speed and sea state are related as shown in Table 2.

Table 2 Sea State, Wave Height (h_a) and Windspeed

Sea State	Wind Speed (kn)	WaveHeight, ft
1 (smooth)	<7	1
2 (slight)	7-12	1-3
3 (moderate)	12-16	3-5
4 (rough)	16-19	5-8
5 (very rough)	19-23	8-12
6 (high)	23-30	12-20
7 (very high)	30-45	20-40

Functional relationships between sea state S, windspeed, V_W, RMS wave height σ_z, and average wave height h_a can be defined through the following equations.

$$\begin{aligned} V_W &= 3.2S^{0.8} \\ \sigma_z &= 0.031S^2 \\ h_a &= 0.08S^2 \end{aligned} \tag{10}$$

which implies that $\sigma_z = 0.3875 h_a$.

4 RANDOM CLUTTER SAMPLES

The APL report [2] advocates generating random clutter samples with a Weibull density function. Instead, we prefer to use Gamma distributed variates as described in Appendix A and advocated in [3]. When these Gamma distributed variates are used as clutter RCS samples and combined using standard I&Q signal processing, they lead to the K-Distribution for the received signal power. One downside of using the Gamma model is that generation of these variates is computationally intensive. As a baseline, we used the Gamma distribution 'm-file' available on the Mathworks web-site software archive. To generate random variates, this algorithm generated one sample at a time using nonlinear transformation of uniform variates. Because of the required looping and conditional processing this method is inefficient for generating large vectors of samples. Thus, the code was 'vectorized', using the same numeric algorithm to process entire vectors of samples rather than single samples. The resulting code produces samples with equivalent distributions, but in about 15% of the required CPU time.

5 CLUTTER DOPPLER SPECTRUM

Sea surface wave motion imposes an aspect dependent Doppler shift on the clutter waveform. The clutter spectrum is modeled as Gaussian $\aleph(V_D, \sigma_v^2)$ where:

$$V_D = \begin{cases} 0.85\sqrt{V_W}\cos\Theta & \text{Polarization} = \text{H} \\ 0.15 V_W \cos\Theta & \text{Polarization} = \text{V} \end{cases} \qquad (11)$$
$$\sigma_v = 0.23 V_W \ (m/s)$$

Clutter attenuation by MTI filtering is considered under a separate memo.

6 MTI IMPROVEMENT

Moving target improvement (MTI) circuits are used to cancel radar returns from stationary or low speed objects such as land and trees or even sea surface-induced returns. Of particular interest is a standard 3-pulse tapped delay line MTI filter as shown in Figure 3. Here, the [complex] output pulse sample is a weighted sum of the current pulse and the prior two pulses with the indicated weightings. The frequency domain response for a simple feedforward MTI filter is [4]:

$$|H(f_d)| = 2^N \sin^N\left(\frac{\pi f_d}{PRF}\right) \qquad (12)$$

where N is the number of delays, f_d is the Doppler frequency and PRF is the pulse repetition frequency of the radar. As can be seen, this MTI response has the desired null at zero, but the null repeats periodically at integer multiples of $f_d = PRF / \pi$. Recalling that the Doppler offset for a target flying with velocity v and being observed by a radar with wavelength λ is $f_d = \frac{2v}{\lambda}$, we see that the MTI filter will have nulls

every 42.8 m/s for a 3.5 GHz radar using a 1 KHz PRF (see Appendix A—Radar Model for radar parameters and PRF design). A composite graph showing the Doppler signature for vertically polarized sea clutter with 15, 30 and 45 Knot winds along with the 3-pulse MTI response is shown in Figure 4. As can be seen, as the windspeed increases, the width and mean of the sea clutter spectrum increases. As this happens, less and less of the distribution falls within the clutter notch suggesting that as windspeed (sea state) increases, the clutter rejection ratio for the MTI filter will decrease. Our task, then is to compute the MTI output power as a function of windspeed.

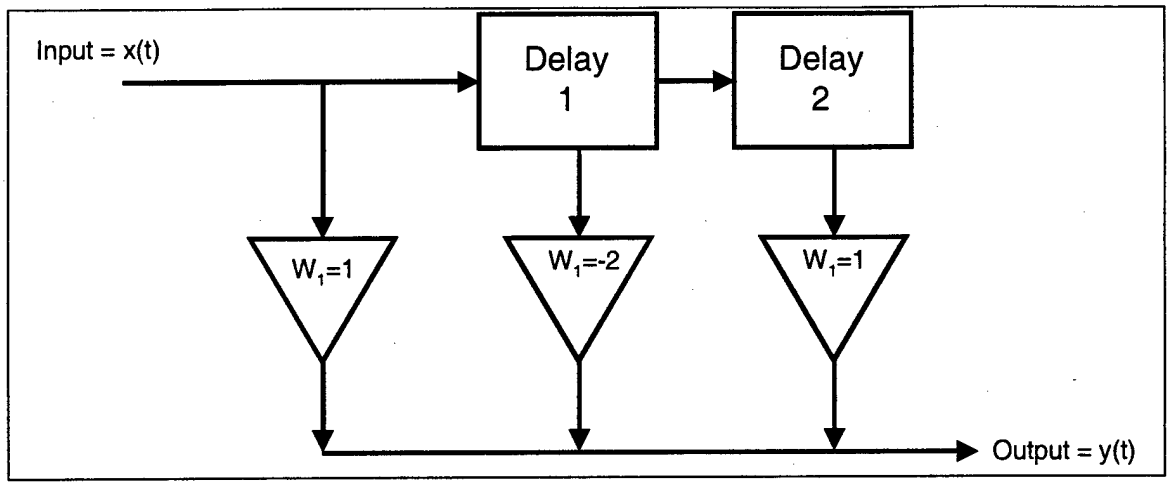

Figure 3. 3-Pulse MTI Canceler

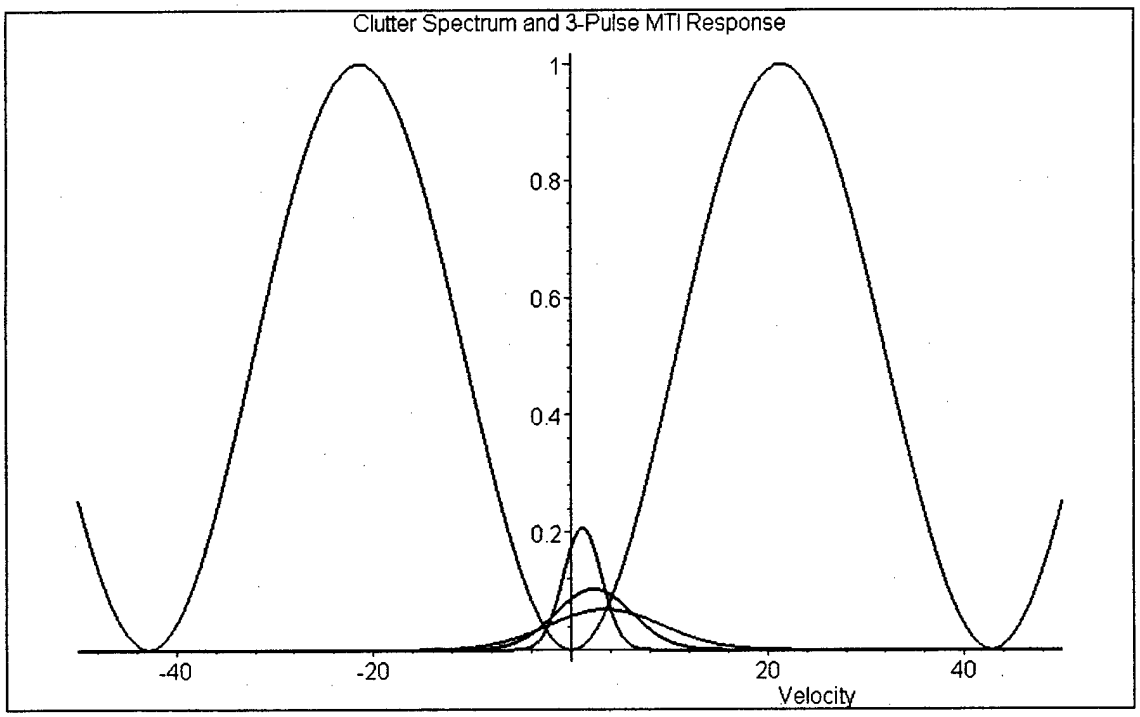

Figure 4. MTI Response and Sea Clutter Doppler Spectrum

The output clutter power will be proportional to the area under the product of the clutter spectrum and the MTI response. This conceptually simple formulation leads to an integral that did not yield to our closed-form integration attempts, so we follow another approach to compute the output clutter power. Following [5], we realize that we wish to find the output power of the MTI filter with weight vector W and with random input signal X. Thus:

$$\begin{aligned} \sigma_c^2 &= E\{W^{'} X X^{'*} W^*\} \\ &= W^{'} M_c W^* \end{aligned} \tag{13}$$

where M_c is the covariance matrix of the clutter, * denotes complex conjugation and ' denotes transposition. Given the Gaussian clutter spectrum specified in Section 5 with variance σ_v^2 and mean V_D:

$$P_c(f) = \frac{1}{\sqrt{2\pi}\sigma_v} e^{\frac{-1}{2}\left(\frac{f-V_D}{\sigma_v}\right)^2} \tag{14}$$

the covariance matrix is defined as:

$$M_c(k,l) = \exp\left\{-2\pi^2\sigma_v^2(k-l)^2T^2 - j2\pi V_D(k-l)T\right\} \tag{15}$$

where T is the pulse recurrence interval (*1/PRF*). Evaluating equation (13) with *W={1, -2, 1}* we get

$$\sigma_c^2 = 6 + 2e^{-8\pi^2\sigma_v^2T^2}\cos(4\pi V_D T) - 8e^{-2\pi^2\sigma_v^2T^2}\cos(2\pi V_D T)^1 \tag{16}$$

By defining the MTI improvement factor to be $I = \sigma_c^2 / \max\left\{|H(f)|^2\right\} = \sigma_c^2 / 16$ we can evaluate the performance of the MTI filter as function of windspeed (using equation (11)), radar frequency and *PRF*. Using the 1 KHz *PRF* and 3.5 GHz center frequency of interest yields Figure 5.

[1] Care must be taken when evaluating this equation to ensure that all units are scaled to the proper Doppler domain.

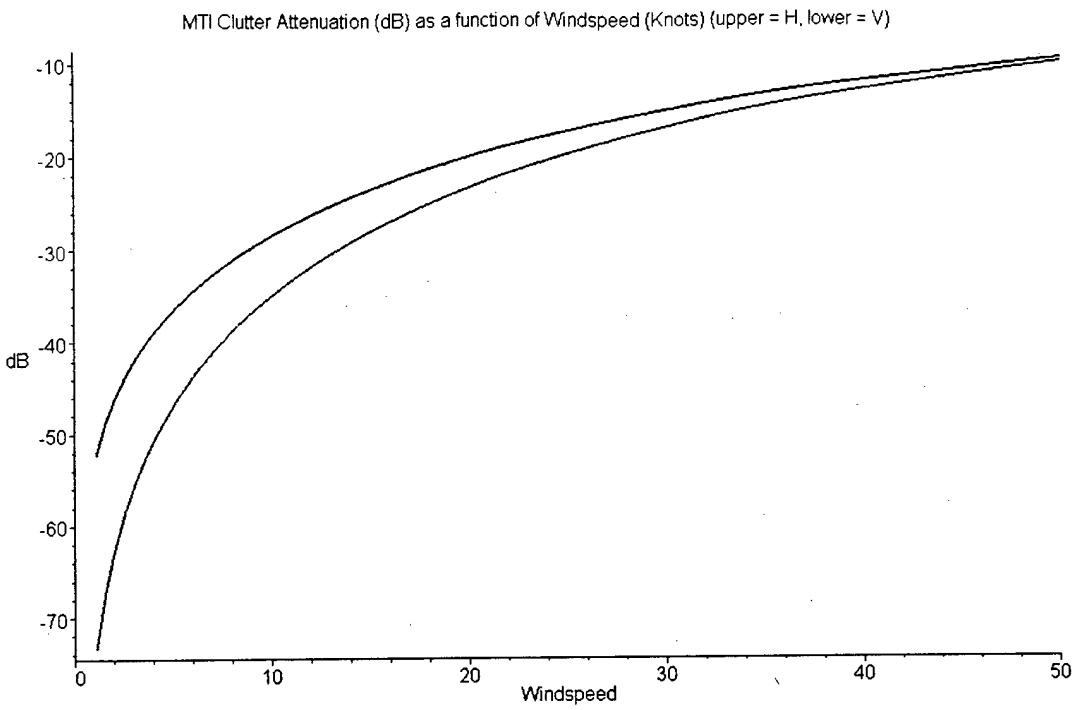

Figure 5. MTI Improvement factor for 3 Pulse canceler at 1 KHz and 3.5 GHz.

As can be seen in the figure, cancellation is quite good for lower windspeeds, achieving 30dB or better for winds below 10 Knots. As the windspeed increases, clutter rejection becomes poor, approaching –10dB as the wind increases to 45 Knots.

7 Summary

A sea clutter model has been developed and implemented in the Matlab® programming environment. The model includes the following features:

- Sea Clutter RCS as a function of:
  - Grazing Angle
  - Sea State (windspeed)
  - Polarization
  - Frequency
  - Radar look direction w.r.t wind direction
- Clutter Doppler Signature
- Statistical (random) RCS Sample Generation

Additionally, the MTI improvement factor was computed for this sea clutter model, and performance curves were plotted for a low PRF waveform using a 3-pulse canceler.

8 REFERENCES

1 Long, M.W., "Airborne Early Warning System Concepts", Artech House, 1992.

2 "Clutter Models for Shipboard Radar Applications: 0.5 to 70 GHz)", Applied Physics Laboratory Report F2A-88-0-307R2, NAAW-88-062R2, October 1, 1988.

3 Watts, S. and K.D. Ward, "Spatial Correlation in K-Distributed Sea Clutter," IEE Proceedings, Vol 134 Pt. F, No. 6, October 1987.

4 Skolnik, M., "Radar Handbook, Second Edition," McGraw-Hill, 1990, p. 15.23

5 Lewis, B.L. *et al* (eds) "Aspects of Radar Signal Processing" Artech House, 1986, pp. 434-464 ("Performance of Cascaded MTI and Coherent Integration Filters in a Clutter Environment" by G.A. Andrews)

Appendix C

Simulation of Non-Gaussian, Complex Sea Scatter

James K. Sangston

1.0 Gaussian Clutter

Simulation of complex, non-Gaussian sea scatter builds on the simulation of complex Gaussian sea scatter. We assume the returns are independent and identically distributed (i.i.d.) in both time and space. Hence it suffices to describe how to generate a single sample of sea scatter.

Let

$$\begin{aligned} u_a &= \text{uniform random number} \\ u_b &= \text{uniform random number} \\ c_i &= \text{phase clutter return} \\ c_q &= \text{clutter return} \\ c &= c_i + c_q = \text{complex clutter return} \end{aligned}$$

Then

$$\begin{aligned} c_i &= = \sqrt{-2\sigma_0 \ln(u_a)}\cos(2\pi u_b) \\ c_q &= = \sqrt{-2\sigma_0 \ln(u_a)}\sin(2\pi u_b) \end{aligned}$$

generates a single, complex Gaussian return whose amplitude PDF is

$$\begin{aligned} f(|c|) &= \frac{|c|}{\sigma_0}\exp(-\frac{|c|^2}{2\sigma_0}) \\ &= \text{Rayleigh distributed} \end{aligned}$$

where σ represents the clutter power level.

2.0 K-Distributed Clutter

To build a simulation for non-Gaussian clutter we will let the amplitude statistics be K distributed of which the Rayleigh distribution is a special case. The extension of the Gaussian simulation

of the non-Gaussian simulation with K distributed amplitude statistics is straight forward. We simply replace σ_0, which in the Gaussian case is a fixed number, with a gamma-distributed random variable σ where

$$\begin{aligned} f(\sigma) &= \frac{\nu^\nu}{\sigma_0 \Gamma(\nu)} \sigma^{\nu-1} \exp\Big(-\frac{\nu\sigma}{\sigma_0}\Big) \\ &= \text{Gamma PDF} \end{aligned}$$

In this distribution

$$\begin{aligned} E\{\sigma\} &= \sigma_0 = \text{average power level} \\ \nu &= \text{shape parameter} \end{aligned}$$

As $\nu \to \infty$, the distribution reverts to Gaussian. Thus, in this case we generate

$$\begin{aligned} &u_a = \text{uniform random number} \\ &u_b = \text{uniform random number} \\ &\sigma = \text{gamma distributed random variable} \\ &c_i = \sqrt{-2\sigma \ln(u_a)} \cos(2\pi u_b) \\ &c_q = \sqrt{-2\sigma \ln(u_a)} \sin(2\pi u_b) \end{aligned}$$

In this case the PDF of the amplitude is given by

$$\begin{aligned} f(|c|) &= \int_0^\infty \frac{|c|}{p} \exp\Big(-\frac{|c|^2}{2\sigma}\Big) \frac{\nu^\nu}{\sigma_0 \Gamma(\nu)} \sigma^{\nu-1} \exp\Big(-\frac{\nu\sigma}{\sigma_0}\Big)\, d\sigma \\ &= \left(\frac{\sqrt{2\nu}}{\sigma_0}\right)^{\nu+1} \frac{|c|^\nu}{2^{\nu-1}\Gamma(\nu)} K_{\nu-1}\left(\frac{2\nu}{\sigma_0}|c|\right) \end{aligned}$$

where $K_{\nu-1}(\cdot)$ is the modified Bessel function of the second kind.

The question now arises as to how to choose the parameter ν as a function of the range resolution length. Over a number of years the general observation has been made that as resolution increases (*i.e.*, as the resolution length decreases), the clutter is observed to be more non-Gaussian (*i.e.*, spikier). Since spikier clutter implies a smaller ν, we are led to hypothesize a relationship of the form

$$\nu = Al^q$$

where

ν = is the shape parameter in the K distribution
l = is the range resolution length (meters)
A = is a constant
q = is a constant

A study by Watts and Ward (*IEE Proceedings* vol. 134 Pb F, No. 6, October 1987, pp 526-532) suggests that a good choice for q is

$$q = \frac{5}{8}$$

However, this same study shows that A can vary greatly as a function of sea state, location, *etc.* To start, I would recommend setting $A = 0.1$. for a 1 μs pulse width (*i.e.*, $l = 300$ m), this gives $\nu = 3.5$, which is moderately spiky clutter. For a 5 μs pulse width it gives $\nu = 9.6$, which is probably indistinguishable from Gaussian clutter. Initially, we recommend choosing

$$\nu = 0.1 l^{\frac{5}{8}}$$

Table of Contents

Monopulse DOA Estimation of Two Unresolved Rayleigh Targets

W.D. Blair
Georgia Tech Research Institute
Georgia Institute of Technology
Atlanta, Georgia 30332-0857
dale.blair@gtri.gatech.edu

M. Brandt-Pearce
Dept. of Electrical Engineering
University of Virginia
Charlottesville, Virginia 22903
mb-p@virginia.edu

ABSTRACT

The measurements of the two closely-spaced targets will be merged when the target echoes are not resolved in angle, range, or radial velocity (*i.e.*, Doppler processing). The Cramer Rao lower bound (CRLB) is developed for the Direction-Of-Arrival (DOA) estimation of two unresolved Rayleigh targets using a standard monopulse radar. Then the modified CRLB is used to give insight into the boresight pointing for monopulse DOA estimation of two unresolved targets. Monopulse processing is considered for DOA estimation of two unresolved Rayleigh targets with known relative Radar Cross Section (RCS). The performance of the DOA estimator is studied via Monte Carlo simulations and compared to the modified CRLB.

Keywords: Radar Signal Processing, Target Tracking, Sensor Resolution

1. INTRODUCTION

While the problem of tracking multiple targets has been studied extensively in recent years, the issue of finite sensor resolution has been completely ignored in almost all studies [1]. Typically, the targets are assumed to be detected with a given probability of detection in the presence of false alarms and clutter, and the target measurements are modeled as the true values plus independent Gaussian errors [2]. However, when two targets are closely spaced with regard to the resolution of the sensor, the measurements from the two targets can be merged into a single measurement. The Joint Probabilistic Data Association (JPDA) algorithm [2] was extended in [3] to develop the JPDAM algorithm, which includes possibly merged measurements (*i.e.*, unresolved targets). Multiple Hypothesis Tracking (MHT) [4] was extended in [5] to include possibly unresolved measurements. In the JPDAM algorithm or MHT, merged measurements are modeled as a "power" weighted centroid of the two targets. While the application of the results of this paper can be used to enhance the JPDAM and MHT algorithms, the focus of this paper is the generation of two Direction-Of-Arrival (DOA) estimates for tracking two unresolved targets rather than the use of a centroid for the two targets.

Monopulse is a simultaneous lobing technique for determining the angular location of a source of radiation or of a "target" that reflects part of the energy incident upon it [6]. In an amplitude comparison monopulse radar system, a pulse of energy is transmitted directly at the predicted position of the target, and the target echo is received with two beams that are squinted relative to the predicted position of the target. (Note that two beams are required for each angular coordinate.) Traditionally, the DOA of a target is estimated with the in-phase part (*i.e.*, the real part) of the monopulse ratio, which is formed by dividing the difference of the two received signals by their sum. When target echoes interfere (*i.e.*, the echoes are not resolved in the frequency or time domains), the DOA estimate indicated by the in-phase monopulse ratio can wander far beyond the angular separation of the targets [6]. In [7], Daum studied the angular estimation accuracies of a standard monopulse radar system for two unresolved targets and showed that the estimation accuracies decline significantly as the variance of the target amplitude fluctuations increases. A generalized maximum likelihood ratio test is developed in [8] for detecting the presence of unresolved Rayleigh targets. While the problem of DOA estimation of unresolved targets has been addressed in several studies involving array signal processing [9,10] and multiple-beam monopulse (*i.e.*, more than two beams per angular coordinate) [11], the work of Sherman in [6,12] is the only technique that utilizes a standard monopulse system in the DOA estimation of two unresolved targets.

Since the hardware of many existing systems provide output signals for standard monopulse,

techniques which directly use this output can be implemented in timely and cost-efficient manner without the development of new hardware. Sherman proposed in [6,12] the use of complex monopulse ratios from two pulses separated sufficiently in time so that the relative phase of the two targets changes, but sufficiently close in time so that the amplitudes of the two targets remain fixed. Sherman then used the five measured quantities (*i.e.*, the two complex monopulse ratios and the ratio of the measured amplitudes of the sum signal) to compute the DOAs of the two targets, the two relative phases, and the ratio of the target amplitudes. In [12], the in-phase and quadrature monopulse ratios and the Method of Moments (MM) were used to develop estimators of the DOAs for tracking two unresolved, fixed-amplitude targets with known relative Radar Cross Section (RCS). Berkowitz and Sherman showed in [13] that under similar assumptions the in-phase monopulse ratios from the two angular coordinates and the ratio of the measured amplitudes from two pulses can be used to estimate the centroid of the two targets and the slope of the line connecting them. However, achieving two pulses with echoes that satisfy the requirements of Sherman's technique is questionable. Furthermore, Sherman utilized a deterministic formulation of the problem to develop his approach. Thus, to date, the results of Sherman have not been further developed and reported in the literature, and no algorithm is available for estimating the DOAs of two unresolved Rayleigh targets.

In this paper, the results on monopulse statistics drived in [8] are used to develop estimators that generate two DOA estimates to be used in tracking rather than relying in the centroid measurement used in the JPDAM. The use of two DOA estimates will be critical for the tracking of two aircraft flying in formation or separating ballistic missiles, where the flight paths result in the targets being unresolved for more than a couple of measurements.

Some background material and notation are given in Section 2, while the probability distribution of the monopulse measurements for two unresolved Rayleigh targets is given in Section 3. In Section 4, the conditional Cramer Rao Lower Bounds (CRLBs) are developed for the DOA estimation of two unresolved Rayleigh targets using a standard monopulse radar. The modified CRLBs (MCRLB) [14], which are needed to remove the dependence on the received amplitudes, are calculated and then used to study the effects of antenna boresight pointing on the DOA estimation. The DOA estimation for the case of two unresolved targets with known relative RCS is treated in Section 5, where the mean of the in-phase monopulse ratio and the variance of the in-phase and quadrature monopulse ratios are utilized to estimate the DOAs of the two targets. Simulation results that illustrate the performance of the DOA estimators and compares it to the MCRLB are also given in Section 5. Concluding remarks are given in Section 6.

2. DEFINITIONS AND BACKGROUND

The in-phase and quadrature parts of the sum and difference signals for two unresolved Rayleigh targets can be written as

$$s_I = \alpha_1 \cos\phi_1 + \alpha_2 \cos\phi_2 + n_{SI} \tag{1}$$

$$s_Q = \alpha_1 \sin\phi_1 + \alpha_2 \sin\phi_2 + n_{SQ} \tag{2}$$

$$d_I = \alpha_1\eta_1 \cos\phi_1 + \alpha_2\eta_2 \cos\phi_2 + n_{dI} \tag{3}$$

$$d_Q = \alpha_1\eta_1 \sin\phi_1 + \alpha_2\eta_2 \sin\phi_2 + n_{dQ} \tag{4}$$

where α_i is the Rayleigh distributed amplitude of the received signal from target i, ϕ_i is phase of the received signal from target i, η_i is the DOA for target i, and

$$n_{SI} \sim N(0,\sigma_S^2) \qquad n_{SQ} \sim N(0,\sigma_S^2)$$
$$n_{dI} \sim N(0,\sigma_d^2) \qquad n_{dQ} \sim N(0,\sigma_d^2)$$

The notation $N(\bar{x},\sigma^2)$ denotes a Gaussian distribution with mean $\bar{x}$ and variance σ^2. For this paper, the errors n_{SI}, n_{SQ}, n_{dI}, and n_{dQ}, are assumed to be independent.

Letting Λ and ψ denote the measured amplitude and phase of the sum signal gives

$$s_I = \Lambda \cos\psi \qquad s_Q = \Lambda \sin\psi \tag{5}$$

Then the observed SNR will be defined as

$$\Re_o = \frac{\Lambda^2}{2\sigma_S^2} \tag{6}$$

Since α_1 and α_2 are Rayleigh distributed and ϕ_1 and ϕ_2 are uniformly distributed on $(-\pi,\pi]$, s_I and s_Q are Gaussian random variables. Applying the transformation of random variables in (5) to the PDF of s_I and s_Q gives the PDF of the observed SNR as

$$f(\Re_o|\Re_R) = \frac{1}{\Re_R+1}\exp\Big[-\frac{\Re_o}{\Re_R+1}\Big], \qquad \Re_o \geq 0 \tag{7}$$

where $\Re_R$ is the SNR parameter of the Rayleigh signal given by

$$\Re_R = \frac{E[\alpha_1^2]}{2\sigma_S^2} + \frac{E[\alpha_2^2]}{2\sigma_S^2} = \Re_{R1} + \Re_{R2} \tag{8}$$

where $E[\cdot]$ denotes the expected value. Since the relative RCS of the targets is assumed to be known, let $\Re_{R2} = \lambda\Re_{R1}$, $\lambda > 0$. Then $\Re_R = (1+\lambda)\Re_{R1}$. For N subpulses at distinct frequencies (*i.e.*, independent), the Maximum Likelihood (ML) estimate of $\Re_R$ is given by

$$\widehat{\Re}_R = Y_N - 1, \qquad Y_N = \frac{1}{N}\sum_{k=1}^{N}\Re_{ok} \tag{9}$$

where $\Re_{ok}$ denotes the observed SNR for subpulse k. Then $\widehat{\Re}_R$ is an unbiased, efficient estimator of $\Re$ with variance given by $\mathrm{VAR}[\widehat{\Re}_R|\Re_R] = N^{-1}(\Re_R+1)^2$.

Denoting $s = s_I + js_Q$ and $d = d_I + jd_Q$, the in-phase and quadrature parts of the monopulse ratio are given by

$$y_I = \mathrm{Re}(\frac{d}{s}) = \frac{s_I d_I + s_Q d_Q}{s_I^2 + s_Q^2} \qquad y_Q = \mathrm{Im}(\frac{d}{s}) = \frac{s_I d_Q - s_Q d_I}{s_I^2 + s_Q^2} \tag{10}$$

3. STATISTICS OF THE MONOPULSE RATIOS

The PDF of the monopulse ratios, y_I and y_Q, for a single pulse can be obtained by application of the transformation of random variables in (5) and (10) to $f(s_I, s_Q, d_I, d_Q|\Phi)$, where Φ denotes the parameter set $\{\Re_{R1}, \Re_{R2}, \eta_1, \eta_2, \sigma_S, \sigma_d\}$. Integrating the result with respect to ψ and conditioning the density on Λ in the form of $\Re_o$ gives

$$f(y_I, y_Q|\Re_o, \Phi) = f(y_I|\Re_o, \Phi) f(y_Q|\Re_o, \Phi) \tag{11}$$

where

$$f(y_I|\Re_o, \Phi) = N\Big(\frac{\Re_{R1}\eta_1 + \Re_{R2}\eta_2}{\Re_{R1} + \Re_{R2} + 1}, \frac{q}{2\Re_o}\Big) \tag{12}$$

$$f(y_Q|\Re_o, \Phi) = N\Big(0, \frac{q}{2\Re_o}\Big) \tag{13}$$

$$q = \Big[\frac{\sigma_d^2}{\sigma_S^2} + \frac{\Re_{R1}\eta_1^2 + \Re_{R2}\eta_2^2 + \Re_{R1}\Re_{R2}(\eta_1 - \eta_2)^2}{\Re_{R1} + \Re_{R2} + 1}\Big] \tag{14}$$

Thus, y_I and y_Q are conditionally independent, Gaussian random variables with a common variance. The mean of y_I is a "power" weighted average of the DOAs of the two targets, while the mean of y_Q is zero.

Using N subpulses at distinct frequencies to ensure that the targets' amplitudes are independent for each subpulse, the ML estimate of $\bar{y}_I$, the mean of y_I given Λ, is given by

$$\hat{y}_I = \Big[\sum_{n=1}^{N} \Re_{on}\Big]^{-1} \sum_{k=1}^{N} \Re_{ok} y_{Ik} = \frac{1}{NY_N} \sum_{k=1}^{N} \Re_{ok} y_{Ik} \tag{15}$$

where $\Re_{ok}$ and y_{Ik} denote the observed SNR and in-phase monopulse ratio for subpulse k and Y_N is given by (9). Since the y_{Ik} are Gaussian random variables, $\hat{y}_I$ is the minimum variance estimate of $\bar{y}_I$ and a Gaussian random variable with variance given by

$$\sigma_{\hat{y}_I}^2 = q\Big[\sum_{k=1}^{N} 2\Re_{ok}\Big]^{-1} = \frac{q}{2NY_N} \tag{16}$$

Since the y_{Ik} are Gaussian, $\sigma^2_{\hat{y}_I}$ is the conditional CRLB for $\bar{y}_I$ given $\{\Re_{ok}\}_{k=1}^N$. The term conditional here is used to denote the fact that the Fisher information and CRLB are developed with the amplitude-conditioned PDF. While $\sigma^2_{\hat{y}_I}$ provides the variance of $\hat{y}_I$ for real-time or actual tracking, $\sigma^2_{\hat{y}_I}$ cannot be used for performance prediction because it is a function of $\{\Re_{ok}\}_{k=1}^N$, which are measured quantities. The MCRLB [14] is obtained by averaging the conditional Fisher information with respect to the measured amplitudes of the received pulses. While the MCRLB is a somewhat looser bound than the CRLB, it can be used for performance prediction. Since $f(y_I|\Re_o, \Phi)$ satisfies the regularity conditions with respect to $\bar{y}_I$ [14], the MCRLB is a lower bound on the covariance of any unbiased estimator of $\bar{y}_I$. The MCRLB of $\bar{y}_I$ is given by

$$\tilde{J}_{y_I}(\bar{y}_I|N, \Phi) = E\left[\sigma^{-2}_{\hat{y}_I}\middle|N, \Phi\right]^{-1} = \frac{q}{2N(\Re_{R1} + \Re_{R2} + 1)} \tag{17}$$

Figure 1 gives a comparison of the MCRLBs of $\bar{y}_I$ for a single target and two unresolved, equal-amplitude targets versus the total SNR in a single frequency (*i.e.*, $N = 1$). The MCRLB of $\bar{y}_I$ for a single target is obtained by setting $\Re_{R2} = 0$ in (17). For the two-target case, the total SNR is given by $\Re_{R1} + \Re_{R2} = 2\Re_{R1}$. In order to obtain $\bar{y}_I = 0$ in both cases, the single target was set at the boresight, and the two targets were situated symmetrically about the boresight (*i.e.*, $\eta_1 = -\eta_2$) and separated by one-half of a beamwidth with $\eta_1 = 0.4$. Figure 1 shows that a total SNR of 14 dB gives a MCRLB of 0.02 for the single-target case and 0.095 for the two-target case. Figure 1 also shows that doubling the energy in a single-frequency waveform to obtain a total SNR of 17 dB gives a MCRLB of 0.01 for the single-target case and 0.09 for the two-target case. Thus, doubling the energy in a single-frequency pulse gives only a small reduction in the MCRLB for the two-target case. However, if the energy in the pulse was doubled and a second frequency is added so that two independent observations of the unresolved targets is obtained, the variance would be reduced by 50 percent because the errors are Gaussian (not shown in figure). Therefore, frequency agility is critical to improving the monopulse angle estimation when two unresolved targets are present.

4. CONDITIONAL AND MODIFIED CRLBS FOR DOA ESTIMATION

The conditional and modified CRLBs associated with η_1 and η_2 are developed in this section. The MCRLB is used here to study the effects of antenna pointing on the DOA estimation and it is used in Section 5 to assess the performance of the DOA estimators.

The conditional Fisher Information Matrix (FIM) [15, p. 79] associated with η_1 and η_2 based on N observations of y_I and y_Q is given by

$$I_{y_I, y_Q}(\eta_1, \eta_2|N, \{\Re_{ok}\}_{k=1}^N, \Phi) = \tag{18}$$

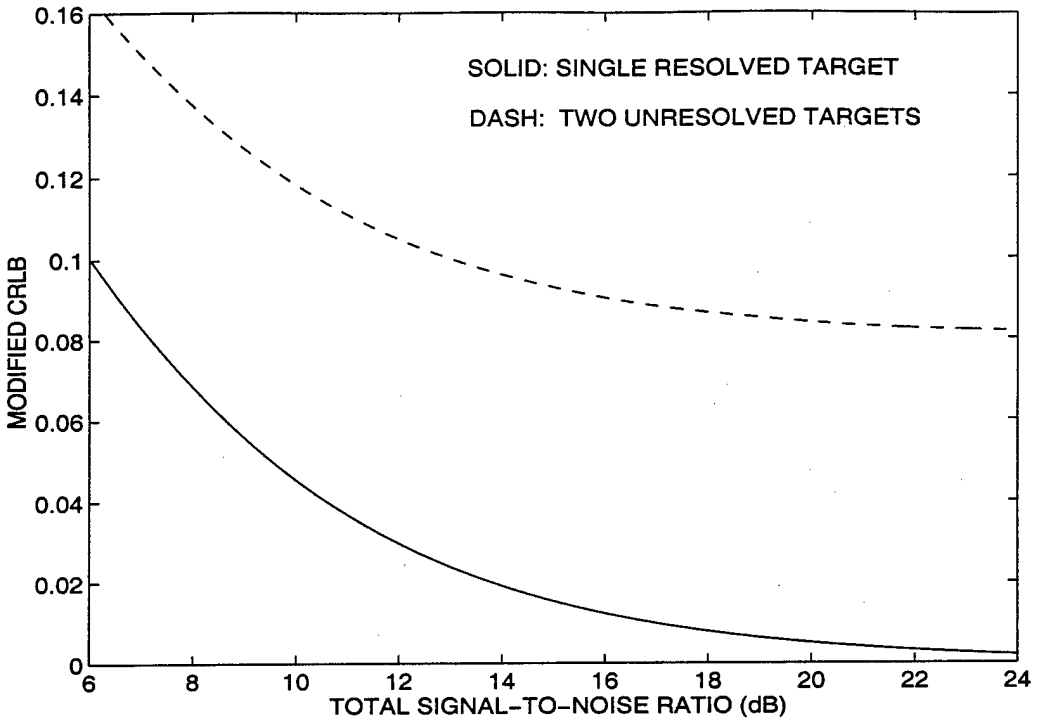

Figure 1. MCRLBs of $\bar{y}_I$ for a single pulse and single target at the boresight and two targets separated by one-half beamwidth and symmetric about the boresight

$$-\sum_{k=1}^{N}\begin{bmatrix} E\Big[\dfrac{\partial^2 \ln f(y_{Ik}, y_{Qk}|\Re_{ok},\Phi)}{\partial \eta_1^2}\Big|\Re_{ok},\Phi\Big] & E\Big[\dfrac{\partial^2 \ln f(y_{Ik}, y_{Qk}|\Re_{ok},\Phi)}{\partial \eta_1 \partial \eta_2}\Big|\Re_{ok},\Phi\Big] \\ E\Big[\dfrac{\partial^2 \ln f(y_{Ik}, y_{Qk}|\Re_{ok},\Phi)}{\partial \eta_1 \partial \eta_2}\Big|\Re_{ok},\Phi\Big] & E\Big[\dfrac{\partial^2 \ln f(y_{Ik}, y_{Qk}|\Re_{ok},\Phi)}{\partial \eta_2^2}\Big|\Re_{ok},\Phi\Big] \end{bmatrix}$$

where $f(y_{Ik}, y_{Qk}|\Re_{ok},\Phi)$ is the PDF of the monopulse ratios for pulse k. Using (11), (12) and (13) in (18) gives

$$I_{y_I,y_Q}(\eta_1,\eta_2|N,\{\Re_{ok}\}_{k=1}^N,\Phi) = \frac{2N\Re_{R1}\Re_{R2}}{q(\Re_{R1}+\Re_{R2}+1)^2} \tag{19}$$
$$\times \begin{bmatrix} \dfrac{\Re_{R1}}{\Re_{R2}}\Big[Y_N + \dfrac{2}{q}\Big(\eta_1 + \Re_{R2}\Delta\eta\Big)^2\Big] & Y_N + \dfrac{2}{q}\Big(\eta_1 + \Re_{R2}\Delta\eta\Big)\Big(\eta_2 - \Re_{R1}\Delta\eta\Big) \\ Y_N + \dfrac{2}{q}\Big(\eta_1 + \Re_{R2}\Delta\eta\Big)\Big(\eta_2 - \Re_{R1}\Delta\eta\Big) & \dfrac{\Re_{R2}}{\Re_{R1}}\Big[Y_N + \dfrac{2}{q}\Big(\eta_2 - \Re_{R1}\Delta\eta\Big)^2\Big] \end{bmatrix}$$

where $\Delta\eta = \eta_1 - \eta_2 > 0$. The dependence of $I_{y_I,y_Q}(\eta_1,\eta_2|N,\{\Re_{ok}\}_{k=1}^N,\Phi)$ on Y_N can removed by averaging over the observed SNR, $\{\Re_{ok}\}_{k=1}^N$, thereby deriving the modified FIM,

$$\tilde{I}_{y_I,y_Q}(\eta_1,\eta_2|N,\Phi) = E[I_{y_I,y_Q}(\eta_1,\eta_2|N,\{\Re_{ok}\}_{k=1}^N,\Phi)|N,\Phi)] \tag{20}$$

which is equivalent to setting $Y_N = E[Y_N|\Phi] = \Re_{R1} + \Re_{R2} + 1$ in (19) since Y_N appears only linearly.

A bound on the covariance of any unbiased estimator of η_1 and η_2 [15, p. 79] is given by the conditional CRLB,

$$COV\begin{bmatrix}\hat{\eta}_1\\ \hat{\eta}_2\end{bmatrix} \geq J_{y_I,y_Q}(\eta_1,\eta_2|N,\{\Re_{ok}\}_{k=1}^N,\Phi) = \Big[I_{y_I,y_Q}(\eta_1,\eta_2|N,\{\Re_{ok}\}_{k=1}^N,\Phi)\Big]^{-1} \tag{21}$$

where

$$J_{y_I,y_Q}(\eta_1,\eta_2|N,\{\Re_{ok}\}_{k=1}^N,\Phi) = \frac{q^2}{4N\Re_{R1}\Re_{R2}\Delta\eta^2} \tag{22}$$
$$\times\begin{bmatrix} \frac{\Re_{R2}}{\Re_{R1}}\Big[1+\frac{2}{qY_N}\Big(\eta_2-\Re_{R1}\Delta\eta\Big)^2\Big] & -1-\frac{2}{qY_N}\Big(\eta_1+\Re_{R2}\Delta\eta\Big)\Big(\eta_2-\Re_{R1}\Delta\eta\Big)\\ -1-\frac{2}{qY_N}\Big(\eta_1+\Re_{R2}\Delta\eta\Big)\Big(\eta_2-\Re_{R1}\Delta\eta\Big) & \frac{\Re_{R1}}{\Re_{R2}}\Big[1+\frac{2}{qY_N}\Big(\eta_1+\Re_{R2}\Delta\eta\Big)^2\Big]\end{bmatrix}$$

Since $f(y_I,y_Q|\Re_o,\Phi)$ satisfies the regularity conditions with respect to η_1 and η_2 [14], the MCRLB is a lower bound on the covariance of any unbiased estimator of η_1 and η_2 [14]. The MCRLB, $\tilde{J}_{y_I,y_Q}(\eta_1,\eta_2|N,\Phi)$, is derived by using the modified FIM of (20) instead of the conditional FIM of (19) in (21). Thus, the MCRLB, $\tilde{J}_{y_I,y_Q}(\eta_1,\eta_2|N,\Phi)$, is obtained by setting $Y_N = E[Y_N|\Phi] = \Re_{R1}+\Re_{R2}+1$ in (22) and given by

$$\tilde{J}_{y_I,y_Q}(\eta_1,\eta_2|N,\Phi) = \frac{q^2}{4N\Re_{R1}\Re_{R2}\Delta\eta^2} \tag{23}$$
$$\times\begin{bmatrix} \frac{\Re_{R2}}{\Re_{R1}}\Big[1+\frac{2(\eta_2-\Re_{R1}\Delta\eta)^2}{q(\Re_{R1}+\Re_{R2}+1)}\Big] & -1-\frac{2(\eta_1+\Re_{R2}\Delta\eta)(\eta_2-\Re_{R1}\Delta\eta)}{q(\Re_{R1}+\Re_{R2}+1)}\\ -1-\frac{2(\eta_1+\Re_{R2}\Delta\eta)(\eta_2-\Re_{R1}\Delta\eta)}{q(\Re_{R1}+\Re_{R2}+1)} & \frac{\Re_{R1}}{\Re_{R2}}\Big[1+\frac{2(\eta_1+\Re_{R2}\Delta\eta)^2}{q(\Re_{R1}+\Re_{R2}+1)}\Big]\end{bmatrix}$$

Although the MCRLB is known to be a somewhat looser bound than the CRLB, it is needed to remove the dependence on the received amplitudes so that performance prediction can be accomplished. The diagonal elements of $\tilde{J}_{y_I,y_Q}(\eta_1,\eta_2|N,\Phi)$ give the MCRLBs for $\hat{\eta}_1$ and $\hat{\eta}_2$ and are used to assess the efficiency [15, p. 71] of the DOA estimators in the next section.

The MCRLB of (23) can be used to study the effects of sensor pointing on the DOA estimation. For this study, the effects of the antenna gain pattern are not assumed to be included in λ, the relative RCS of the two targets. The effects of the antenna gain pattern can instead be included in the anaylsis of the MCRLB by using

$$\widetilde{\Re}_{R1} = \Re_{R1}\cos^4\Big(\frac{\eta_1\pi}{4\eta_{bw}}\Big) \tag{24}$$

$$\widetilde{\Re}_{R2} = \Re_{R2}\cos^4\Big(\frac{\eta_2\pi}{4\eta_{bw}}\Big) \tag{25}$$

in (23) for $\Re_{R1}$ and $\Re_{R2}$, respectively. The η_{bw} denotes the DOA value at the one-way, half-power point on the antenna gain pattern of the sum channel. Thus, at $\eta_1 = \eta_{bw}$, $\widetilde{\Re}_{R1} = \Re_{R1} - 6$ dB. For a monopulse error slope k_m in beamwidths, $2\eta_{bw} \approx k_m$. For all of the examples in this paper, $\eta_{bw} = 0.8$.

Figure 2(a) shows the average MCRLB for two 19 dB targets (*i.e.*, $\Re_{R1} = \Re_{R2} = 19$ dB in (24) and (25) for $N = 1$) separated by one-half beamwidth (*i.e.*, $\Delta\eta = \eta_{bw} = 0.8$) versus the DOA of target 1, η_1, for $N = 1$, 2, 4, 8 and 16 subpulses. The average MCRLB is the average of the two diagonal elements of (23). For each case in Figure 2(a), the energy in the transmitted pulse is fixed and it is divided into N subpulses at different frequencies. Thus, for $N = 8$ subpulses, $\Re_{R1} = \Re_{R2} = 10$ dB in (24) and (25). The DOA for target 2 is given by $\eta_2 = \eta_1 - \Delta\eta$. Thus, $\eta_1 = 0$ in Figure 2(a) corresponds to target 1 on the antenna boresight, while $\eta_1 = 0.8$ corresponds to target 2 on the antenna boresight. Also, $\eta_1 = -0.2$ in Figure 2(a) corresponds to pointing the antenna boresight on the outside of the two targets. The average of the two MCRLBs in Figure 2(a) shows that pointing the antenna boresight exactly between the two targets (*i.e.*, $\eta_1 = 0.4$) gives the smallest average MCRLB for $N = 4$, 8, and 16 and the largest bound for pointing between the targets when $N = 1$. For $N = 1$, the minimum average MCRLB is achieved by pointing the antenna boresight just to the outside of one of the two targets. Figure 2(a) also shows that the average MCRLB is rather insensitive to the antenna boresight when it is positioned between the two targets. For $N = 16$, the rapid increases in the average MCRLB near the edges of the plot are due the rapid increase of the MCRLB for the weaker target. To illustrate this point, Figure 2(b) gives the individual MCRLBs of the two targets for $N = 4$ and 8. Figure 2(b) shows that pointing the antenna boresight closer to target 1 gives a smaller MCRLB for η_1 and larger MCRLB for η_2. Note the rapid increase in the MCRLB of the weaker target when the antenna is pointed to the outside of one of the two targets. Also, note that the reduction in the MCRLB gained through frequency agility (*i.e.*, $N = 8$ rather than $N = 4$) is lost due to the low subpulse SNR at $\eta_1 = -0.15$ for η_2 and $\eta_1 = 0.95$ for η_1.

If the DOA estimate for a single target is desired, the individual MCRLBs for the DOA of each target are of interest. Figure 2(b) shows the individual MCRLBs indicating that pointing closer to or beyond the target of interest minimizes the MCRLB for that target. The minimum MCRLB for η_1 with $N = 4$ is 0.015 at $\eta_1 = -0.3$ and with $N = 8$ is 0.012 at $\eta_1 = -0.2$. For $N = 1$ (not shown in Figure 2(b)), the minimum MCRLB for η_1 is 0.012 at $\eta_1 = -0.5$. For the single target DOA estimation, an optimal pointing angle always exists and moves towards the target of interest as N increases for this separation of the two targets, target amplitudes, and beamwidth. For $N > 1$, note that pointing away from the intefering target is optimal in

the single DOA estimate case, whereas pointing between the targets is optimal when estimating both DOAs.

Figure 2(c) gives further insight into the pointing of the antenna boresight for the DOA estimation of two unresolved targets. Using eight frequencies (*i.e.*, $N = 8$) to simultaneously estimate both DOAs gives a minimum MCRLBs for the individual targets of 0.028 with the antenna boresight pointed exactly between the two targets, as seen also in Figure 2(a). If the eight subpulses are used in two dwells of four subpulses each, the two DOAs can be sequentially estimated by using the first dwell to estimate the nearer target DOA, and using the second to estimate the other target DOA. This method also gives a minimum MCRLB of 0.028 obtained by pointing to the outside of the targets. Further analysis showed that if the separation between the targets is larger than one half of the beamwidth (*i.e.*, $\Delta\eta > \eta_{bw}$), sequential estimation yields a lower MCRLB, whereas if the separation is less than one half the beamwidth, simultaneous estimation provides the best performance bound (not shown). Therefore, for equal amplitude targets, the case $\Delta\eta = \eta_{bw}$ shown in Figure 2(c) denotes a boundary in the decision process for the optimal pointing strategy.

Figure 3(a) shows the average MCRLB for two 19 dB targets (*i.e.*, $\Re_{R1} = \Re_{R2} = 19$ dB in (24) and (25) for $N = 1$) separated by one-fourth beamwidth (*i.e.*, $\Delta\eta = 0.5\eta_{bw} = 0.4$) versus η_1 for $N = 1,\ 2,\ 4,\ 8$, and 16 subpulses. Thus, $\eta_1 = 0$ in Figure 3(a) corresponds to target 1 on the antenna boresight, while $\eta_1 = 0.4$ corresponds to target 2 on the antenna boresight. The average of the two MCRLBs in Figure 3(a) shows that pointing the antenna boresight exactly between the two targets (*i.e.*, $\eta_1 = 0.2$) gives the smallest average MCRLB for all values of N. Figure 3(a) also shows that increasing the number of frequencies from $N = 8$ to $N = 16$ actually results in an increase in the average MCRLB. Note that this result differs from that shown in Figure 2(a), and it is thought to be the result of a low subpulse SNR at $N = 16$ and a lower average MCRLB in 3(a) compared to that in 2(a).

Figure 3(b) gives insight into the pointing of the antenna boresight for the DOA estimation of a single target in the presence of another target for one-fourth beamwidth separation. It is interesting to note the minimum MCRLB for single DOA estimation corresponds to pointing between the two equal amplitude targets for $N = 8$, in contrast to the results of Figure 2(b). A comparision of the sequential and the simultaneous estimation algorithms for this case in a manner similar to that of Figure 2(c) indicates that it is always advantageous to use simultaneous estimation.

Figure 4(a) shows the MCRLB for a 19 dB target and a 16 dB target (*i.e.*, $\Re_{R1} = 2\Re_{R2} = 19$ dB) separated by one-fourth beamwidth versus η_1 for $N = 1,\ 2,\ 4$ and 8 subpulses. For the

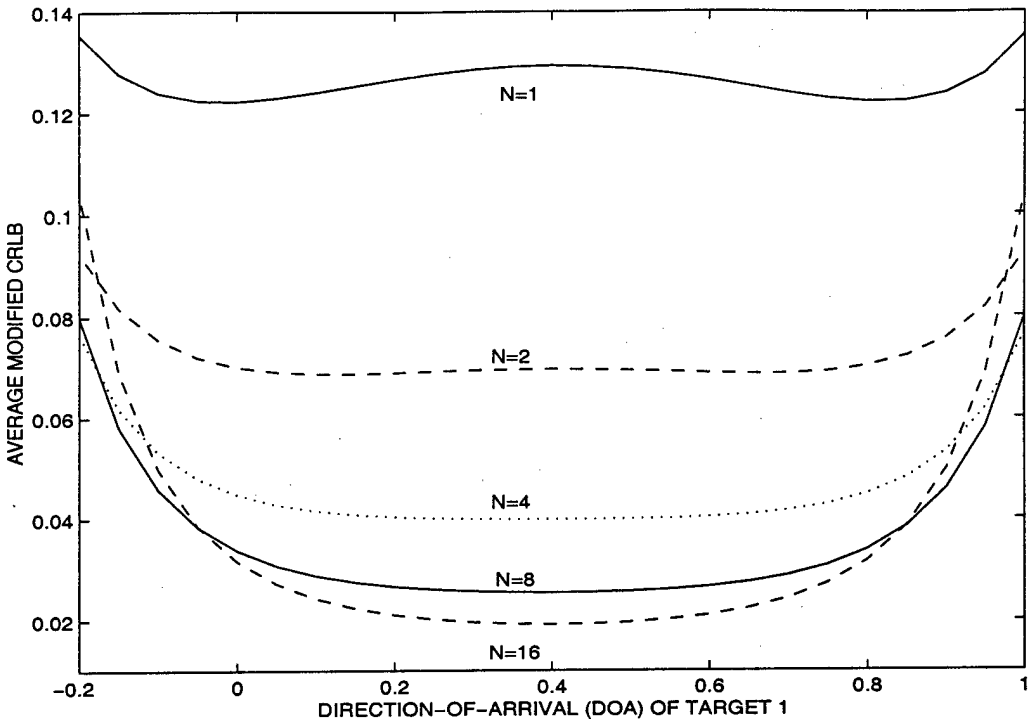

Figure 2(a) Average MCRLB for η_1 and η_2 with $\Delta\eta = \eta_{bw}$ and two 19 dB targets

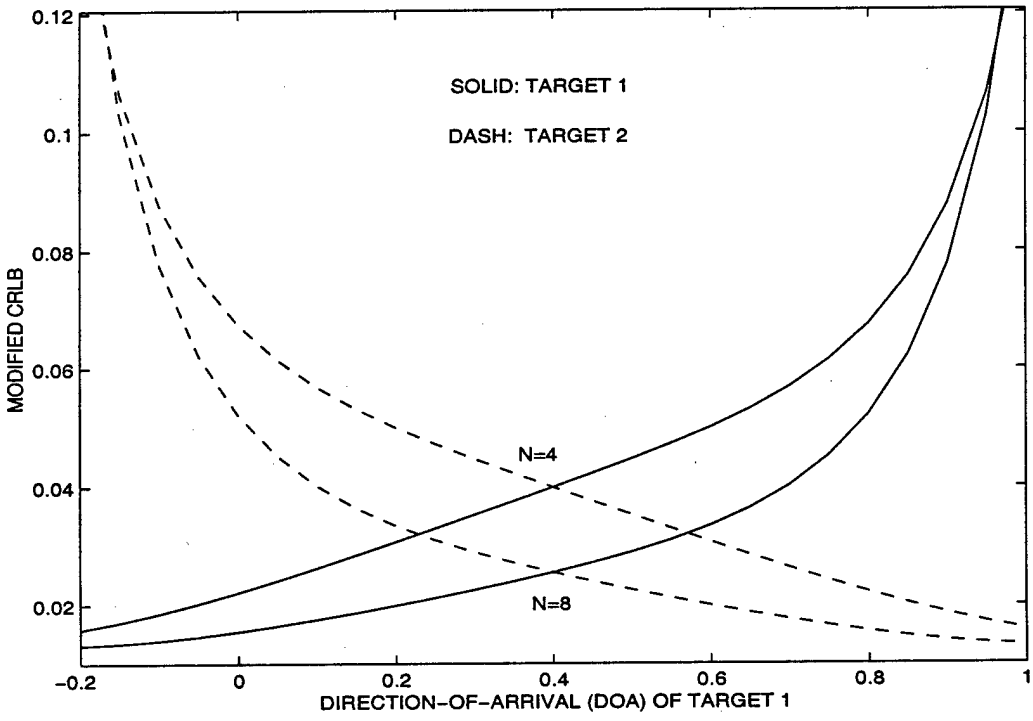

Figure 2(b) MCRLBs for η_1 and η_2 with $\Delta\eta = \eta_{bw}$ and two 19 dB targets

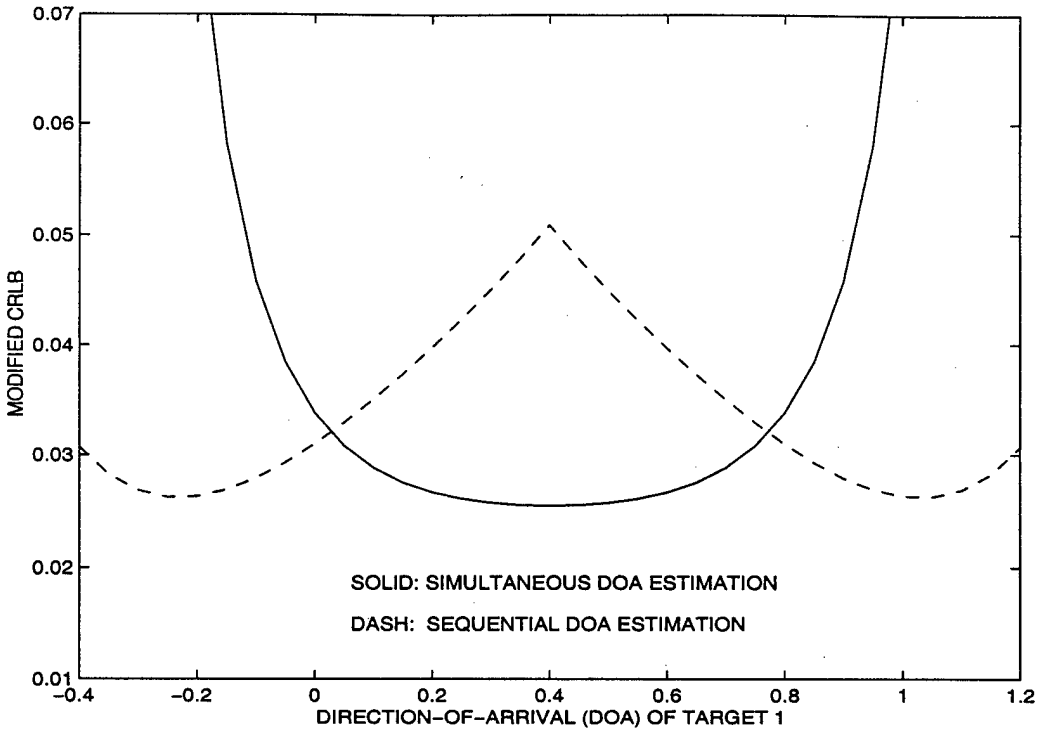

Figure 2(c) MCRLBs for sequential and simultaneous estimation of η_1 and η_2 with $\Delta\eta = \eta_{bw}$, two 19 dB targets, and eight subpulses of equal energy (Sequential: $N = 4$ in two consecutive dwells; simultaneous: $N = 8$ in one dwell)

$N = 1$ and 2 cases, the optimal pointing strategy is to stear the antenna boresight slightly towards the stronger target, while for the other cases, stearing should lean toward the weaker target. It appears that the simultaneous DOA estimator favors pointing towards the lower power target when subpulse powers are too low ($N = 4$ or 8), perhaps to avoid very low SNR observations. Note also that the advantages of frequency agility have been achieved by $N = 4$ and the degradation in performance due to low subpulse SNR can be seen by the steepening of the graph at extreme values of η_1 for $N = 8$. The MCRLB for the single target DOA estimator shown in Figure 4(b) agrees with the results for the equal energy case of Figure 3(b) that for a low number of subpulses the antenna should be pointed at or outside the position of the targets and for a higher number of subpulses it should point on the inside. For the case of two unequal amplitude targets, the pointing strategy for sequential estimation is less clear. Figure 4(b) suggests an approach. The first dwell may be in the neighborhood of the strongest target to obtain the least error in the DOA estimate of that target. The pointing of the second dwell is then chosen to minimize the bound in estimating the DOA of the second target.

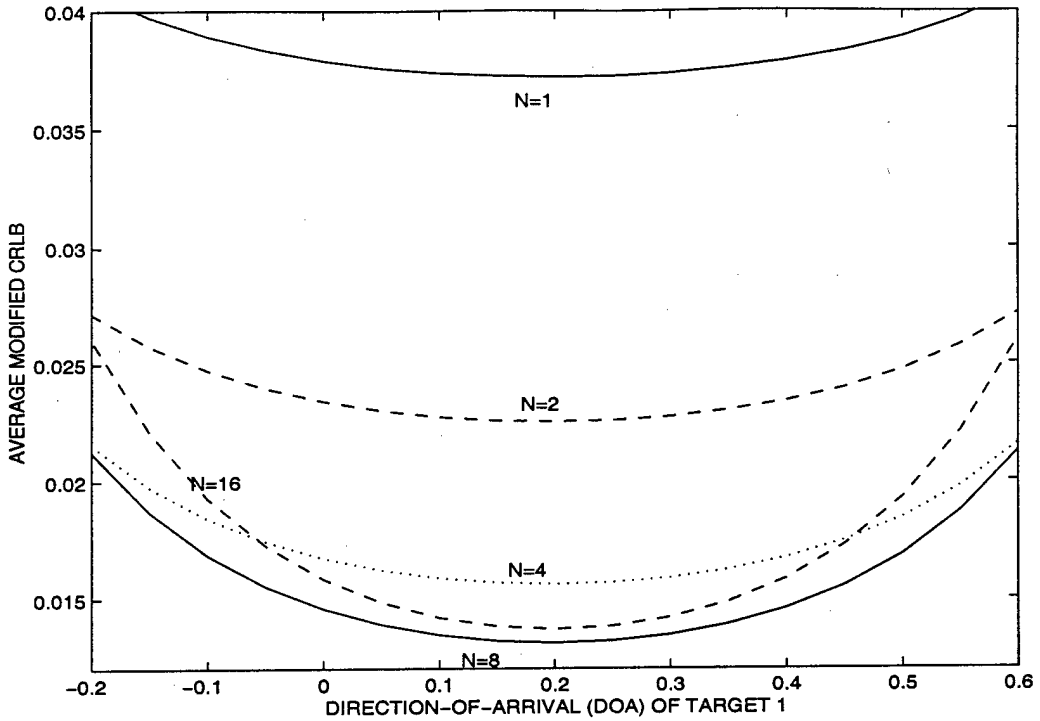

Figure 3(a) Average MCRLB for η_1 and η_2 with $\Delta\eta = 0.5\eta_{bw}$ and two 19 dB targets

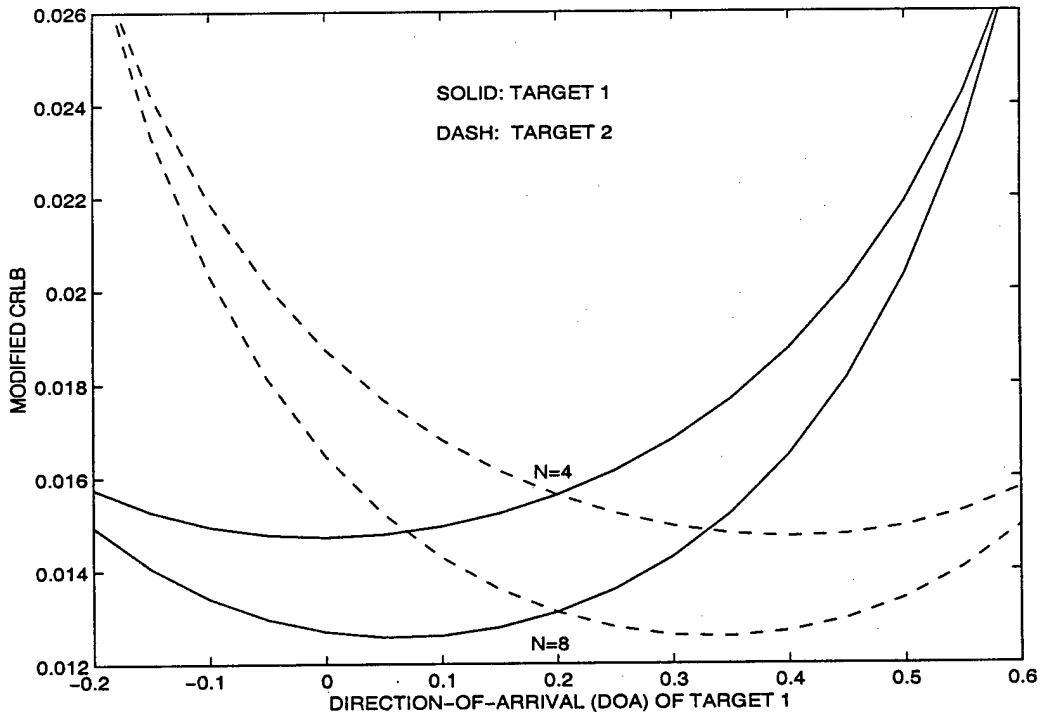

Figure 3(b) MCRLBs for η_1 and η_2 with $\Delta\eta = 0.5\eta_{bw}$ and two 19 dB targets

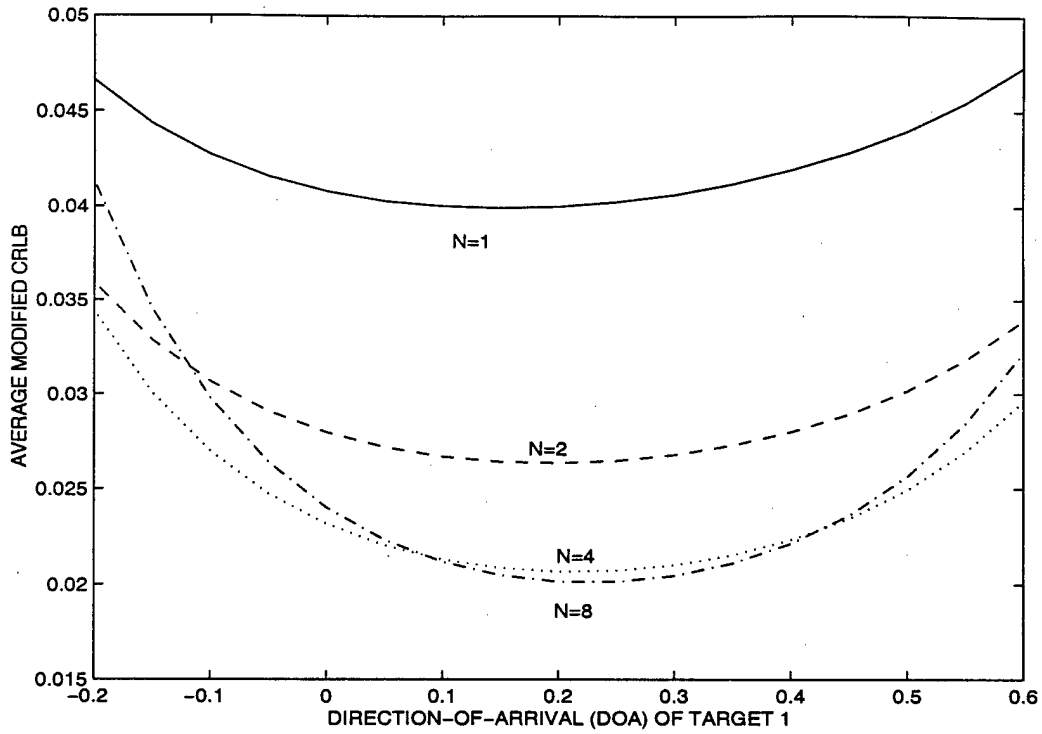

Figure 4(a) Average MCRLB for η_1 and η_2 with $\Delta\eta = 0.5\eta_{bw}$ and 16 dB and 19 dB targets

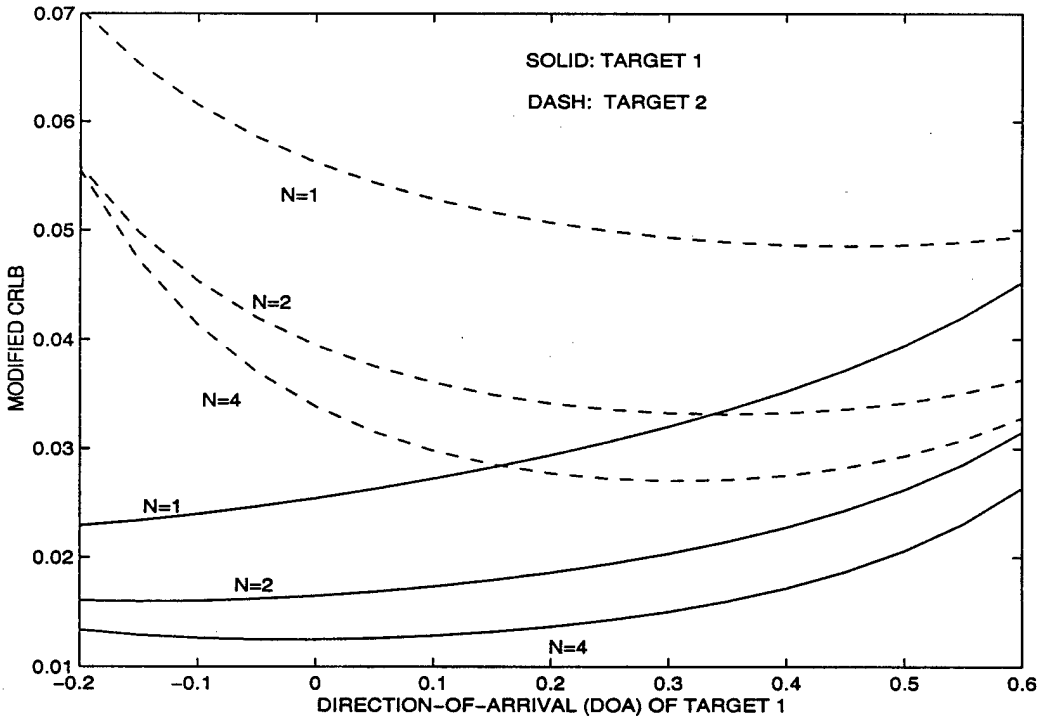

Figure 4(b) MCRLBs for η_1 and η_2 with $\Delta\eta = 0.5\eta_{bw}$ and 13 dB and 19 dB targets

5. DOA ESTIMATION FOR TWO UNRESOLVED TARGETS

As seen in the previous section, the pointing of the antenna boresight affects the information obtained during a radar dwell. Based on the results of Section 4, two sensor pointing strategies are set forth. The simultaneous pointing strategy that was found to be optimal for targets separated by less than one-half beamwidth involves pointing between the targets and estimating both DOAs from data gathered in one dwell. This case is referred to as the fully unresolved case. The second strategy proposed, applicable to targets which are separated by more than one-half of a beamwidth, is the sequential strategy in which the DOAs are estimated from data gathered from two consecutive dwells, each pointing in the general direction of one target. This case can be thought of as a partially resolved target scenario since estimation of each parameter can be performed individually. In this section, a DOA estimation algorithm based on the Method of Moments (MM) for the fully unresolved two-target case is proposed. The partially resolved target case is briefly discussed in [16].

For the case of two fully unresolved Rayleigh targets, the antenna boresight is pointed between the targets and the DOA estimation of both targets is accomplished simultaneously via MM. For the MM, two sample moments are required for the estimation of two DOAs. Since the observations y_{Ik} are not stationary, sample moments cannot be used directly. Thus, $\hat{y}_I$ from (15) will be used to obtain the first expression as

$$\hat{y}_I = \frac{\Re_{R1}\eta_1 + \Re_{R2}\eta_2}{\Re_{R1} + \Re_{R2} + 1} \tag{26}$$

Let $\Delta\eta = \eta_1 - \eta_2 > 0$, so that $\eta_1 > \eta_2$. Then, since $\Re_{R2} = \lambda\Re_{R1}$, where $\lambda > 0$,

$$\eta_1 \approx \hat{y}_I + \frac{\lambda}{1+\lambda}\Delta\eta \qquad \eta_2 \approx \hat{y}_I - \frac{1}{1+\lambda}\Delta\eta \tag{27}$$

Since the y_{Ik} are nonstationary, Gaussian random variables, the second expression for DOA estimation will be obtained by forming a Chi-squared random variable with $2N-1$ degrees of freedom from y_{Ik}, $\Re_{ok}$, and $\hat{y}_I$ and setting the random variable equal to its mean. Thus, for $N > 1$, let

$$X_N = [\, y_{I1} - \hat{y}_I \quad \cdots \quad y_{IN} - \hat{y}_I \quad y_{Q1} \quad \cdots \quad y_{QN} \,] \tag{28}$$

$$R_N = 2\ \mathrm{diag}[\, \Re_{o1} \quad \cdots \quad \Re_{oN} \quad \Re_{o1} \quad \cdots \quad \Re_{oN} \,] \tag{29}$$

Since for $N = 1$, $\hat{y}_I = y_{I1}$, let $X_1 = y_{Q1}$ and $R_1 = 2\Re_{o1}$. Also let

$$v_N = X_N^T R_N X_N q^{-1} \tag{30}$$

where q is given by (14). Since the conditional PDF of the in-phase and quadrature monopulse ratios are Gaussian with variance given by (11) through (14), v_N is a Chi-squared random variable with $2N-1$ degrees of freedom. Then

$$E[v_N] = 2N-1 \qquad \text{VAR}[v_N] = 2(2N-1) \tag{31}$$

Setting v_N equal to its mean gives

$$\hat{q} = \frac{X_N^T R_N X_N}{2N-1}, \qquad N \geq 1 \tag{32}$$

Since for $\Delta\eta > 1.0$ the targets would be processed as partially unresolved targets, assume that $\Delta\eta < 1.0$. Thus, pointing the antenna boresight between the targets allows the approximation of q by

$$q \approx \frac{\sigma_d^2}{\sigma_S^2} + \frac{\lambda \Re_{R1}}{1+\lambda}\Delta\eta^2 \tag{33}$$

Inserting $\hat{q}$ in (32) for q and using (33) in (27) gives the DOA estimates as

$$\hat{\eta}_1 = \hat{y}_I + \sqrt{\frac{\lambda\tilde{q}}{\hat{\Re}_R}}, \qquad \hat{\eta}_2 = \hat{y}_I - \sqrt{\frac{\tilde{q}}{\lambda\hat{\Re}_R}} \tag{34}$$

where

$$\tilde{q} = \begin{cases} 0, & \hat{q} \leq \sigma_d^2\sigma_S^{-2} \\ \dfrac{4\eta_{bw}^2\lambda}{(1+\lambda)^2}\hat{\Re}_R, & \hat{q} \geq \dfrac{4\eta_{bw}^2\lambda}{(1+\lambda)^2}\hat{\Re}_R + \sigma_d^2\sigma_S^{-2} \\ \hat{q} - \sigma_d^2\sigma_S^{-2}, & \text{otherwise} \end{cases} \tag{35}$$

and η_{bw} is defined in conjunction with (24) and (25). The first case of (35) is introduced to ensure that the DOA estimates are real numbers, while the second is introduced to prevent the difference of the two DOA estimates from being unreasonably large. Limiting the difference of the two DOA estimates was found to be critical when correcting the known relative RCS λ for the effects of the antenna gain pattern of the sum channel.

Note that $\tilde{q}$ can be expressed as a function of v_N. Also, note that for a twice differentiable function $g(x)$,

$$E[g(x)] \approx g(\bar{x}) + g''(\bar{x})\sigma_x^2 \tag{36}$$

where $\bar{x} = E[x]$, $\sigma_x^2 = \text{VAR}[x]$, and $g''(\bar{x})$ is the second derivative of $g(x)$ with respect to x evaluated at $x = \bar{x}$. Using (36) with (34) gives approximations of the variances of the DOA estimates for $q \gg \sigma_d^2\sigma_S^{-2}$ as

$$\text{VAR}[\hat{\eta}_1|\Phi] \approx q\left[\frac{1}{2NY_N} + \frac{\lambda q}{\Re_R(2N-1)(q-\sigma_d^2\sigma_S^{-2})}\right] \tag{37}$$

$$\text{VAR}[\hat{\eta}_2|\Phi] \approx q\left[\frac{1}{2NY_N} + \frac{q}{\lambda\Re_R(2N-1)(q-\sigma_d^2\sigma_S^{-2})}\right] \tag{38}$$

Setting $q = \hat{q}$ in (37) and (38) and by analysis of simulation results $q(q - \sigma_d^2 \sigma_S^{-2})^{-1} = 1.5$ was found to provide relatively good estimates of the variances for the DOA estimates, which are given by

$$\hat{\sigma}^2_{\hat{\eta}_1} = \hat{q}\left[\frac{1}{2NY_N} + \frac{1.5\lambda}{\hat{\Re}_R(2N-1)}\right] \tag{39}$$

$$\hat{\sigma}^2_{\hat{\eta}_2} = \hat{q}\left[\frac{1}{2NY_N} + \frac{1.5}{\lambda\hat{\Re}_R(2N-1)}\right] \tag{40}$$

Monte Carlo simulations with 40000 experiments were conducted to study the performance of the DOA estimators for various values of N, $\Delta\eta$, and λ. While the relative RCS of the two targets is assumed to be known, the effect of the antenna gain pattern is not assumed to be included in λ. The effects of the antenna gain pattern were included in the simulation of (1)-(4) by using

$$\tilde{\alpha}_1 = \alpha_1 \cos\left(\frac{\eta_1 \pi}{4\eta_{bw}}\right) \tag{41}$$

$$\tilde{\alpha}_2 = \alpha_2 \cos\left(\frac{\eta_2 \pi}{4\eta_{bw}}\right) \tag{42}$$

for α_1 and α_2, respectively. The effects of the antenna gain pattern were addressed in the DOA estimation by using a modified λ in (34) and (35), which is given by

$$\tilde{\lambda} = \lambda \frac{\cos^4\left(\frac{\tilde{\eta}_2 \pi}{4\eta_{bw}}\right)}{\cos^4\left(\frac{\tilde{\eta}_1 \pi}{4\eta_{bw}}\right)} \tag{43}$$

where $\tilde{\eta}_1$ and $\tilde{\eta}_2$ are the DOA estimates that result from ignoring the effects of the antenna gain pattern. The multiplier modification to λ was restricted to greater than 0.25 and less than 4. Also, during the simulations, only measurements with $NY_N > 20$ dB were utilized in the DOA estimation and $\eta_{bw} = 0.8$, the same value as that used in Section 4.

The effect of N on the DOA estimation was studied using $\Delta\eta = 0.4$ and setting $N\Re_{R1} = N\Re_{R2} = 22$ dB (*i.e.*, without the effects of the antenna pattern). The sample averages of the errors in the DOA estimates for target 1 are shown versus the DOA of target 1 in Figure 5(a). The DOA for target 2 is given by $\eta_2 = \eta_1 - \Delta\eta$. Thus, $\eta_1 = 0$ in Figure 5(a) corresponds to target 1 on the antenna boresight, while $\eta_1 = 0.4$ corresponds to target 2 on the antenna boresight. Figure 5(a) shows that the sample average errors are rather small for each case of N and have the smaller magnitudes when the antenna boresight is pointed between the two

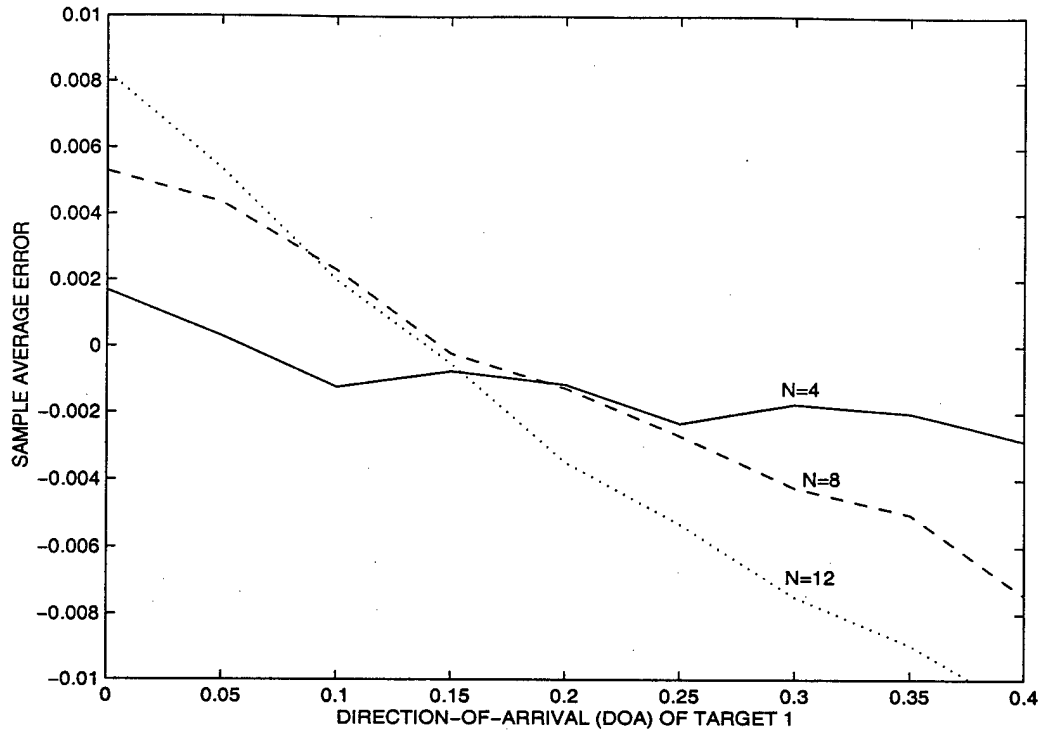

Figure 5(a) Averages of Errors in DOA Estimates of Target 1 for $\Delta\eta = 0.5\eta_{bw}$ and $\lambda = 1$

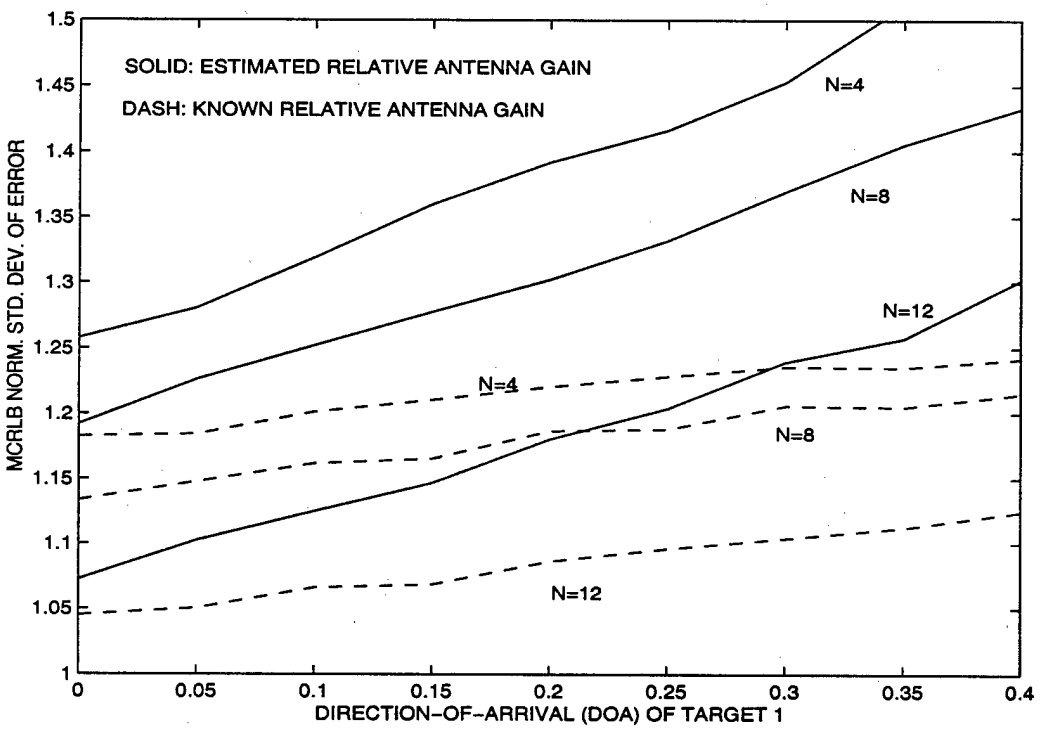

Figure 5(b) Modified CRLB of Target 1 for $\Delta\eta = 0.5\eta_{bw}$ and $\lambda = 1$

targets (*i.e.*, $\eta_1 \approx 0.2$). The sample standard deviations of the errors in the DOA estimates for target 1 normalized by the MCRLB are shown versus the DOA of target 1 in Figure 5(b) by the solid lines. Figure 5(b) shows that the efficiency of the MM estimator improves (*i.e.*, sample variance approaches the MCRLB) as N increases from 4 to 12 and is best when the antenna boresight is pointed at target 1 (*i.e.*, $\eta_1 = 0$). However, the MM estimators are shown to be rather inefficient in Figure 5(b). In order to assess the effects of the estimation of the antenna gain pattern effects on the relative RCS on the efficiency of the MM estimators, the simulation studies were conducted with $\tilde{\lambda}$ as a known quantity rather than an estimated quantity (*i.e.*, the true values of η_1 and η_2 were used in (43)). For $\tilde{\lambda}$ known, the sample standard deviations of the errors in the DOA estimates for target 1 normalized by the MCRLB are shown versus the DOA of target 1 in Figure 5(b) by the dashed lines. Figure 5(b) shows that the efficiency of the MM estimators are degraded rather significantly by the estimation of $\tilde{\lambda}$. Thus, if the two targets are under track, the target state estimates should be used to predict the effects of the antenna gain pattern. Figure 5(b) in conjunction with Figure 3(a) also shows that increasing the number of subpulses at distinct frequencies in a radar pulse improves the accuracy and efficiency of the DOA estimation.

The effect of $\Delta\eta$ on DOA estimation was studied using $N = 8$ and setting $\Re_{R1} = \Re_{R2} = 13$ dB. The averages and standard deviations of the errors in the DOA estimates for target 1 are shown in Figures 6(a) and 6(b) for various DOAs of target 1 and $\Delta\eta = 0.2,\ 0.4,\ 0.6$, and 0.8. The DOA estimation for $\Delta\eta = 0.8$ is significantly degraded when compared to that for $\Delta\eta = 0.2$ or 0.4. Thus, when two targets are separated by about one-half of the one-way beamwidth, sequential DOA estimation with two consecutive dwells at the individual targets will be better than the simultaneous DOA estimation with a single dwell. This observation agrees with those of Section 4.

The effect of λ on DOA estimation was studied using $N = 8$, $\Delta\eta = 0.4$, and $\Re_{R1} = 16$ dB. The sample averages and standard deviations of the errors in the DOA estimates for targets 1 and 2 are shown in Figures 7(a) and 7(b) for the positive DOAs of target 1, the corresponding negative DOAs of target 2, and $\lambda = 1,\ 0.5$, and 0.25 (*i.e.*, $\Re_{R2} = 16,\ 13$, and 10 dB). The $\eta_1 = 0$ in Figures 7(a) and 7(b) corresponds to target 1 on the antenna boresight and $\eta_2 = -0.4$, while $\eta_2 = 0$ corresponds to target 2 on the antenna boresight and $\eta_1 = 0.4$. The accuracy of the DOA estimation for target 1 improves as $\Re_{R2}$ decreases, while accuracy of the DOA estimation for target 2 degrades as $\Re_{R2}$ decreases. The errors were also normalized by the standard deviation estimates of (39) and (40) and the sample standard deviations of those errors are given in Figure 7(c), which indicates that the variances estimates of (39) and (40) are reasonably good. Figure 7(c) also shows that the variance estimates are best for a target at the antenna boresight.

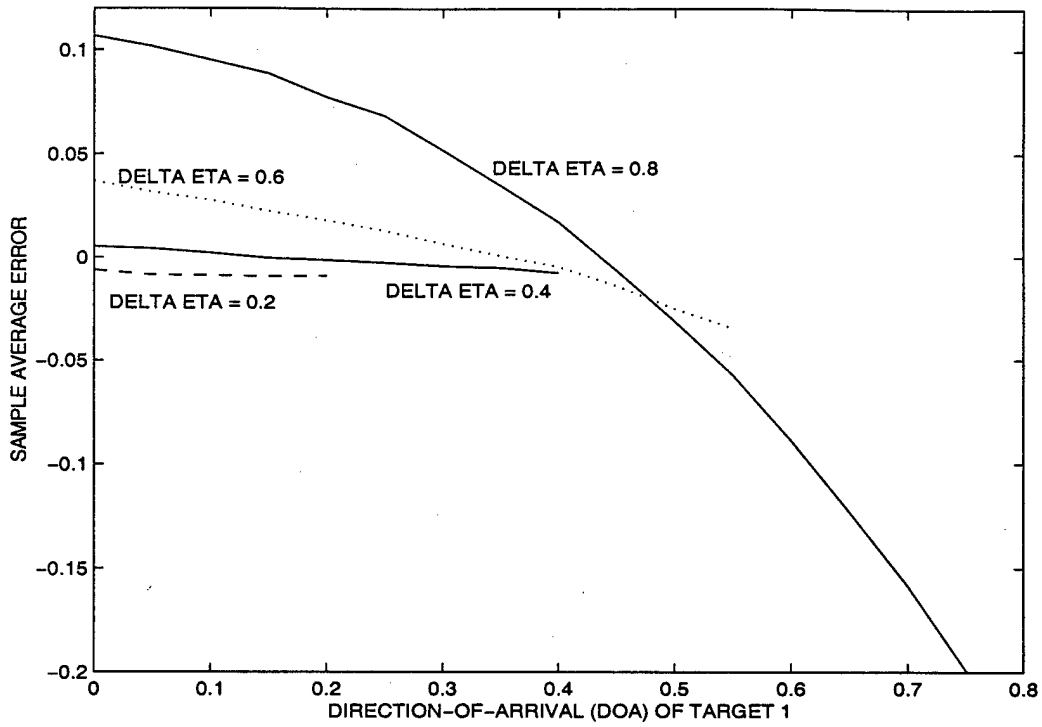

Figure 6(a) Averages of Errors in DOA Estimates of Target 1 for $N = 8$ and $\lambda = 1$

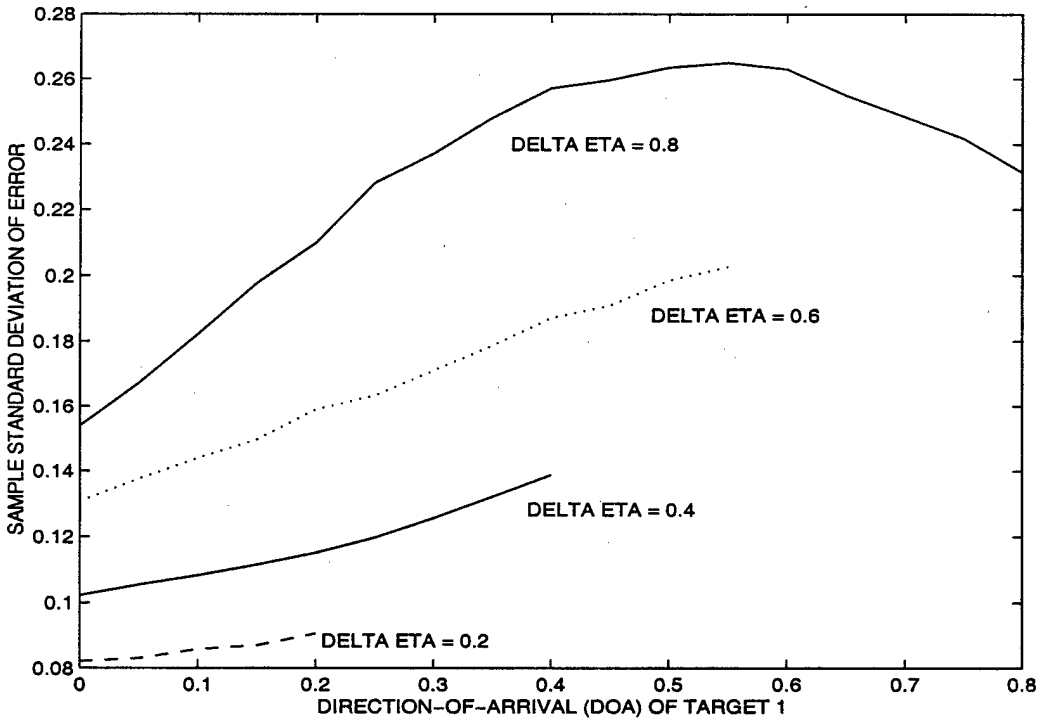

Figure 6(b) Sample Standard Deviations of Errors in DOA Estimates of Target 1 for $N = 8$ and $\lambda = 1$

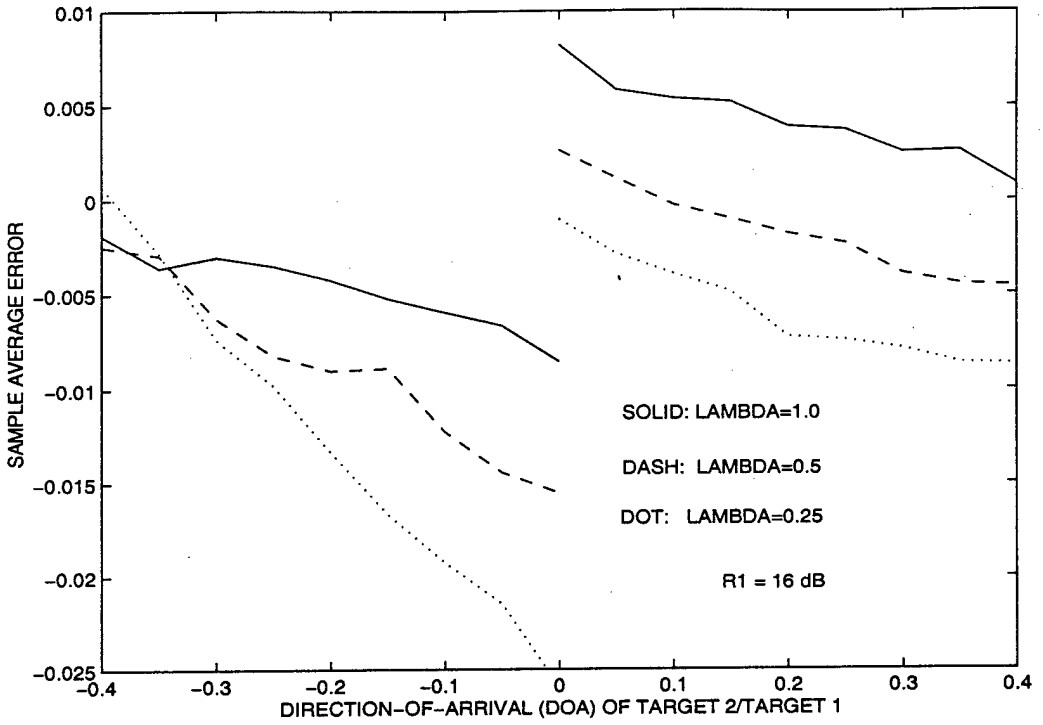

Figure 7(a) Averages of Errors in DOA Estimates for $N = 8$ and $\Delta\eta = 0.5\eta_{bw}$

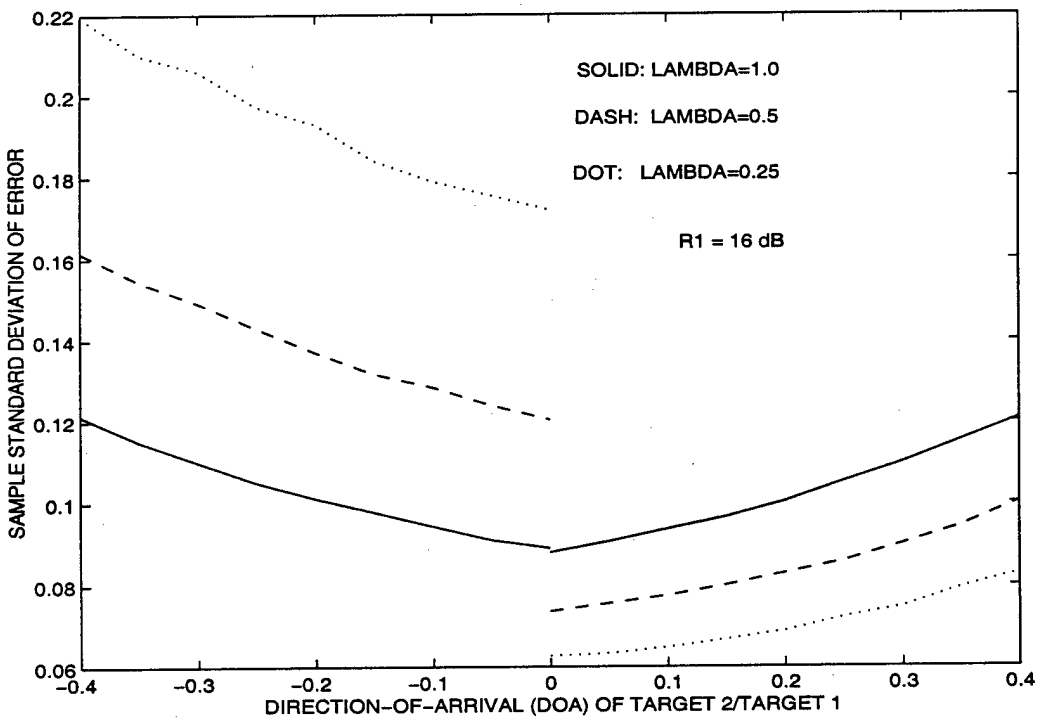

Figure 7(b) Standard Deviations of Errors in DOA Estimates for $N = 8$ and $\Delta\eta = 0.5\eta_{bw}$

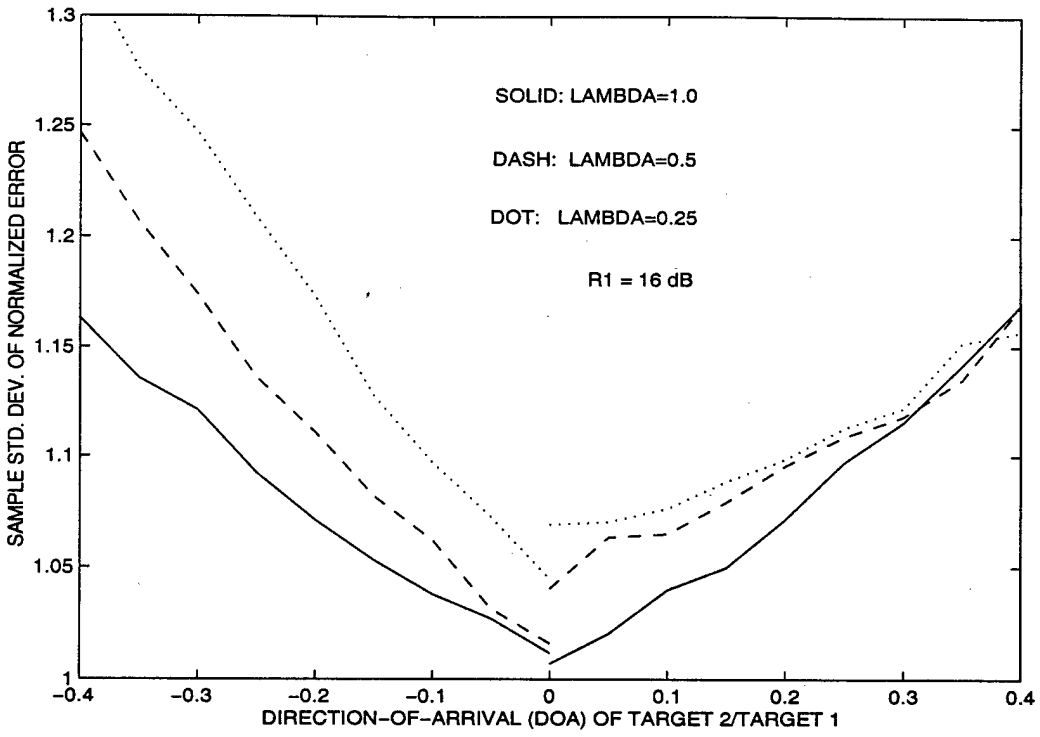

Figure 7(c) Sample Standard Deviations of Errors in DOA Estimates Normalized by the Estimates of Standard Deviations for $N = 8$ and $\Delta\eta = 0.5\eta_{bw}$

6. CONCLUDING REMARKS

The conditional CRLB and modified CRLB were developed for monopulse DOA estimation of two unresolved Rayleigh targets. The MCRLB was used to investigate the effects of frequency diversity and antenna boresight steering on the DOA estimation. For a given waveform energy, the accuracy of the DOA estimation was found to improve as the number of distinct frequencies increases and the expected subpulse energy remains above a few dB. The study revealed two sensor pointing strategies for the DOA estimation: simultaneous and sequential. The simultaneous pointing strategy involves pointing between the targets and estimating both DOAs from data gathered in one dwell, while the sequential pointing strategy involves estimating the DOAs with data gathered from two consecutive dwells, each pointing in the general direction of one target. While the relative performance of the two pointing stategies depend on the SNRs of the two targets and the number of subpulses, the simultaneous pointing strategy was found to be better for targets separated by less than one-half beamwidth, while the sequential pointing strategy was found to be better for targets that are separated by more than one-half of a beamwidth.

An estimation algorithm based on the Method of Moments (MM) was developed for the simultaneous DOA estimation of two unresolved Rayleigh targets with known relative amplitude.

In the DOA estimation, the effects of the antenna gain pattern were treated as unknown and addressed in the DOA estimation with a one-step iteration on the DOA estimates. In other words, the initial DOA estimates obtained by ignoring the effects of the antenna gain were used to predict the effect of the antenna gain on the relative amplitude of the two targets for DOA estimation. The performances of the DOA estimators were studied via Monte Carlo simulations and compared to the MCRLB. The results of the Monte Carlo simulations confirmed the predicted benefits of frequency diversity and showed that frequency diversity also improves the efficiency [15] of the estimators. The results support the use of simultaneous DOA estimation when the targets are separated by less than one-half of a beamwidth and sequential DOA estimation when the targets are separated by more than one-half of a beamwidth. The results also show that the efficiency of the MM estimators are degraded rather significantly by the estimation of the effects of the antenna gain. Thus, if the two targets are under track, the target state estimates should be used to predict the effects of the antenna gain pattern. Furthermore, for tracking closely-spaced targets with merged or unresolved measurements, this paper provides for new approaches to the processing of the unresolved measurements as two DOA measurements rather than the conventional single DOA measurement of the centroid.

REFERENCES

1. F. Daum, "A System Approach to Multiple Target Tracking," in *Multitarget-Multisensor Tracking: Applications and Advances, Vol. II,* edited by Y. Bar-Shalom, Artech House, Inc., Norwood, MA, 1992.
2. Y. Bar-Shalom and X.R. Li, *Multitarget-Multisensor Tracking: Principles and Techniques,* YBS Publishers, Box U-157, Storrs, CT, 06296-3157, 1995.
3. K.C. Chang and Y. Bar-Shalom, "Joint Probabilistic Data Association for Multitarget Tracking with Possibly Unresolved Measurements and Maneuvers," *IEEE Trans. on Auto. Cont.,* July 1984, pp. 585-594.
4. Blackman, S.S., *Multiple-Target Tracking with Radar Applications,* Artech House, Inc., Norwood, MA, 1986.
5. W. Koch and G. Van Keuk, "Multiple Hypothesis Track Maintenance with Possibly Unresolved Measurements," *IEEE Trans. Aero. Elect. Sys.,* July 1997, pp. 883-892.
6. S.M. Sherman, *Monopulse Principles and Techniques,* Artech House, Inc., Dedham, MA, 1984.
7. F. E. Daum, "Angular Estimation Accuracy for Unresolved Targets," *Proc. of 1987 American Control Conference,* Minneapolis, MN, June 1987, pp. 1135-36.
8. W.D. Blair and M. Brandt-Pearce, "Unresolved Rayleigh Target Detection Using Monopulse Measurements," *IEEE Trans. Aero. Elect. Sys.,* April 1998, pp. 543-552.
9. A. A. Ksienski and R. B. McGhee, "A Decision Theoretic Approach to the Angular Resolution and Parameter Estimation Problem for Multiple Targets," *IEEE Trans. Aero. Elect. Sys.,* May 1968, pp. 443-455.
10. S. Haykin, J. Litva, and T.J. Shepherd, Eds., *Radar Array Processing,* Springer-Verlag, New York, NY, 1993.
11. P. Z. Peebles and R. S. Berkowitz, "Multiple-Target Monopulse Radar Processing Techniques," *IEEE Trans. Aero. Elect. Sys.,* Nov. 1968, pp. 845-854.
12. S. M. Sherman, "Complex Indicated Angles Applied To Unresolved Targets and Multipath," *IEEE Trans. Aero. and Elect. Sys.,* Jan. 1971, pp. 160-170.
13. R. S. Berkowitz and S. M. Sherman, "Information Derivable from Monopulse Radar Measurements of Two Unresolved Targets," *IEEE Trans. Aero. and Elect. Sys.,* Sept. 1971, pp. 1011-1013.
14. F. Gini, R. Reggiannini, and U. Mengali, "The Modified Cramer-Rao Bound in Vector Parameter Estimation," *IEEE Trans. on Communications,* vol. 46, No. 1, pp. 52-60, January 1998.
15. H. L., Van Trees, *Detection, Estimation, and Modulation Theory,* John Wiley & Sons, Inc., 1968.
16. W.D. Blair, G.A. Watson, and M. Brandt-Pearce, "Monopulse Tracking of Two Unresolved Rayleigh Targets," *Proceedings of the Signal and Data Processing of Small Targets 1997,* SPIE's International Symposium, San Diego, CA, July 1997.

NNJPDA for Possibly Merged Monopulse Measurements

W. D. Blair
Georgia Tech Research Institute
Georgia Institute of Technology
Atlanta, Georgia 30332-0857
dale.blair@gtri.gatech.edu

Abstract–The Nearest Neighbor Joint Probabilistic Data Association Algorithm (NNJPDA) algorithm is extended to include the possibility of merged monopulse measurements of Rayleigh targets. The monopulse signals are incorporated into the data association as a feature to discriminate between merged and resolved measurements. A summary of monopulse processing and the NNJPDA algorithm is given, along with a technique for predicting the measurement variance of merged monopulse measurements.

I. INTRODUCTION

While the problem of tracking multiple targets has been studied extensively in recent years, the issue of finite sensor resolution has been completely ignored in almost all of the studies [1]. Typically, the targets are assumed to be detected with a given probability of detection in the presence of false alarms and clutter, and the target measurements are modeled as the true values plus independent Gaussian errors [2]. However, when two targets are closely spaced with regard to the resolution of the sensor, the measurements from the two targets can be merged into a single measurement. The Joint Probabilistic Data Association (JPDA) algorithm [2] was extended in [3] to develop the JPDAMM algorithm, which includes possibly merged measurements (*i.e.*, unresolved targets). Multiple hypothesis tracking (MHT) [4] was extended in [5] to include possibly unresolved measurements. Since MHT is a very complex algorithm and is rather computational expensive to implement, the JPDA may be preferred over the MHT for many applications. However, the JPDA can be rather complex when more than two targets are closely-spaced and tracks formed with JPDA on closely-spaced targets often coalesce. A simplified, *ad hoc* technique for approximating the measurement-to-track association probabilities of the JPDA is proposed in [6] and the resulting algorithm is referred to as the "cheap" JPDA. Also in [6], the Nearest Neighbor Joint Probabilistic Data Association (NNJPDA) algorithm is proposed to reduce the complexity and track coalescence of the JPDA. In the NNJPDA, the approximate measurement-to-track association probabilities of the "cheap" JPDA are used to make the assignments of measurements to tracks.

In this paper, the NNJPDA algorithm is extended to include the possibility of merged monopulse [7] measurements of Rayleigh targets to form the NNJPDA for Merged Measurements (NNJPDAMM). The NNJPDA algorithm is extended to accommodate possibly merged measurements by adding a pseudo-track for each collection of tracks that is a candidate for a merged measurement. The predicted states of the targets are used to estimate the variance of the merged monopulse measurement, which is inflated by the presence of unresolved targets. A generalized maximum likelihood ratio test for detecting the presence of unresolved Rayleigh targets with monopulse measurements is developed in [8], and the features of the monopulse signals used in [8] to detect the presence of unresolved Rayleigh targets are also used in the NNJPDAMM to improve the data association.

Section II gives some definitions and background material, while Section III summarizes the NNJPDA algorithm. The NNJPDA algorithm is extended to develop the NNJPDAMM in Section IV. Concluding remarks are given in Section V.

II. DEFINITIONS AND BACKGROUND

Some background on target tracking and monopulse radar systems is given in this section.

A. Dynamical System for Tracking

The dynamics of a target in track is often modeled as

$$X_{k+1} = F_k X_k + G_k V_k \tag{1}$$

with observations

$$Z_k = h_k(X_k) + W_k \tag{2}$$

where X_k is the kinematic state of the target at time k, F_k is the linear constraint on the dynamics, G_k is the input matrix, V_k is the process noise that represents the uncertainty in the dynamical constraint, $h_k(\cdot)$ is a nonlinear function relating the target state to the measurements, and W_k is the sensor error. Both W_k and V_k are typically treated as Gaussian error processes, where $W_k \sim N(0, R_k)$ and $V_k \sim N(0, Q_k)$. The notation $N(\bar{x}, \sigma^2)$ denotes a Gaussian distribution with mean $\bar{x}$ and variance σ^2. Typical radar systems measure the position of targets in polar or spherical coordinates, while the kinematic state of the target is often represented in Cartesian coordinates.

B. Monpulse Radar

Monopulse is a simultaneous lobing technique for determining the angular location of a source of radiation or of a "target" that reflects part of the energy incident upon it [7]. In an amplitude comparison monopulse radar system, a pulse of energy is transmitted directly at the predicted position of the target, and the target echo is received with two beams that are squinted relative to the predicted position of the target (note that two beams are required for each angular coordinate). Traditionally, the angle-of-arrival of a target is estimated with the in-phase part (*i.e.*, the real part) of the monopulse ratio, which is formed by dividing the difference of the two received signals by their sum.

The in-phase and quadrature parts of the sum and difference signals for two unresolved Rayleigh targets can be written as

$$s_I = \alpha_1 \cos\phi_1 + \alpha_2 \cos\phi_2 + n_{SI} \quad (3)$$

$$s_Q = \alpha_1 \sin\phi_1 + \alpha_2 \sin\phi_2 + n_{SQ} \quad (4)$$

$$d_I = \alpha_1\eta_1 \cos\phi_1 + \alpha_2\eta_2 \cos\phi_2 + n_{dI} \quad (5)$$

$$d_Q = \alpha_1\eta_1 \sin\phi_1 + \alpha_2\eta_2 \sin\phi_2 + n_{dQ} \quad (6)$$

where α_i is the Rayleigh distributed amplitude of the received signal from target i, ϕ_i is phase of the received signal from target i, η_i is the direction-of-arrival (DOA) parameter for target i, and

$$n_{SI} \sim N(0,\sigma_S^2) \qquad n_{SQ} \sim N(0,\sigma_S^2)$$
$$n_{dI} \sim N(0,\sigma_d^2) \qquad n_{dQ} \sim N(0,\sigma_d^2)$$

For this paper, n_{SI}, n_{SQ}, n_{dI}, and n_{dQ} are assumed to be independent. In a typical monopulse system, the angle-of-arrival θ is approximated by

$$\theta \approx \frac{\theta_{BW}}{k_m}\eta \quad (7)$$

where $1 < k_m < 2$, and θ_{BW} is the 3-dB beamwidth of the antenna pattern (*i.e.*, the angle between the two one-half power points of the antenna pattern). The linear approximation to the monopulse error function is usually appropriate for $-0.75\theta_{BW} \le \theta \le 0.75\theta_{BW}$.

Letting Λ and ψ denote the measured amplitude and phase of the sum signal gives

$$s_I = \Lambda\cos\psi \qquad s_Q = \Lambda\sin\psi \quad (8)$$

Then the observed signal-to-noise ratio (SNR) will be defined as

$$\Re_o = \frac{\Lambda^2}{2\sigma_S^2} \quad (9)$$

Since α_1 and α_2 are Rayleigh distributed and ϕ_1 and ϕ_2 are uniformly distributed on $(-\pi,\pi]$, s_I and s_Q are Gaussian random variables. Applying the transformation of random variables in (8) to the probability density function (pdf) of s_I and s_Q gives the pdf of the observed SNR as

$$f(\Re_o|\Re) = \frac{1}{\Re+1}\exp\Big[-\frac{\Re_o}{\Re+1}\Big], \qquad \Re_o \ge 0 \quad (10)$$

where $\Re$ is the SNR parameter of the Rayleigh signal given by

$$\Re = \frac{E[\alpha_1^2]}{2\sigma_S^2} + \frac{E[\alpha_2^2]}{2\sigma_S^2} = \Re_1 + \Re_2 \quad (11)$$

where $E[\cdot]$ denotes the expected value. For N subpulses at distinct frequencies (*i.e.*, independent), the maximum likelihood (ML) estimate of $\Re$ is given by

$$\hat{\Re} = Y_N - 1, \qquad Y_N = \frac{1}{N}\sum_{k=1}^{N}\Re_{ok} \quad (12)$$

where $\Re_{ok}$ denotes the observed SNR for subpulse k. Then $\hat{\Re}$ is an unbiased, efficient estimator of $\Re$ with variance given by $\mathrm{VAR}[\hat{\Re}|\Re] = N^{-1}(\Re+1)^2$.

Then the pdf of Y_N is given by

$$f(Y_N|\Re) = \frac{N^N}{(N-1)!}\frac{Y_N^{N-1}}{(\Re+1)^N}\exp\left[-\frac{NY_N}{\Re+1}\right], \; Y_N > 0 \quad (13)$$

which is the Erlang density. The pdf of (13) can be shown to be equivalent to the pdf of NY_N given in [9, p. 404]. Letting $\Re_{th}$ be the detection threshold value for Y_N gives the probability of a false alarm as

$$P_{fa} = \int_{\Re_{th}}^{\infty} f(x|\Re=0)\,dx = \frac{\Gamma(N, N\Re_{th})}{\Gamma(N)} \quad (14)$$

and the probability of detection is given by

$$P_D = \int_{\Re_{th}}^{\infty} f(x|\Re)\,dx = \frac{\Gamma(N, \frac{N\Re_{th}}{\Re+1})}{\Gamma(N)} \quad (15)$$

where $\Gamma(\cdot)$ and $\Gamma(\cdot,\cdot)$ are the Gamma and Incomplete Gamma functions of [10], respectively.

Denoting $s = s_I + js_Q$ and $d = d_I + jd_Q$, the in-phase and quadrature parts of the monopulse ratio are given by

$$y_I = \mathrm{Re}\Big(\frac{d}{s}\Big) = \frac{s_I d_I + s_Q d_Q}{s_I^2 + s_Q^2} \quad (16)$$

$$y_Q = \mathrm{Im}\Big(\frac{d}{s}\Big) = \frac{s_I d_Q - s_Q d_I}{s_I^2 + s_Q^2} \quad (17)$$

Let H_0 denote the hypothesis of no unresolved targets (*i.e.*, Target 1 only), and H_1 denote the hypothesis

of two unresolved targets (*i.e.*, Targets 1 and 2). Then the pdfs of y_I and y_Q for a single pulse are given by

$$f(y_I|H_1,\Re_o) = N\Big(\frac{\Re_1\eta_1+\Re_2\eta_2}{\Re_1+\Re_2+1},\sigma_1^2\Big) \quad (18)$$

$$f(y_Q|H_1,\Re_o) = N\Big(0,\sigma_1^2\Big) \quad (19)$$

where

$$\sigma_1^2 = \frac{q}{2\Re_o} \quad (20)$$

$$q = \Big[\frac{\sigma_d^2}{\sigma_S^2} + \frac{\Re_1\eta_1^2+\Re_2\eta_2^2+\Re_1\Re_2(\eta_1-\eta_2)^2}{\Re_1+\Re_2+1}\Big] \quad (21)$$

with q being introduced for later reference. The y_I and y_Q are conditionally independent, Gaussian random variables with a common variance. The mean of y_I is a "power" weighted average of the DOAs of the two targets, while the mean of y_Q is zero. The pdfs of y_I and y_Q for a single target are given by

$$f(y_I|H_0,\Re_o) = N\Big(\frac{\Re_1}{\Re_1+1}\eta_1,\sigma_0^2\Big) \quad (22)$$

$$f(y_Q|H_0,\Re_o) = N\Big(0,\sigma_0^2\Big) \quad (23)$$

where

$$\sigma_0^2 = \frac{p}{2\Re_o} \quad (24)$$

$$p = \Big[\frac{\sigma_d^2}{\sigma_s^2} + \frac{\Re_1}{\Re_1+1}\eta_1^2\Big] \quad (25)$$

with p being introduced for later reference.

Using N subpulses at distinct frequencies to ensure that the amplitudes of the targets for are independent the subpulses, the ML estimate of $\bar{y}_I$, the mean of y_I given Λ, is given by

$$\hat{y}_I = \Big[\sum_{n=1}^{N}\Re_{on}\Big]^{-1}\sum_{k=1}^{N}\Re_{ok}y_{Ik} = \frac{1}{NY_N}\sum_{k=1}^{N}\Re_{ok}y_{Ik} \quad (26)$$

where $\Re_{ok}$ and y_{Ik} denote the observed SNR and in-phase monopulse ratio for subpulse k and Y_N is given by (12). Since the y_{Ik} are Gaussian random variables, $\hat{y}_I$ is the minimum variance estimate of $\bar{y}_I$ under H_0 and H_1 and a Gaussian random variable with variance under H_0 given by

$$\sigma_{\hat{y}_I}^2 = p\left[\sum_{k=1}^{N}2\Re_{ok}\right]^{-1} = \frac{p}{2NY_N} \quad (27)$$

The variance of $\hat{y}_I$ under H_1 is given by (27) with $p=q$. Typically, $\hat{y}_I$ is taken as the estimate of the DOA parameter, which gives the angle-of-arrival estimate as

$$\hat{\theta} = \frac{\theta_{BW}}{k_m}\hat{y}_I \quad (28)$$

III. NNJPDA Algorithm

When multiple detections occur near the predicted position of a target, a technique for selecting the detection for tracking is required. Nearest Neighbor (NN) and the probabilistic data association filter (PDAF) [2] are two common techniques for addressing this data association problem. In the standard NN data association, the measurement that has the largest likelihood of associating with a target is assigned to the target and used for tracking. In the PDAF, all of the detections are assigned to the target and used for tracking. However, neither the NN nor the PDAF address the problem of data association for closely-spaced targets. The JPDA is an extension of the PDAF to include closely-spaced targets. However, the JPDA is rather complex when more than two targets are closely spaced and tracks formed with the JPDA on closely-spaced targets often coalesce.

The NNJPDA is an *ad hoc* technique for assigning measurements to tracks. One measurement is assigned to one track in the NNJPDA, whereas in the JPDA, multiple measurements can be used to update a track and a measurement can be used to update multiple tracks. In the NNJPDA, simple approximations to the measurement-to-track association probabilities of the JPDA are used as the metric for assigning measurements to tracks. Using the approximate association probabilities, the most probable measurement-to-track association is made and all candidate associations that include either the measurement or the track are removed from consideration. Using the approximate association probabilities of the remaining candidate associations, the new most probable measurement-to-track association is made and all candidate associations that include either the measurement or the track are removed from consideration. This process continues until all measurements have been assigned to tracks or all of the tracks have been assigned to measurements.

The likelihood of association of track i and measurement j at time k is approximated by

$$C_k^{ij} = \frac{1}{\sqrt{|2\pi S_k^{ij}|}} \times \exp\Big[-\frac{1}{2}\big(Z_k^j - h_k(X_k^i)\big)^T(S_k^{ij})^{-1}\big(Z_k^j - h_k(X_k^i)\big)\Big] \quad (29)$$

where S_k^{ij} is the covariance of the measurement residual, $Z_k^j - h_k(X_k^i)$, of track i and measurement j. Let

$$\Sigma_k^{ti} = \sum_{j=1}^{M_k^r} C_k^{ij} \quad (30)$$

$$\Sigma_k^{rj} = \sum_{i=1}^{M_k^t} C_k^{ij} \quad (31)$$

where M_k^r is the number of measurements at time k, and M_k^t is the number of tracks at time k. Then the approximate association probability of track i and measurement

j at time k for the NNJPDA [6] is given by

$$P_k^{ij} = \frac{C_k^{ij}}{\Sigma_k^{ti} + \Sigma_k^{rj} - C_k^{ij} + B} \tag{32}$$

where B is included to account for nonunity probability of detection and the presence of clutter and false alarms.

In the NNJPDA, the measurement-to-track assignment that gives the largest P_k^{ij} is made and all candidate associations that include either measurement j or track i are removed from consideration. Using the remaining candidate associations, the measurement-to-track assignment that gives the new largest P_k^{ij} is made and all candidate associations that include either measurement j or track i are removed from consideration. This process continues until all measurements have been assigned to tracks or all of the tracks have been assigned to measurements.

IV. NNJPDAMM Algorithm

The NNJPDAMM algorithm is an extension of the NNJPDA to include the possibility of merged measurements. The NNJPDAMM is obtained from the NNJPDA by adding a pseudotrack for each pair of tracks that are a potentially unresolved. The monopulse measurements are also included as a feature [8] to improve the data association. While the NNJPDAMM can be extended beyond pairs of unresolved tracks, only pairs are considered in this paper. For the pseudotrack, the means and variances of the monopulse measurements are estimated with (18), while (22) is used for the resolved measurements. The monopulse feature of the merged measurements are included with (18) through (21), while (22) through (25) are used to include the feature of the resolved monopulse measurements. While the NNJPDAMM can be applied to monopulse systems with two angular coordinates, only one angular coordinate is considered in this section. Also, the NNJPDA is modified to allow for targets of different detection probabilities.

For resolved measurement j and resolved track i with probability of detection P_{Di}, let the likelihood of association be approximated by

$$\tilde{C}_k^{ij} = \frac{P_{Di}}{(2\pi\hat{p})^N}\sqrt{\frac{|A_N|}{|2\pi S_k^{ij}|}}\exp\Big[-\frac{1}{2\hat{p}}B_N^T A_N B_N\Big] \tag{33}$$
$$\times \exp\Big[-\frac{1}{2}(Z_k^j - h_k(X_k^i))^T (S_k^{ij})^{-1}(Z_k^j - h_k(X_k^i))\Big]$$

where for $N > 1$,

$$B_N = [\,y_{I1} - \hat{y}_I \quad \cdots \quad y_{IN} - \hat{y}_I \quad y_{Q1} \quad \cdots \quad y_{QN}\,]^T \tag{34}$$

$$A_N = 2\,\mathrm{diag}[\,\Re_{o1} \quad \cdots \quad \Re_{oN} \quad \Re_{o1} \quad \cdots \quad \Re_{oN}\,] \tag{35}$$

$$\hat{p} = \frac{\sigma_d^2}{\sigma_S^2} + \hat{y}_I^2 \tag{36}$$

and for $N = 1$, $X_1 = y_{Q1}$ and $R_1 = 2\Re_{o1}$. The y_{Im} and y_{Qm} are the in-phase and quadrature monopulse ratios for pulse m, while $\Re_{om}$ is the observed SNR of (9) for pulse m. The variance of the monopulse angle measurement for S_k^{ij} is given by

$$\hat{\sigma}_\theta^2 = \frac{\theta_{bw}^2}{k_m^2}\sigma_{\hat{y}_I}^2 = \frac{\hat{p}\theta_{bw}^2}{2k_m^2 N Y_N} \tag{37}$$

Note that all of the monopulse measurements and parameters in (34) through (37) correspond to measurement j.

For potentially merged measurement j and potentially unresolved track i composed of tracks l and n, let the likelihood of association be approximated by

$$\tilde{C}_k^{ij} = \frac{P_{Di}}{(2\pi q)^N}\sqrt{\frac{|A_N|}{|2\pi S_k^{ij}|}}\exp\Big[-\frac{1}{2\hat{q}}B_N^T A_N B_N\Big] \tag{38}$$
$$\times \exp\Big[-\frac{1}{2}(Z_k^j - \bar{h}_k(X_k^l, X_k^n))^T (S_k^{ij})^{-1}(Z_k^j - \bar{h}_k(X_k^l, X_k^n))\Big]$$

where $\bar{h}_k(X_k^i, X_k^l)$ is the predicted measurement of the unresolved track and

$$\hat{q} = \frac{\sigma_d^2}{\sigma_S^2} + \frac{\hat{\Re}_l\hat{\eta}_l^2 + \hat{\Re}_n\hat{\eta}_n^2 + \hat{\Re}_l\hat{\Re}_n(\hat{\eta}_l - \hat{\eta}_n)^2}{\hat{\Re}_l + \hat{\Re}_n + 1} \tag{39}$$

with $\hat{\Re}_n$ denoting the predicted SNR of target n and η_n denoting the predicted DOA parameter for target n. The predicted probability of detection of the unresolved track i is given by (15) with $\Re = \hat{\Re}_l + \hat{\Re}_n$. The variance of the monopulse angle measurement for S_k^{ij} is estimated by

$$\hat{\sigma}_\theta^2 = \frac{\theta_{bw}^2}{k_m^2}\sigma_{\hat{y}_I}^2 = \frac{\hat{q}\theta_{bw}^2}{2k_m^2 N Y_N} \tag{40}$$

Note that all of the monopulse measurements and parameters in (38) through (40) correspond to measurement j as a merged measurement of tracks l and n.

Let

$$\tilde{\Sigma}_k^{rj} = \sum_{i=1}^{M_k^t + M_k^{mt}} \tilde{C}_k^{ij} \tag{41}$$

$$\tilde{\Sigma}_k^{ti} = \sum_{j=1}^{M_k^r} \tilde{C}_k^{ij} \tag{42}$$

where M_k^t is the number of tracks, M_k^{mt} is the number of potentially merged tracks at time k. Then for measurement j and (resolved or unresolved) track i, let the association probabilities of the NNJPDAMM be approximated by

$$\tilde{P}_k^{ij} = \frac{\tilde{C}_k^{ij}}{\tilde{\Sigma}_k^{tj} + \tilde{\Sigma}_k^{ri} - \tilde{C}_k^{ij} + B_k^i} \tag{43}$$

where B_k^i is included to account for nonunity probability of detection of track i and the presence of clutter and false alarms. Then

$$B_k^i = M_k^r \frac{1 - P_{Di} P_G}{V_k} \tag{44}$$

where V_k is the volume of the gating region and P_G is the probabilty of gating the target.

In order to include the possibility of a missed detection, let $j = 0$ denote the case of no measurement

$$\tilde{P}_k^{i0} = \frac{B_k^i}{\tilde{\Sigma}_k^{ri} + B_k^i} \tag{45}$$

In the NNJPDAMM, the measurement-to-track assignment that gives the largest P_k^{ij} is made and all candidate associations that include either measurement j or track i are removed from consideration. If track i is an an unresolved track composed of track l and track n, then both tracks l and n are removed as candidates for measurement-to-track assignment. Using the remaining candidate associations, the measurement-to-track assignment that gives the new largest P_k^{ij} is made and all candidate associations that include either measurement j or track i are removed from consideration. This process continues until all all of the tracks have been assigned to a measurement or a missed detection.

V. CONCLUDING REMARKS

Simulation studies are planned to assess the performance of the NNJPDAMM algorithm and compare its performance with that of the standard JPDAMM algorithm in [2]. The monopulse features and measurements statistics will be added to the JPDAMM prior to that comparison. Also, a computer simulation of a phased array radar will be used to compare the performances of the JPDAMM and NNJPDAMM and study the effects of both algorithms on the radar resources required for tracking closely-spaced targets.

A pseudotrack was introduced for potentially unresolved tracks to extend the NNJPDA algorithm to include the possibility of merged monopulse measurements. While the NNJPDAMM algorithm was restricted to pairs of unresolved tracks, the pseudotrack concept is extendable to multiple unresolved tracks. The pseudotrack concept can be used to extend other measurement-to-track assignment techniques such as those in [2] to include merged measurements. The statistics of the merged monopulse measurements and the features of the monopulse measurements used in the NNJPDAMM algorithm can also be used to improved the performance of the JPDAMM in [2].

While the data association for possibly merged monopulse measurements is addressed with the NNJPDAMM, the track filtering with merged monopulse measurements is not part of the NNJPDAMM. In the track filtering, a merged measurement can be treated as a single merged measurement to simultaneously update both tracks as in the JPDAM [2]. On the other hand, the merged monopulse measurements of two unresolved tracks can be used as in [12] to generate two separate measurements for updating the two tracks.

The extension of the NNJPDAMM algorithm to two angular coordinates will be complicated by the fact that the monopulse features may indicate a merged measurement in one angular coordinate and a resolved measurement in the other coordinate. Also, using the technique in [12] for the track filtering with monopulse measurements in two coordinates will be complicated by an ambiguity in the angular position of the two measurements.

REFERENCES

1. F. Daum, "A System Approach to Multiple Target Tracking," in *Multitarget-Multisensor Tracking: Applications and Advances, Vol. II,* edited by Y. Bar-Shalom, Artech House, Inc., Norwood, MA, 1992.
2. Y. Bar-Shalom and X.R. Li, *Multitarget-Multisensor Tracking: Principles and Techniques,* YBS Publishers, Box U-157, Storrs, CT, 06296-3157, 1995.
3. K.C. Chang and Y. Bar-Shalom, "Joint Probabilistic Data Association for Multitarget Tracking with Possibly Unresolved Measurements and Maneuvers," *IEEE Trans. on Auto. Cont.,* July 1984, pp. 585-594.
4. S.S. Blackman, *Multiple-Target Tracking with Radar Applications,* ARTECH House, Inc., Norwood, MA, 1986.
5. W. Koch and G. Van Keuk, "Multiple Hypothesis Track Maintenance with Possibly Unresolved Measurements," *IEEE Trans. Aero. Elect. Sys.,* July 1997, pp. 883-892.
6. R.J. Fitzgerald, "Development of Practical PDA Logic for Multitarget Tracking by Microprocessor," in *Multitarget/Multisensor Tracking: Applications and Advances, Vol. I,* edited by Y. Bar-Shalom, Artech House, Inc., Norwood, MA, 1990.
7. S.M. Sherman, *Monopulse Principles and Techniques,* Artech House, Inc., Dedham, MA, 1984.
8. W.D. Blair and M. Brandt-Pearce, "Unresolved Rayleigh Target Detection Using Monopulse Measurements," *IEEE Trans. Aero. Elect. Sys.,* April 1998, pp. 543-552.
9. J.V. DiFranco and W.L. Rubin, *Radar Detection,* Artech House, Inc. Dedham, MA, 1980.
10. M. Abramowitz and I.A. Stegun, Ed., *Handbook of Mathematical Functions, with Formulas, Graphs, and Mathematical Tables,* U.S. Government Printing Office, Washington, DC, 1972, and John Wiley & Sons, Inc. 1972.
11. H. Van Trees, *Detection, Estimation, and Modulation Theory: Part I,* John Wiley & Sons, New York, NY, 1968.
12. W.D. Blair and M. Brandt-Pearce, "Monopulse DOA Estimation for Two Unresolved Rayleigh Targets," submitted to *IEEE Trans. Aero. Elect. Sys.,* Dec 1998.

NNJPDA for Tracking Closely-Spaced Rayleigh Targets With Possibly Merged Measurements*

W.D. Blair
Georgia Tech Research Institute
Georgia Institute of Technology
Atlanta, Georgia 30332-0857

M. Brandt-Pearce
Dept. of Electrical Engineering
University of Virginia
Charlottesville, Virginia 22903

ABSTRACT

The measurements of the two closely-spaced targets will be merged when the target echoes are not resolved in angle, range, or radial velocity (*i.e.*, Doppler processing). The modified Cramer Rao lower bound (CRLB) is given for monopulse direction-of-arrival (DOA) estimation for two unresolved Rayleigh targets and used to give insight into the antenna boresight pointing. A monopulse processing technique is given for DOA estimation of two unresolved Rayleigh targets. The Nearest Neighbor Joint Probabilistic Data Association Algorithm (NNJPDA) algorithm is extended to include the possibility of merged monopulse measurements of Rayleigh targets. The monopulse signals are incorporated into the data association as a feature to discriminate between merged and resolved measurements.

Keywords: Unresolved Objects, Target Tracking, Data Association, Radar Signal Processing

1. INTRODUCTION

While the problem of tracking multiple targets has been studied extensively in recent years, the issue of finite sensor resolution has been completely ignored in almost all studies [1]. Typically, the targets are assumed to be detected with a given probability of detection in the presence of false alarms and clutter, and the target measurements are modeled as the true values plus independent Gaussian errors [2]. However, when two targets are closely spaced with regard to the resolution of the sensor, the measurements from the two targets can be merged into a single measurement. In a monopulse radar, the direction-of-arrival (DOA) estimate computed from merged measurements (*i.e.*, the echoes are not resolved in the frequency or time domains) can wander far beyond the angular separation of the targets [3,4]. The failure to detect the presence of this interference can be catastrophic to the performance of the tracking algorithm, since its position and velocity estimates determine the association of any subsequent measurements to the target.

A generalized likelihood ratio test for detecting the presence of unresolved Rayleigh targets is developed in [5]. While the test in [5] helps to prevent castastrophic track loss through data rejection, it does not take advantage of the information available in the merged data, which may be problematic if the targets are unresolved for several consecutive dwells. In [6], the information in the merged measurements is exploited to form DOA estimates for both targets. In this paper, the detection algorithm of [5] and the DOA estimation algorithm of [6] are utilized to develop a technique for tracking closely-spaced Rayleigh targets with possibly merged measurements.

The Joint Probabilistic Data Association (JPDA) algorithm [3] was extended in [7] to develop the JPDAM algorithm, which includes possibly merged measurements. Multiple Hypothesis Tracking (MHT) [8] was extended in [9] to include possibly unresolved measurements. In the JPDAM algorithm and MHT approach, merged measurements are modeled as a "power" weighted centroid of the two targets. Since MHT is a very complex algorithm and is rather computationally expensive to implement, the JPDA may be preferred over the MHT for many applications. However, the JPDA can be rather complex when more than two targets are closely-spaced and tracks formed with JPDA on closely-spaced targets often coalesce. A simplified, *ad hoc* technique for approximating the measurement-to-track association probabilities of the JPDA is presented in [10] and the resulting algorithm is re-

* This work accomplished through funding from the Office of Naval Research, Arlington, VA through contract N00014-99-1-0084.

ferred to as the "cheap" JPDA. Also in [10], the Nearest Neighbor Joint Probabilistic Data Association (NNJPDA) algorithm is presented to reduce the complexity and track coalescence of the JPDA. In the NNJPDA, the approximate measurement-to-track association probabilities of the "cheap" JPDA are used to make the assignments of measurements to tracks.

In [11], the results of [5] were utilized to extend the NNJPDA to accommodate the possibility of merged measurements. In this paper, the results of [11] and [6] are incorporated to address the tracking of closely-spaced Rayleigh target with possibly merged measurements. Using the results in [6], DOA estimates for both targets are used in tracking rather than relying in the centroid measurement used in the JPDAM. The use of two DOA estimates is critical for the tracking of two aircraft flying in formation or separating ballistic missiles, where the flight paths result in the targets being unresolved for more than a couple of dwells.

Some background material and notation are given in Section 2, while the probability distribution of the monopulse measurements for two unresolved Rayleigh targets is given in Section 3. In Section 4, the Modified Cramer Rao Lower Bounds (MCRLBs) [12] are presented for the DOA estimation of two unresolved Rayleigh targets and used to study the effects of antenna boresight pointing on the DOA estimation. The DOA estimator for the case of two unresolved targets is derived in Section 5. The extension of the NNJPDA to include possibly merged measurements in [11] is given in Section 6 along with a discussion of the interface with the track filter. Concluding remarks are given in Section 7.

2. DEFINITIONS AND BACKGROUND

Some background on target tracking and monopulse radar systems is given in this section.

2.1. Dynamical System for Tracking

The dynamics of a target in track is often modeled as

$$X_{k+1} = F_k X_k + G_k V_k \tag{1}$$

with observations

$$Z_k = h_k(X_k) + W_k \tag{2}$$

where X_k is the kinematic state of the target at time k, F_k is the linear constraint on the dynamics, G_k is the input matrix, V_k is the process noise that represents the uncertainty in the dynamical constraint, $h_k(\cdot)$ is a nonlinear function relating the target state to the measurements, and W_k is the sensor error. Both W_k and V_k are typically treated as Gaussian error processes, where $W_k \sim N(0, R_k)$ and $V_k \sim N(0, Q_k)$. The notation $N(\bar{X}, P)$ denotes a Gaussian distribution with mean $\bar{X}$ and covariance P. Typical radar systems measure the position of targets in polar or spherical coordinates, while the kinematic state of the target is often represented in Cartesian coordinates.

2.2. Monpulse Radar

The in-phase and quadrature parts of the sum and difference signals for two unresolved Rayleigh targets can be written as

$$s_I = \alpha_1 \cos\phi_1 + \alpha_2 \cos\phi_2 + n_{SI} \qquad s_Q = \alpha_1 \sin\phi_1 + \alpha_2 \sin\phi_2 + n_{SQ} \tag{3}$$

$$d_I = \alpha_1\eta_1 \cos\phi_1 + \alpha_2\eta_2 \cos\phi_2 + n_{dI} \qquad d_Q = \alpha_1\eta_1 \sin\phi_1 + \alpha_2\eta_2 \sin\phi_2 + n_{dQ} \tag{4}$$

where α_i is the Rayleigh distributed amplitude of the received signal from target i, ϕ_i is phase of the received signal from target i, η_i is the DOA parameter for target i, and

$$n_{SI} \sim N(0, \sigma_S^2) \qquad n_{SQ} \sim N(0, \sigma_S^2) \qquad n_{dI} \sim N(0, \sigma_d^2) \qquad n_{dQ} \sim N(0, \sigma_d^2)$$

For this paper, the errors n_{SI}, n_{SQ}, n_{dI}, and n_{dQ}, are assumed to be independent. The DOA parameter is given by

$$\eta_i = \frac{G_\Delta(\theta_i)}{G_\Sigma(\theta_i)} \approx \frac{k_m}{\theta_{bw}}\theta_i \tag{5}$$

where θ_i is the off-boresight angle of target i, $G_\Delta(\theta_i)$ is the difference channel voltage gain at θ_i, $G_\Sigma(\theta_i)$ is the sum channel voltage gain at θ_i, k_m is the monopulse error slope in units of beamwidths, and θ_{bw} is the one-half beamwidth of the sum-channel antenna pattern. For $|\theta_i| < \theta_{bw}$, the linear approximation of the relationship between η_i and θ_i is rather accurate.

Letting Λ and ψ denote the measured amplitude and phase of the sum signal gives

$$s_I = \Lambda \cos \psi \qquad s_Q = \Lambda \sin \psi \tag{6}$$

Then the observed SNR will be defined as

$$\Re_o = \frac{\Lambda^2}{2\sigma_S^2} \tag{7}$$

Since α_1 and α_2 are Rayleigh distributed and ϕ_1 and ϕ_2 are uniformly distributed on $(-\pi, \pi]$, s_I and s_Q are Gaussian random variables. Applying the transformation of random variables in (6) to the pdf of s_I and s_Q gives the pdf of the observed SNR as

$$f(\Re_o|\Re_R) = \frac{1}{\Re_R + 1} \exp\Big[- \frac{\Re_o}{\Re_R + 1}\Big], \qquad \Re_o \geq 0 \tag{8}$$

where $\Re_R$ is the SNR parameter of the Rayleigh signal given by

$$\Re_R = \frac{E[\alpha_1^2]}{2\sigma_S^2} + \frac{E[\alpha_2^2]}{2\sigma_S^2} = \Re_{R1} + \Re_{R2} \tag{9}$$

where $E[\cdot]$ denotes the expected value. Since the relative RCS of the targets is assumed to be known from the track filter, let $\Re_{R2} = \lambda \Re_{R1}$, $\lambda > 0$. Then $\Re_R = (1 + \lambda)\Re_{R1}$. For N subpulses at distinct frequencies (*i.e.*, independent), the Maximum Likelihood (ML) estimate of $\Re_R$ is given by

$$\widehat{\Re}_R = Y_N - 1, \qquad Y_N = \frac{1}{N} \sum_{k=1}^{N} \Re_{ok} \tag{10}$$

where $\Re_{ok}$ denotes the observed SNR for subpulse k. Then $\widehat{\Re}_R$ is an unbiased, efficient estimator of $\Re_R$ with variance given by $\mathrm{VAR}[\widehat{\Re}_R|\Re_R] = N^{-1}(\Re_R + 1)^2$. Note that the detection threshold is assumed to be sufficently high so that the case of $Y_N < 1.0$ need not be considered. Also, if the RCS of a target is tracked or estimated over multiple dwells, $\widehat{\Re}_R$ should be modified on each dwell to account for beam pointing losses and changes in the waveform.

Then the pdf of Y_N is given by

$$f(Y_N|\Re_R) = \frac{N^N}{(N-1)!} \frac{Y_N^{N-1}}{(\Re_R + 1)^N} \exp\left[- \frac{NY_N}{\Re_R + 1} \right], \; Y_N > 0 \tag{11}$$

which is the Erlang density. The pdf of (11) can be shown to be equivalent to the pdf of NY_N given in [13, p. 404]. Letting $\Re_{th}$ be the detection threshold value for Y_N gives the probabilities of a false alarm and detection as

$$P_{fa} = \int_{\Re_{th}}^{\infty} f(x|\Re_R = 0)\, dx = \frac{\Gamma(N, N\Re_{th})}{\Gamma(N)} \qquad P_D = \int_{\Re_{th}}^{\infty} f(x|\Re_R)\, dx = \frac{\Gamma(N, \frac{N\Re_{th}}{\Re_R + 1})}{\Gamma(N)} \tag{12}$$

where $\Gamma(\cdot)$ and $\Gamma(\cdot, \cdot)$ are the Gamma and Incomplete Gamma functions of [14], respectively.

Denoting $s = s_I + j s_Q$ and $d = d_I + j d_Q$, the in-phase and quadrature parts of the monopulse ratio are given by

$$y_I = \mathrm{Re}\big(\frac{d}{s}\big) = \frac{s_I d_I + s_Q d_Q}{s_I^2 + s_Q^2} \qquad y_Q = \mathrm{Im}\big(\frac{d}{s}\big) = \frac{s_I d_Q - s_Q d_I}{s_I^2 + s_Q^2} \tag{13}$$

In conventional monopulse systems, the angle-of-arrival estimate for a target i that is resolved is obtained by

$$\hat{\theta}_i = \frac{\theta_{bw}}{k_m} y_I \tag{14}$$

3. STATISTICS OF THE MONOPULSE RATIOS

The pdf of the monopulse ratios, y_I and y_Q, for a single pulse can be obtained by application of the transformation of random variables in (5) and (13) to $f(s_I, s_Q, d_I, d_Q|\Phi)$, where Φ denotes the parameter set $\{\Re_{R1}, \Re_{R2}, \eta_1, \eta_2, \sigma_S, \sigma_d\}$. Integrating the result with respect to ψ and conditioning the density on Λ in the form of $\Re_o$ gives

$$f(y_I, y_Q|\Re_o, \Phi) = f(y_I|\Re_o, \Phi) f(y_Q|\Re_o, \Phi) \tag{15}$$

where

$$f(y_I|\Re_o, \Phi) = N\Big(\frac{\Re_{R1}\eta_1 + \Re_{R2}\eta_2}{\Re_{R1} + \Re_{R2} + 1}, \frac{q}{2\Re_o}\Big) \qquad f(y_Q|\Re_o, \Phi) = N\Big(0, \frac{q}{2\Re_o}\Big) \tag{16}$$

$$q = \Big[\frac{\sigma_d^2}{\sigma_S^2} + \frac{\Re_{R1}\eta_1^2 + \Re_{R2}\eta_2^2 + \Re_{R1}\Re_{R2}(\eta_1 - \eta_2)^2}{\Re_{R1} + \Re_{R2} + 1}\Big] \tag{17}$$

Thus, y_I and y_Q are conditionally independent, Gaussian random variables with a common variance. The mean of y_I is a "power" weighted average of the DOAs of the two targets, while the mean of y_Q is zero. The pdf of the monopulse ratios, y_I and y_Q, for a single pulse of a resolved target is given by setting $\Re_{R2} = 0$ in (16) and (17).

Using N subpulses at distinct frequencies to ensure that the targets' amplitudes are independent for each subpulse, the ML estimate of $\bar{y}_I$, the mean of y_I given Λ, is given by

$$\hat{y}_I = \Big[\sum_{n=1}^{N} \Re_{on}\Big]^{-1} \sum_{k=1}^{N} \Re_{ok} y_{Ik} = \frac{1}{NY_N} \sum_{k=1}^{N} \Re_{ok} y_{Ik} \tag{18}$$

where $\Re_{ok}$ and y_{Ik} denote the observed SNR and in-phase monopulse ratio for subpulse k and Y_N is given by (10). Since the y_{Ik} are Gaussian random variables, $\hat{y}_I$ is the minimum variance estimate of $\bar{y}_I$ and a Gaussian random variable with variance given by

$$\sigma_{\hat{y}_I}^2 = q\Big[\sum_{k=1}^{N} 2\Re_{ok}\Big]^{-1} = \frac{q}{2NY_N} \tag{19}$$

Since the y_{Ik} are Gaussian, $\sigma_{\hat{y}_I}^2$ is the conditional CRLB for $\bar{y}_I$ given $\{\Re_{ok}\}_{k=1}^N$. The term conditional here is used to denote the fact that the Fisher information and CRLB are developed with the amplitude-conditioned pdf. While $\sigma_{\hat{y}_I}^2$ provides the variance of $\hat{y}_I$ for real-time or actual tracking, $\sigma_{\hat{y}_I}^2$ cannot be used for performance prediction because it is a function of $\{\Re_{ok}\}_{k=1}^N$, which are measured quantities. The MCRLB [12] is obtained by averaging the conditional Fisher information with respect to the measured amplitudes of the received pulses. While the MCRLB is a somewhat looser bound than the CRLB, it can be used for performance prediction. Since $f(y_I|\Re_o, \Phi)$ satisfies the regularity conditions with respect to $\bar{y}_I$ [14], the MCRLB is a lower bound on the variance of any unbiased estimator of $\bar{y}_I$. The MCRLB of $\bar{y}_I$ is given by

$$\tilde{J}_{y_I}(\bar{y}_I|N, \Phi) = E\big[\sigma_{\hat{y}_I}^{-2}|N, \Phi\big]^{-1} = \frac{q}{2N(\Re_{R1} + \Re_{R2} + 1)} \tag{20}$$

Figure 1 gives a comparison of the MCRLBs of $\bar{y}_I$ for a single target and two unresolved, equal-amplitude targets versus the total SNR in a single frequency (*i.e.*, $N = 1$). The MCRLB of $\bar{y}_I$ for a single target is obtained by setting $\Re_{R2} = 0$ in (17) and (20). For the two-target case, the total SNR is given by $\Re_{R1} + \Re_{R2} = 2\Re_{R1}$. In order

to obtain $\bar{y}_I = 0$ in both cases, the single target was set at the boresight, and the two targets were situated symmetrically about the boresight (*i.e.*, $\eta_1 = -\eta_2$) and separated by one-half of a beamwidth with $\eta_1 = 0.4$. Figure 1 shows that a total SNR of 14 dB gives a MCRLB of 0.02 for the single-target case and 0.095 for the two-target case. Figure 1 also shows that doubling the energy in a single-frequency waveform to obtain a total SNR of 17 dB gives a MCRLB of 0.01 for the single-target case and 0.09 for the two-target case. Thus, doubling the energy in a single-frequency pulse gives only a small reduction in the MCRLB for the two-target case. However, if the energy in the pulse was doubled and a second frequency is added so that two independent observations of the unresolved targets is obtained, the variance would be reduced by 50 percent because the errors are Gaussian (not shown in figure). Therefore, frequency agility is critical to improving the monopulse angle estimation when two unresolved targets are present.

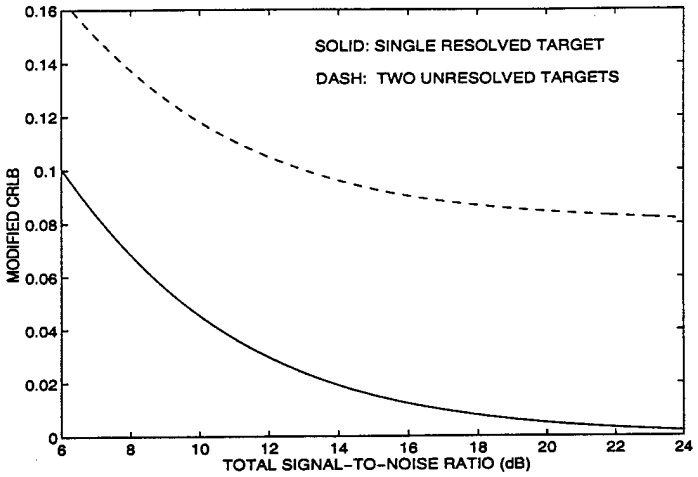

Figure 1. MCRLBs of $\bar{y}_I$ for a single pulse and single target at the boresight and two targets separated by one-half beamwidth and symmetric about the boresight

4. MODIFIED CRLBS FOR DOA ESTIMATION

The MCRLBs associated with η_1 and η_2 are given and used to study the effects of antenna pointing on the DOA estimation. In [6], the MCRBs of η_1 and η_2 were derived with the pdfs of (16) by averaging over the observed SNR yielding

$$\tilde{J}_{y_I,y_Q}(\eta_1,\eta_2|N,\Phi) = \frac{q^2}{4N\Re_{R1}\Re_{R2}\Delta\eta^2}\begin{bmatrix} \frac{\Re_{R2}}{\Re_{R1}}\Big[1+\frac{2(\eta_2-\Re_{R1}\Delta\eta)^2}{q(\Re_{R1}+\Re_{R2}+1)}\Big] & -1-\frac{2(\eta_1+\Re_{R2}\Delta\eta)(\eta_2-\Re_{R1}\Delta\eta)}{q(\Re_{R1}+\Re_{R2}+1)} \\ -1-\frac{2(\eta_1+\Re_{R2}\Delta\eta)(\eta_2-\Re_{R1}\Delta\eta)}{q(\Re_{R1}+\Re_{R2}+1)} & \frac{\Re_{R1}}{\Re_{R2}}\Big[1+\frac{2(\eta_1+\Re_{R2}\Delta\eta)^2}{q(\Re_{R1}+\Re_{R2}+1)}\Big] \end{bmatrix} \tag{21}$$

The diagonal elements of $\tilde{J}_{y_I,y_Q}(\eta_1,\eta_2|N,\Phi)$ give the MCRLBs for $\hat{\eta}_1$ and $\hat{\eta}_2$.

The MCRLB of (21) can be used to study the effects of sensor pointing on the DOA estimation. For this study, the effects of the antenna gain pattern are not assumed to be included in λ, the relative RCS of the two targets. The effects of the antenna gain pattern can instead be included in the anaylsis of the MCRLB by using

$$\tilde{\Re}_{R1} = \Re_{R1}\cos^4\Big(\frac{\eta_1\pi}{4\eta_{bw}}\Big) \qquad \tilde{\Re}_{R2} = \Re_{R2}\cos^4\Big(\frac{\eta_2\pi}{4\eta_{bw}}\Big) \tag{22}$$

in (21) for $\Re_{R1}$ and $\Re_{R2}$, respectively. The η_{bw} denotes the DOA value at the one-way, half-power point on the antenna gain pattern of the sum channel. Thus, at $\eta_1 = \eta_{bw}$, $\tilde{\Re}_{R1} = \Re_{R1} - 6$ dB. For a monopulse error slope k_m in beamwidths, $2\eta_{bw} \approx k_m$. For all of the examples in this paper, $\eta_{bw} = 0.8$.

Figure 2(a) shows the average MCRLB for two 19 dB targets (*i.e.*, $\Re_{R1} = \Re_{R2} = 19$ dB in (22) for $N = 1$) separated by one-half beamwidth (*i.e.*, $\Delta\eta = \eta_{bw} = 0.8$) versus the DOA of target 1, η_1, for $N = 1$, 2, 4, 8 and 16 subpulses. The average MCRLB is the average of the two diagonal elements of (21). For each case in Figure 2(a), the energy in the transmitted pulse is fixed and it is divided into N subpulses at different frequencies. Thus, for $N = 8$ subpulses, $\Re_{R1} = \Re_{R2} = 10$ dB in (22). The DOA for target 2 is given by $\eta_2 = \eta_1 - \Delta\eta$. Thus, $\eta_1 = 0$ in Figure 2(a) corresponds to target 1 on the antenna boresight, while $\eta_1 = 0.8$ corresponds to target 2 on the

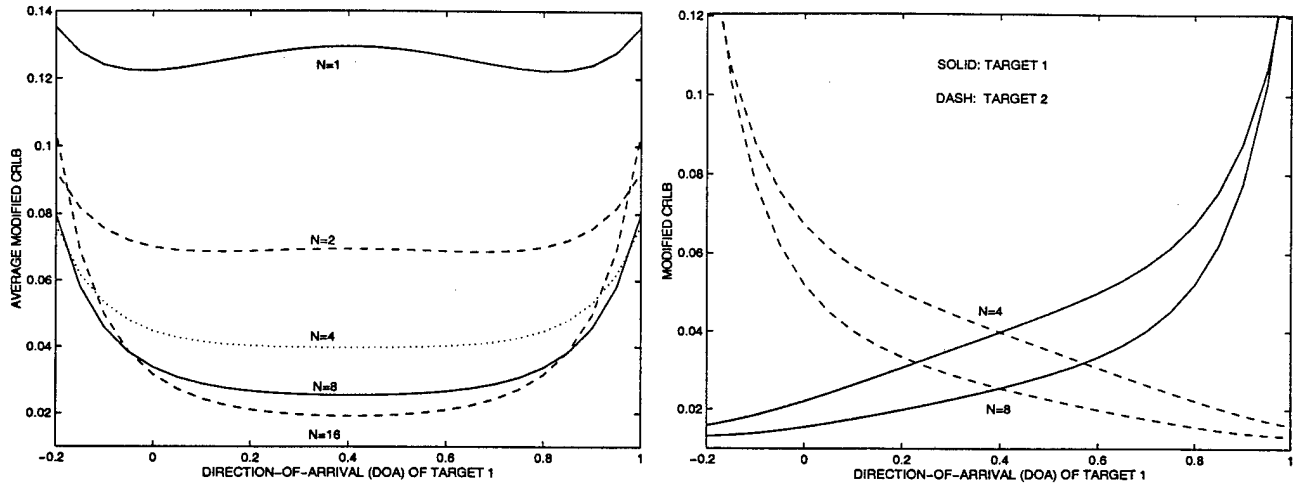

Figure 2. MCRLB for η_1 andη_2 with $\Delta\eta = \eta_{bw}$ and two 19 dB targets: (a) Averaged over both targets, (b) Each target

antenna boresight. Also, $\eta_1 = -0.2$ in Figure 2(a) corresponds to pointing the antenna boresight on the outside of the two targets. The average of the two MCRLBs in Figure 2(a) shows that pointing the antenna boresight exactly between the two targets (*i.e.*, $\eta_1 = 0.4$) gives the smallest average MCRLB for $N = 4$, 8, and 16 and the largest bound for pointing between the targets when $N = 1$. For $N = 1$, the minimum average MCRLB is achieved by pointing the antenna boresight just to the outside of one of the two targets. Figure 2(a) also shows that the average MCRLB is rather insensitive to the antenna boresight when it is positioned between the two targets. For $N = 16$, the rapid increases in the average MCRLB near the edges of the plot are due the rapid increase of the MCRLB for the weaker target. To illustrate this point, Figure 2(b) gives the individual MCRLBs of the two targets for $N = 4$ and 8. Figure 2(b) shows that pointing the antenna boresight closer to target 1 gives a smaller MCRLB for η_1 and larger MCRLB for η_2. Note the rapid increase in the MCRLB of the weaker target when the antenna is pointed to the outside of one of the two targets. Also, note that the reduction in the MCRLB gained through frequency agility (*i.e.*, $N = 8$ rather than $N = 4$) is lost due to the low subpulse SNR at $\eta_1 = -0.15$ for η_2 and $\eta_1 = 0.95$ for η_1.

If the DOA estimate for a single target is desired, the individual MCRLBs for the DOA of each target are of interest. Figure 2(b) shows the individual MCRLBs indicating that pointing closer to or beyond the target of interest minimizes the MCRLB for that target. The minimum MCRLB for η_1 with $N = 4$ is 0.015 at $\eta_1 = -0.3$ and with $N = 8$ is 0.012 at $\eta_1 = -0.2$. For $N = 1$ (not shown in Figure 2(b)), the minimum MCRLB for η_1 is 0.012 at $\eta_1 = -0.5$. For the single target DOA estimation, an optimal pointing angle always exists and moves towards the target of interest as N increases for this separation of the two targets, target amplitudes, and beamwidth. For $N > 1$, note that pointing away from the intefering target is optimal in the single DOA estimate case, whereas pointing between the targets is optimal when estimating both DOAs.

Figure 3 gives further insight into the pointing of the antenna boresight for the DOA estimation of two unresolved targets. Using eight frequencies (*i.e.*, $N = 8$) to simultaneously estimate both DOAs gives a minimum MCRLBs for the individual targets of 0.028 with the antenna boresight pointed exactly between the two targets, as seen also in Figure 2(a). If the eight subpulses are used in two dwells of four subpulses each, the two DOAs can be sequentially estimated by using the first dwell to estimate the nearer target DOA, and using the second to estimate the other target DOA. This method also gives a minimum MCRLB of 0.028 obtained by pointing to the outside of the targets. Further analysis showed that if the separation between the targets is larger than one half of the beamwidth (*i.e.*, $\Delta\eta > \eta_{bw}$), sequential estimation yields a lower MCRLB, whereas if the separation is less than one half the beamwidth, simultaneous estimation provides the best performance bound (not shown). Therefore, for equal amplitude targets, the case $\Delta\eta = \eta_{bw}$ shown in Figure 3 denotes a boundary in the decision process for the optimal pointing strategy.

Figure 4 shows the average MCRLB for two 19 dB targets (*i.e.*, $\Re_{R1} = \Re_{R2} = 19$ dB in (22) for $N = 1$) separated by one-fourth beamwidth (*i.e.*, $\Delta\eta = 0.5\eta_{bw} = 0.4$) versus η_1 for $N = 1$, 2, 4, 8, and 16 subpulses. Thus, $\eta_1 = 0$ in Figure 4(a) corresponds to target 1 on the antenna boresight, while $\eta_1 = 0.4$ corresponds to target 2 on the antenna boresight. The average of the two MCRLBs in Figure 4(a) shows that pointing the antenna boresight exactly between the two targets (*i.e.*, $\eta_1 = 0.2$) gives the smallest average MCRLB for all values of N. Figure 4(a) also shows that increasing the number of frequencies from $N = 8$ to $N = 16$ actually results in an increase in the average MCRLB. Note that this result differs from that shown in Figure 2(a), and it is thought to be the result of a low subpulse SNR at $N = 16$ and a lower average MCRLB in 4(a) compared to that in 2(a).

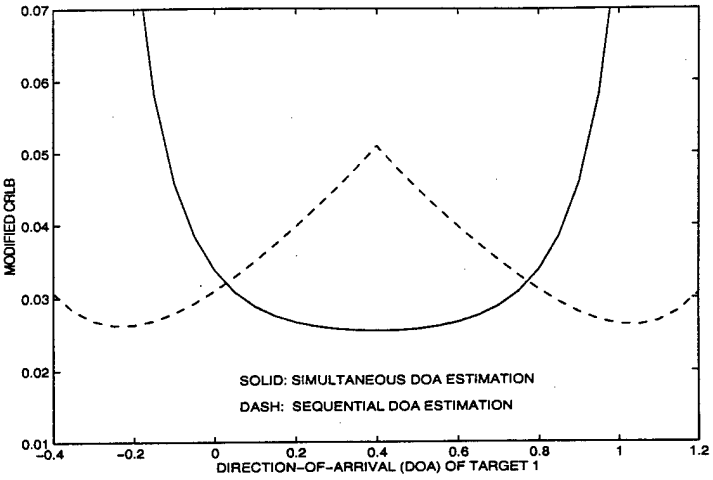

Figure 3. MCRLBs for sequential and simultaneous estimation of η_1 and η_2 with $\Delta\eta = \eta_{bw}$, two 19 dB targets, and eight subpulses of equal energy (Sequential: $N = 4$ in two consecutive dwells; simultaneous: $N = 8$ in one dwell)

Figure 4(b) gives insight into the pointing of the antenna boresight for the DOA estimation of a single target in the presence of another target for one-fourth beamwidth separation. It is interesting to note the minimum MCRLB for single DOA estimation corresponds to pointing between the two equal amplitude targets for $N = 8$, in contrast to the results of Figure 2(b). A comparision of the sequential and the simultaneous estimation algorithms for this case in a manner similar to that of Figure 3 indicates that it is always advantageous to use simultaneous estimation.

Figure 5(a) shows the MCRLB for a 19 dB target and a 16 dB target (*i.e.*, $\Re_{R1} = 2\Re_{R2} = 19$ dB) separated by one-fourth beamwidth versus η_1 for $N = 1$, 2, 4 and 8 subpulses. For the $N = 1$ and 2 cases, the optimal pointing strategy is to stear the antenna boresight slightly towards the stronger target, while for the other cases, stearing should lean toward the weaker target. It appears that the simultaneous DOA estimator favors pointing towards the lower power target when subpulse powers are too low ($N = 4$ or 8), perhaps to avoid very low SNR observations. Note also that the advantages of frequency agility have been achieved by $N = 4$ and the degradation in performance due to low subpulse SNR can be seen by the steepening of the graph at extreme values of η_1 for $N = 8$. The MCRLB for the single target DOA estimator shown in Figure 5(b) agrees with the results for the equal energy case of Figure 4(b) that for a low number of subpulses the antenna should be pointed at or outside the position of the targets and for a higher number of subpulses it should be pointed on the inside. For the case of two unequal amplitude targets, the pointing strategy for sequential estimation is less clear. Figure 5(b) suggests an approach. The first dwell may be in the neighborhood of the strongest target to obtain the least error in the DOA estimate of that target. The pointing of the second dwell is then chosen to minimize the bound in estimating the DOA of the second target.

5. DOA ESTIMATION FOR TWO UNRESOLVED TARGETS

As seen in the previous section, the pointing of the antenna boresight affects the information obtained during a radar dwell. Based on the results of Section 4, two sensor pointing strategies are set forth. The simultaneous pointing strategy that was found to be optimal for targets separated by less than one-half beamwidth involves pointing between the targets and estimating both DOAs from data gathered in one dwell. This case is referred to as the fully unresolved case. The second strategy proposed, applicable to targets which are separated by more than one-half of a beamwidth, is the sequential strategy in which the DOAs are estimated from data gathered from two consecutive dwells, each pointing in the general direction of one target. This case can be thought of as a partially resolved target scenario since estimation of each parameter can be performed individually. In this section, a DOA estimation algorithm based on the Method of Moments (MM) for the fully unresolved two-target case is proposed.

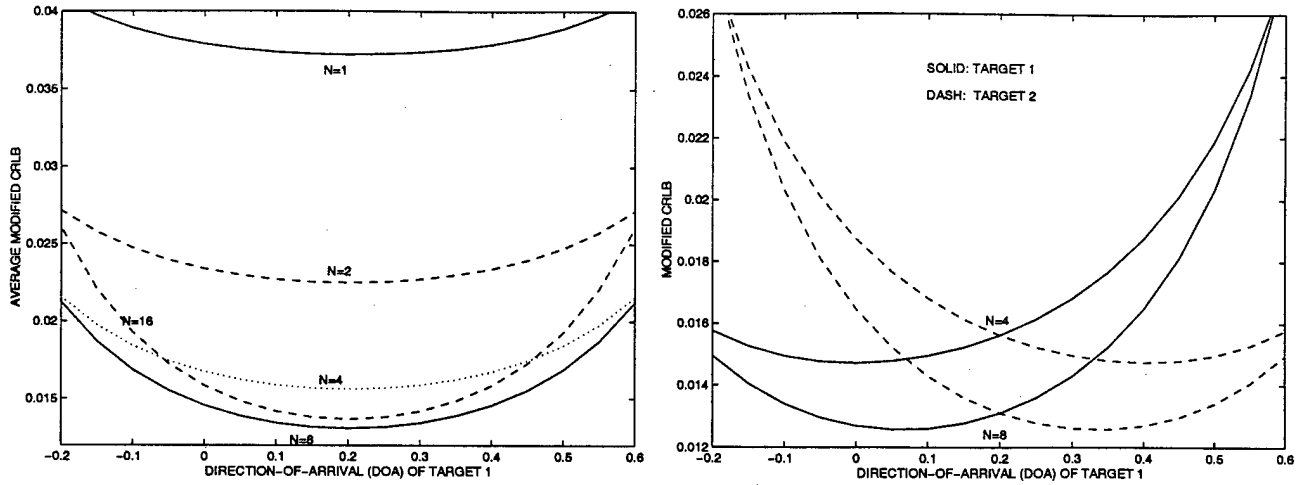

Figure 4. MCRLB for η_1 andη_2 with $\Delta\eta = 0.5\eta_{bw}$ and two 19 dB targets: (a) Averaged over both targets, (b) Each target

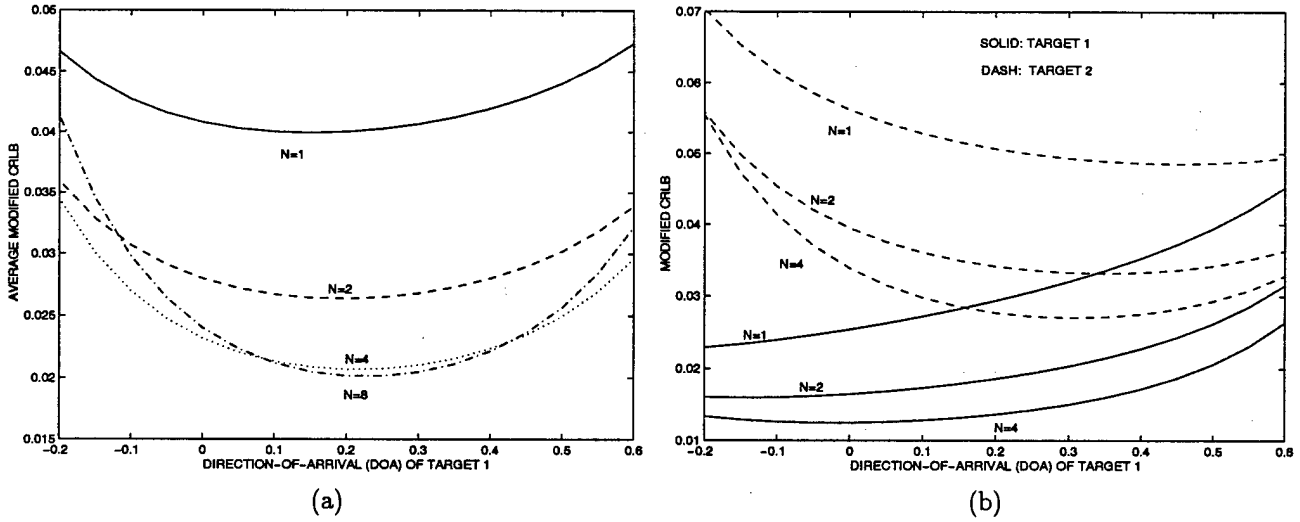

Figure 5. MCRLB for η_1 and η_2 with $\Delta\eta = 0.5\eta_{bw}$: (a) Averaged over 16 dB and 19 dB targets, (b) For 13 dB and 19 dB targets

The partially resolved target case is briefly discussed in [15].

For the case of two fully unresolved Rayleigh targets, the antenna boresight is pointed between the targets and the DOA estimation of both targets is accomplished simultaneously via MM. For the MM, two sample moments are required for the estimation of two DOAs. Since the observations y_{Ik} are not stationary, sample moments cannot be used directly. Thus, $\hat{y}_I$ from (16) will be used to obtain the first expression as

$$\hat{y}_I = \frac{\Re_{R1}\eta_1 + \Re_{R2}\eta_2}{\Re_{R1} + \Re_{R2} + 1} \tag{23}$$

Let $\Delta\eta = \eta_1 - \eta_2 > 0$, so that $\eta_1 > \eta_2$. Then, since $\Re_{R2} = \lambda\Re_{R1}$, where $\lambda > 0$,

$$\eta_1 \approx \hat{y}_I + \frac{\lambda}{1+\lambda}\Delta\eta \qquad \eta_2 \approx \hat{y}_I - \frac{1}{1+\lambda}\Delta\eta \tag{24}$$

Since the y_{Ik} are nonstationary, Gaussian random variables, the second expression for DOA estimation will be obtained by forming a Chi-squared random variable with $2N-1$ degrees of freedom from y_{Ik}, $\Re_{ok}$, and $\hat{y}_I$ and setting the random variable equal to its mean. Thus, for $N > 1$, let

$$B_N = [\, y_{I1} - \hat{y}_I \quad \cdots \quad y_{IN} - \hat{y}_I \quad y_{Q1} \quad \cdots \quad y_{QN} \,] \qquad A_N = 2\,\mathrm{diag}[\, \Re_{o1} \quad \cdots \quad \Re_{oN} \quad \Re_{o1} \quad \cdots \quad \Re_{oN} \,] \tag{25}$$

Since for $N = 1$, $\hat{y}_I = y_{I1}$, let $X_1 = y_{Q1}$ and $R_1 = 2\Re_{o1}$. Also let

$$v_N = B_N^T A_N B_N q^{-1} \tag{26}$$

where q is given by (17). Since the conditional pdf of the in-phase and quadrature monopulse ratios are Gaussian with variance given by (15) through (17), v_N is a Chi-squared random variable with $2N-1$ degrees of freedom. Then

$$E[v_N] = 2N - 1 \qquad \mathrm{VAR}[v_N] = 2(2N-1) \tag{27}$$

Setting v_N equal to its mean gives

$$\hat{q} = \frac{B_N^T A_N B_N}{2N-1}, \qquad N \geq 1 \tag{28}$$

Since for $\Delta\eta > 1.0$ the targets would be processed as partially unresolved targets, assume that $\Delta\eta < 1.0$. Thus, pointing the antenna boresight between the targets allows the approximation of q by

$$q \approx \frac{\sigma_d^2}{\sigma_S^2} + \frac{\lambda\Re_{R1}}{1+\lambda}\Delta\eta^2 \tag{29}$$

Inserting $\hat{q}$ in (29) for q and using (29) in (24) gives the DOA estimates as

$$\hat{\eta}_1 = \hat{y}_I + \sqrt{\frac{\lambda\tilde{q}}{\hat{\Re}_R}}, \qquad \hat{\eta}_2 = \hat{y}_I - \sqrt{\frac{\tilde{q}}{\lambda\hat{\Re}_R}} \tag{30}$$

where

$$\tilde{q} = \begin{cases} 0, & \hat{q} \leq \sigma_d^2\sigma_S^{-2} \\ \dfrac{4\eta_{bw}^2\lambda}{(1+\lambda)^2}\hat{\Re}_R, & \hat{q} \geq \dfrac{4\eta_{bw}^2\lambda}{(1+\lambda)^2}\hat{\Re}_R + \sigma_d^2\sigma_S^{-2} \\ \hat{q} - \sigma_d^2\sigma_S^{-2}, & \text{otherwise} \end{cases} \tag{31}$$

and η_{bw} is defined in conjunction with (22). The first case of (31) is introduced to ensure that the DOA estimates are real numbers, while the second is introduced to prevent the difference of the two DOA estimates from being unreasonably large. Limiting the difference of the two DOA estimates was found to be critical when correcting the known relative RCS λ for the effects of the antenna gain pattern of the sum channel.

Note that $\tilde{q}$ can be expressed as a function of v_N. Also, note that for a twice differentiable function $g(x)$,

$$E[g(x)] \approx g(\bar{x}) + g''(\bar{x})\sigma_x^2 \tag{32}$$

where $\bar{x} = E[x]$, $\sigma_x^2 = \mathrm{VAR}[x]$, and $g''(\bar{x})$ is the second derivative of $g(x)$ with respect to x evaluated at $x = \bar{x}$. Using (32) with (30) gives approximations of the variances of the DOA estimates for $q \gg \sigma_d^2\sigma_S^{-2}$ as

$$\mathrm{VAR}[\hat{\eta}_1|\Phi] \approx q\left[\frac{1}{2NY_N} + \frac{\lambda q}{\Re_R(2N-1)(q-\sigma_d^2\sigma_S^{-2})}\right] \qquad \mathrm{VAR}[\hat{\eta}_2|\Phi] \approx q\left[\frac{1}{2NY_N} + \frac{q}{\lambda\Re_R(2N-1)(q-\sigma_d^2\sigma_S^{-2})}\right] \tag{33}$$

Setting $q = \hat{q}$ in (33) and by analysis of simulation results $q(q - \sigma_d^2\sigma_S^{-2})^{-1} = 1.5$ was found to provide relatively good estimates of the variances for the DOA estimates, which are given by

$$\hat{\sigma}^2_{\hat{\eta}_1} = \hat{q}\left[\frac{1}{2NY_N} + \frac{1.5\lambda}{\widehat{\Re}_R(2N-1)}\right] \qquad \hat{\sigma}^2_{\hat{\eta}_2} = \hat{q}\left[\frac{1}{2NY_N} + \frac{1.5}{\lambda\widehat{\Re}_R(2N-1)}\right] \tag{34}$$

While the relative RCS of the two targets is assumed to be known from the track filter, the effect of the antenna gain pattern is not assumed to be included in λ. The effects of the antenna gain pattern can be included in the DOA estimation by using a modified λ in (30) and (31), which is given by

$$\tilde{\lambda} = \lambda \frac{\cos^4\left(\frac{\tilde{\eta}_2\pi}{4\eta_{bw}}\right)}{\cos^4\left(\frac{\tilde{\eta}_1\pi}{4\eta_{bw}}\right)} \tag{35}$$

where $\tilde{\eta}_1$ and $\tilde{\eta}_2$ are the DOA estimates from the predicted state of the track filter. Note that estimation of the RCSs (or $\Re_{R1}$ and $\Re_{R1}$) of the two targets in the track filtering should account for the beam pointing losses.

6. NNJPDA FOR POSSIBLY MERGED MEASUREMENTS

When multiple detections occur near the predicted position of a target, a technique for selecting the detection for tracking is required. Nearest Neighbor (NN) and the probabilistic data association filter (PDAF) [2] are two common techniques for addressing this data association problem. In the standard NN data association, the measurement that has the largest likelihood of associating with a target is assigned to the target and used for tracking. In the PDAF, all of the detections are assigned to the target and used for tracking. However, neither the NN nor the PDAF address the problem of data association for closely-spaced targets. The JPDA is an extension of the PDAF to include closely-spaced targets. However, the JPDA is rather complex when more than two targets are closely spaced and tracks formed with the JPDA on closely-spaced targets often coalesce.

The NNJPDA is an *ad hoc* technique for assigning measurements to tracks. One measurement is assigned to one track in the NNJPDA, whereas in the JPDA, multiple measurements can be used to update a track and a measurement can be used to update multiple tracks. In the NNJPDA, simple approximations to the measurement-to-track association probabilities of the JPDA are used as the metric for assigning measurements to tracks. Using the approximate association probabilities, the most probable measurement-to-track association is made and all candidate associations that include either the measurement or the track are removed from consideration. This process continues until all measurements have been assigned to tracks or all of the tracks have been assigned to measurements.

The likelihood of association of track i with predicted state $X^i_{k|k-1}$ and measurement j at time k is approximated by

$$C^{ij}_k = \frac{1}{\sqrt{|2\pi S^{ij}_k|}} \exp\Big[-\frac{1}{2}(Z^j_k - h_k(X^i_{k|k-1}))^T (S^{ij}_k)^{-1}(Z^j_k - h_k(X^i_{k|k-1}))\Big] \tag{36}$$

where S^{ij}_k is the covariance of the measurement residual, $Z^j_k - h_k(X^i_{k|k-1})$, of track i and measurement j. Let

$$\Sigma^{ti}_k = \sum_{j=1}^{M^r_k} C^{ij}_k \qquad \Sigma^{rj}_k = \sum_{i=1}^{M^t_k} C^{ij}_k \tag{37}$$

where M^r_k is the number of measurements at time k, and M^t_k is the number of tracks at time k. Then the approximate association probability of track i and measurement j at time k for the NNJPDA [10] is given by

$$P^{ij}_k = \frac{C^{ij}_k}{\Sigma^{ti}_k + \Sigma^{rj}_k - C^{ij}_k + B} \tag{38}$$

where B is included to account for nonunity probability of detection and the presence of clutter and false alarms.

In the NNJPDA, the measurement-to-track assignment that gives the largest P_k^{ij} is made and all candidate associations that include either measurement j or track i are removed from consideration. Using the remaining candidate associations, the measurement-to-track assignment that gives the new largest P_k^{ij} is made and all candidate associations that include either measurement j or track i are removed from consideration. This process continues until all measurements have been assigned to tracks or all of the tracks have been assigned to measurements or a minimum threshold value for P_k^{ij} is not achieved by any of the remaining track and measurement pairs.

The NNJPDAM^3 algorithm is an extension of the NNJPDA to include the possibility of merged monopulse measurements. The NNJPDAM^3 is obtained from the NNJPDA by adding a pseudotrack for each pair of tracks that are potentially unresolved. The monopulse measurements are also included as a feature [5] to improve the data association. While the NNJPDAM^3 can be extended beyond pairs of unresolved tracks, only pairs are considered in this paper. For the pseudotrack, the means and variances of the monopulse measurements are estimated with (18), while (22) is used for the resolved measurements. The monopulse feature of the merged measurements are included with (18) through (21), while (22) through (25) are used to include the feature of the resolved monopulse measurements. While the NNJPDAM^3 can be applied to monopulse systems with two angular coordinates, only one angular coordinate is considered in this section. Also, the NNJPDA is modified to allow for targets of different detection probabilities.

For resolved measurement j and resolved track i with probability of detection P_{Di}, let the likelihood of association be approximated by

$$\tilde{C}_k^{ij} = \frac{P_{Di}}{(2\pi\hat{p})^N}\sqrt{\frac{|A_N|}{|2\pi S_k^{ij}|}}\exp\Big[-\frac{1}{2\hat{p}}B_N^T A_N B_N\Big]\exp\Big[-\frac{1}{2}(Z_k^j - h_k(X_{k|k-1}^i))^T (S_k^{ij})^{-1}(Z_k^j - h_k(X_{k|k-1}^i))\Big] \quad (39)$$

where A_N and B_N are defined in (25) and

$$\hat{p} = \frac{\sigma_d^2}{\sigma_S^2} + \hat{y}_I^2 \quad (40)$$

The variance of the monopulse angle measurements for inclusion in S_k^{ij} is given for measurements within the half power beamwidth by

$$\hat{\sigma}_\theta^2 = \frac{\theta_{bw}^2}{k_m^2}\sigma_{\hat{y}_I}^2 = \frac{\hat{p}\theta_{bw}^2}{2k_m^2 N Y_N} \quad (41)$$

Note that all of the monopulse measurements and parameters in (39) through (41) correspond to measurement j.

For potentially merged measurement j and potentially unresolved track i composed of tracks l and n, let the likelihood of association be approximated by

$$\begin{aligned}\tilde{C}_k^{ij} =& \frac{P_{Di}}{(2\pi\hat{q})^N}\sqrt{\frac{|A_N|}{|2\pi S_k^{ij}|}}\exp\Big[-\frac{1}{2\hat{q}}B_N^T A_N B_N\Big] \\ &\times \exp\Big[-\frac{1}{2}(Z_k^j - \bar{h}_k(X_{k|k-1}^l, X_{k|k-1}^n))^T (S_k^{ij})^{-1}(Z_k^j - \bar{h}_k(X_{k|k-1}^l, X_{k|k-1}^n))\Big]\end{aligned} \quad (42)$$

where $\bar{h}_k(X_{k|k-1}^i, X_{k|k-1}^l)$ is the predicted measurement of the unresolved track based on (16) and (17) with

$$\hat{q} = \frac{\sigma_d^2}{\sigma_S^2} + \frac{\hat{\Re}_l\hat{\eta}_l^2 + \hat{\Re}_n\hat{\eta}_n^2 + \hat{\Re}_l\hat{\Re}_n(\hat{\eta}_l - \hat{\eta}_n)^2}{\hat{\Re}_l + \hat{\Re}_n + 1} \quad (43)$$

with $\hat{\Re}_n$ denoting the predicted SNR of target n and $\hat{\eta}_n$ denoting the predicted DOA parameter for target n. The predicted probability of detection of the unresolved track i is given by (12) with $\Re = \hat{\Re}_l + \hat{\Re}_n$. The variance of the monopulse angle measurement for S_k^{ij} is estimated by

$$\hat{\sigma}_\theta^2 = \frac{\theta_{bw}^2}{k_m^2}\sigma_{\hat{y}_I}^2 = \frac{\hat{q}\theta_{bw}^2}{2k_m^2 N Y_N} \quad (44)$$

Note that all of the monopulse measurements and parameters in (42) through (44) correspond to measurement j as a merged measurement of tracks l and n.

Let

$$\widetilde{\Sigma}_k^{rj} = \sum_{i=1}^{M_k^t + M_k^{ut}} \widetilde{C}_k^{ij} \qquad \widetilde{\Sigma}_k^{ti} = \sum_{j=1}^{M_k^r} \widetilde{C}_k^{ij} \tag{45}$$

where M_k^t is the number of tracks, M_k^{ut} is the number of potentially unresolved tracks at time k. Then for measurement j and (resolved or unresolved) track i, let the association probabilities of the NNJPDAM[3] be approximated by

$$\widetilde{P}_k^{ij} = \frac{\widetilde{C}_k^{ij}}{\widetilde{\Sigma}_k^{tj} + \widetilde{\Sigma}_k^{ri} - \widetilde{C}_k^{ij} + B_k^i} \tag{46}$$

where B_k^i is included to account for nonunity probability of detection of target i and the presence of clutter and false alarms. An option for B_k^i is

$$B_k^i = \max\{M_k^r - M_k^t, 1\} \frac{1 - P_{Di} P_G}{V_k} \tag{47}$$

where V_k denotes the volume of the gating region at time k and P_G is the probability of gating the target. In order to include the possibility of a missed detection, let $j = 0$ denote the case of no measurement

$$\widetilde{P}_k^{i0} = \frac{B_k^i}{\widetilde{\Sigma}_k^{ri} + B_k^i} \tag{48}$$

In the NNJPDAM[3], the measurement-to-track assignment that gives the largest P_k^{ij} is made and all candidate associations that include either measurement j or track i are removed from consideration. If track i is an unresolved track composed of track l and track n, then both tracks l and n are removed as candidates for measurement-to-track assignment. Using the remaining candidate associations, the measurement-to-track assignment that gives the new largest P_k^{ij} is made and all candidate associations that include either measurement j or track i are removed from consideration. This process continues until all of the tracks have been assigned to a measurement or a missed detection.

7. CONCLUDING REMARKS

The modified CRLB for monopulse DOA estimation of two unresolved Rayleigh targets was given and used to investigate the effects of frequency diversity and antenna boresight steering on the DOA estimation. For a given waveform energy, the accuracy of the DOA estimation was found to improve as the number of distinct frequencies increases and the expected subpulse energy remains above a few dB. The study revealed two sensor pointing strategies for the DOA estimation: simultaneous and sequential. The simultaneous pointing strategy involves pointing between the targets and estimating both DOAs from data gathered in one dwell, while the sequential pointing strategy involves estimating the DOAs with data gathered from two consecutive dwells, each pointing in the general direction of one target. While the relative performance of the two pointing stategies depend on the SNRs of the two targets and the number of subpulses, the simultaneous pointing strategy was found to be better for targets separated by less than one-half beamwidth, while the sequential pointing strategy was found to be better for targets that are separated by more than one-half of a beamwidth.

An estimation algorithm based on the Method of Moments (MM) was developed for the simultaneous DOA estimation of two unresolved Rayleigh targets with a relative RCS given from the track filter. The effects of the antenna gain pattern were also treated as known from the track filter. Thus, if the two targets are under track, the target state estimates should be used to predict the effects of the antenna gain pattern and the estimated RCSs should be used to predict the SNR parameters $\Re_{R1}$ and $\Re_{R2}$. Furthermore, for tracking closely-spaced targets with merged or unresolved measurements, this paper provides for a new approach to the processing of the unresolved measurements as two DOA measurements rather than the conventional single DOA measurement of the centroid.

A pseudotrack was introduced for potentially unresolved tracks to extend the NNJPDA algorithm to include the possibility of merged monopulse measurements to from the NNJPDAM^3 algorithm. While the NNJPDAM^3 algorithm has been restricted to pairs of unresolved tracks, the pseudotrack concept is extendable to multiple unresolved tracks. The pseudotrack concept can be used to extend other measurement-to-track assignment techniques such as those in [2] to include merged measurements. The statistics of the merged monopulse measurements and the features of the monopulse measurements used in the NNJPDAM^3 algorithm can also be used to improve the performance of the JPDAMM in [2].

While the data association for possibly merged monopulse measurements is addressed with the NNJPDAM^3, the track filtering with merged monopulse measurements is not part of the NNJPDAM^3. In the track filtering, a merged measurement can be treated as a single merged measurement to simultaneously update both tracks as in the JPDAM [2]. On the other hand, the merged monopulse measurements of two unresolved tracks can be used as in [6] to generate two separate measurements for updating the two tracks. The extension of the NNJPDAM^3 algorithm to two angular coordinates will be complicated by the fact that the monopulse features may indicate a merged measurement in one angular coordinate and a resolved measurement in the other coordinate. Also, using the technique in [6] for the track filtering with monopulse measurements in two coordinates will be complicated by an ambiguity in the angular position of the two measurements. Simulation studies are planned to assess the performance of the NNJPDAM^3 algorithm and compare its performance with that of the standard JPDAMM algorithm in [2]. Also, a computer simulation of a phased array radar will be used to compare the performances of the JPDAMM and NNJPDAM^3 and study the effects of both algorithms on the radar resources required for tracking closely-spaced targets.

REFERENCES

1. F. Daum, "A System Approach to Multiple Target Tracking," in *Multitarget-Multisensor Tracking: Applications and Advances, Vol. II,* edited by Y. Bar-Shalom, Artech House, Inc., Norwood, MA, 1992.
2. Y. Bar-Shalom and X.R. Li, *Multitarget-Multisensor Tracking: Principles and Techniques,* YBS Publishers, Box U-157, Storrs, CT, 06296-3157, 1995.
3. S.M. Sherman, *Monopulse Principles and Techniques,* Artech House, Inc., Dedham, MA, 1984.
4. S. M. Sherman, "Complex Indicated Angles Applied To Unresolved Targets and Multipath," *IEEE Trans. Aero. and Elect. Sys.,* Jan. 1971, pp. 160-170.
5. W.D. Blair and M. Brandt-Pearce, "Unresolved Rayleigh Target Detection Using Monopulse Measurements," *IEEE Trans. Aero. Elect. Sys.,* April 1998, pp. 543-552.
6. W.D. Blair and M. Brandt-Pearce, "Monpulse DOA Estimation for Two Unresolved Rayleigh Targets," submitted to *IEEE Trans. Aero. Elect. Sys.,* Dec. 1998.
7. K.C. Chang and Y. Bar-Shalom, "Joint Probabilistic Data Association for Multitarget Tracking with Possibly Unresolved Measurements and Maneuvers," *IEEE Trans. on Auto. Cont.,* July 1984, pp. 585-594.
8. Blackman, S.S., *Multiple-Target Tracking with Radar Applications,* Artech House, Inc., Norwood, MA, 1986.
9. W. Koch and G. Van Keuk, "Multiple Hypothesis Track Maintenance with Possibly Unresolved Measurements," *IEEE Trans. Aero. Elect. Sys.,* July 1997, pp. 883-892.
10. R.J. Fitzgerald, "Development of Practical PDA Logic for Multitarget Tracking by Microprocessor," in *Multitarget/Multisensor Tracking: Applications and Advances, Vol. I,* edited by Y. Bar-Shalom, Artech House, Inc., Norwood, MA, 1990.
11. W.D. Blair, "NNJPDA for Possibly Merged Monopulse Measurements," *Proc. of 31st Southeastern Symposium on Systems Theory,* Auburn, AL, Mar 21-23, 1999. Dec. 1998.
12. F. Gini, R. Reggiannini, and U. Mengali, "The Modified Cramer-Rao Bound in Vector Parameter Estimation," *IEEE Trans. on Communications,* vol. 46, No. 1, pp. 52-60, January 1998.
13. J.V. DiFranco and W.L. Rubin, *Radar Detection,* Artech House, Inc. Dedham, MA, 1980.
14. M. Abramowitz and I.A. Stegun, Ed., *Handbook of Mathematical Functions, with Formulas, Graphs, and Mathematical Tables,* U.S. Gov. Printing Office, Washington, DC, 1972, and John Wiley & Sons, Inc. 1972.

Steady-State Tracking with LFM Waveforms

Winnie Wong
Georgia Tech Research Institute
Georgia Institute of Technology
Atlanta, Georgia 30332-0857
gt7625a@prism.gatech.edu

W. D. Blair
Georgia Tech Research Institute
Georgia Institute of Technology
Atlanta, Georgia 30332-0857
dale.blair@gtri.gatech.edu

ABSTRACT

The steady-state gains and error covariance are derived for a two-state Kalman filter (i.e., an α, β filter) for tracking with linear frequency modulated (LFM) waveforms. A procedure is given for calculating the α, β gains from the tracking index, Γ, the sample period, T, and the range-Doppler coupling coefficient, Δt. The steady-state error covariance is found to be a simple function of α, β, Δt, T and the measurement noise variance, σ_v^2. The expressions for steady-state gains and error covariance were confirmed numerically with the Kalman filtering equations. A gain scheduling technique for α and β during initialization is also given.

INTRODUCTION

The Kalman filter produces an optimal estimate of the target state when given the motion model and a sequence of sensor measurements corrupted with white Gaussian errors. The computational burden of maintaining the Kalman filter may prohibit its use when many targets are being tracked. Steady-state filters are also good for filter design and analysis. Constant data rate and constant covariances required for steady-state filters are not typically true in real systems, so approximate gains are typically used. The gains are based on the steady-state gains of the Kalman filter and implemented using either using a fixed gain or an easily generated gain schedule. The resultant filter for tracking range and range rate is called the α, β filter, where approximate filter gains α, β may be used instead of the optimal Kalman gains [1]. In [2], the range-Doppler coupling of linear frequency modulated (LFM) waveforms is shown to have a significant effect on tracking accuracy. In the Appendix of [1], the steady-state gains and error covariance are derived for range measurements without range-Doppler coupling. In this paper, the range-Doppler coupling associated with LFM waveforms is included in the measurement equation, and expressions for the steady-state gains and error covariance are calculated.

MATHEMATICAL MODEL

The dynamics model commonly assumed for a target in track is given by

$$X_{k+1} = F_k X_k + G_k w_k \tag{1}$$

where $w_k \sim N(0, Q_k)$ is the process noise, F_k defines a linear constraint on the dynamics and G_k is the input matrix for maneuver. The target state vector X_k contains the range and range rate of the target at time k. The linear measurement model is given by

$$Y_k = H_k X_k + v_k \tag{2}$$

where Y_k is typically the target position measurement and $v_k \sim N(0, R_k)$ is the measurement noise, and H_k is the output matrix that will include range-Doppler coupling.

The measured range and the variance for a LFM waveform and the range-Doppler coupling coefficient for a LFM waveform are given by [2] as

$$y_k = r_k + \Delta t \dot{r}_k + v_k \tag{3}$$

$$\sigma_v^2 = E[v_r] = \frac{\Delta t^2 c^2}{8 f_o^2 \tau^2 \Re} = \frac{c^2}{8 \mathcal{B}^2 \Re} \tag{4}$$

$$\Delta t = \frac{f_0 \tau}{f_2 - f_1} = \frac{f_0 \tau}{\mathcal{B}} \tag{5}$$

where r_k is the true range at time k, $\Re$ is the signal-to-noise ratio, c is the speed of light, f_0 is the nominal carrier frequency, f_1 is the initial frequency, and f_2 is the final frequency. Also $|\mathcal{B}|$ is the bandwidth of the LFM waveform and τ is the pulse length. Note that the demodulation frequency can be modified with the range rate estimate to remove the bias in the range measurement due to range-Doppler coupling. However, if the range rate estimate is used to remove the bias in the range measurements, the measurement errors become correlated with the state estimate and the typical Kalman filter must be modified to account for the state correlated measurement errors.

The Kalman filtering equations associated with the state model in (1) and the measurement model in (2) are given by the following equations.

Time Update:

$$X_{k|k-1} = F_{k-1} X_{k-1|k-1} \tag{6}$$

$$P_{k|k-1} = F_{k-1|k-1} P_{k-1|k-1} F_{k-1}^T + G_{k-1} Q_{k-1} G_{k-1}^T \tag{7}$$

Measurement Update:

$$K_k = P_{k|k-1}H_k^T[H_kP_{k|k-1}H_k^T + R_k]^{-1} = P_{k|k}H_k^TR_k^{-1} \tag{8}$$

$$X_{k|k} = X_{k|k-1} + K_k[Y_k - H_kX_{k|k-1}] \tag{9}$$

$$P_{k|k} = [I - K_kH_k]P_{k|k-1} \tag{10}$$

where the subscript notation $(k|j)$ denotes the state estimate for time k when given measurements through time j. K_k is the Kalman gain that minimizes the mean square error in the state estimate. Also, note that $X_k \sim N(X_{k|k}, P_{k|k})$ with $X_{k|k}$ and $P_{k|k}$ denoting the mean and error covariance of the state estimate, respectively.

THE α, β FILTER

For the Kalman filter in steady–state conditions, $P_{k|k} = P_{k-1|k-1}$, and $P_{k+1|k} = P_{k|k-1}$, and $K_k = K_{k-1}$. For a Kalman filter to achieve these steady-state conditions, the error processes, w_k, and v_k, must have stationary statistics and the data rate must be constant, When the noise processes are not stationary or the data rate is not constant, a filter using the steady-state gains will provide suboptimal estimates. The α, β filter is the steady-state Kalman filter for tracking nearly constant range rate targets. The α, β filter is a single coordinate filter that is based on the assumption that the target is moving with constant range rate plus zero-mean, white Gaussian acceleration errors. Given this assumption, the filter gains α and β are chosen as the steady-state Kalman gains that minimize the mean-square error in the range and range rate estimates.

For the α, β filter for piecewise constant acceleration errors,

$$X_k = [r_k \quad \dot{r}_k]^T \tag{11}$$

$$F_k = F = \begin{bmatrix} 1 & T \\ 0 & 1 \end{bmatrix} \tag{12}$$

$$G_k = G = \begin{bmatrix} \frac{T^2}{2} & T \end{bmatrix}^T \tag{13}$$

$$H_k = H = [1 \quad \Delta t] \tag{14}$$

$$R_k = R = \sigma_v^2 \tag{15}$$

$$Q_k = Q = \sigma_w^2 \tag{16}$$

$$K_k = K = \begin{bmatrix} \alpha & \frac{\beta}{T} \end{bmatrix}^T \tag{17}$$

where r_k and $\dot{r}_k$ are the range and range rate of the target, respectively, σ_v^2 and σ_w^2 are the variances of measurement noise and process noise, respectively, T is the sample period between

measurements, Δt is the range-Doppler coupling coefficient, and α and $\frac{\beta}{T}$ are the steady-state Kalman filter gains.

Let the steady-state error covariance matrix of the filtered estimates for the α, β filter be denoted as

$$P_{k+1|k+1} = P_{k|k} = P = \begin{bmatrix} p_{11} & p_{12} \\ p_{12} & p_{22} \end{bmatrix} \tag{18}$$

Using (14), (15), and (18) in (8) gives the steady-state gain as

$$K_k = K_{k-1} = K = PH^T R^{-1} = \begin{bmatrix} p_{11} + p_{12}\Delta t \\ p_{12} + p_{22}\Delta t \end{bmatrix} \sigma_v^{-2} \tag{19}$$

Using (17) with (19) gives

$$\alpha = (p_{11} + p_{12}\Delta t)\sigma_v^{-2} \tag{20}$$

$$\beta = (p_{12} + p_{22}\Delta t)T\sigma_v^{-2} \tag{21}$$

Inserting (7) into (10) and setting $P_{k|k} = P_{k-1|k-1} = P$ for steady-state conditions gives

$$[I - KH]^{-1} P = FPF^T + GG^T\sigma_w^2 \tag{22}$$

Then

$$[I - KH]^{-1} P = \frac{1}{1 - \alpha - \frac{\beta\Delta t}{T}} \begin{bmatrix} \left(1 - \frac{\beta\Delta t}{T}\right) p_{11} + \alpha\Delta t p_{12} & \left(1 - \frac{\beta\Delta t}{T}\right) p_{12} + \alpha\Delta t p_{22} \\ \frac{\beta}{T} p_{11} + (1-\alpha) p_{12} & \frac{\beta}{T} p_{12} + (1-\alpha) p_{22} \end{bmatrix} \tag{23}$$

$$FPF^T = \begin{bmatrix} p_{11} + 2Tp_{12} + T^2 p_{22} & p_{12} + Tp_{22} \\ p_{12} + Tp_{22} & p_{22} \end{bmatrix} \tag{24}$$

$$GG^T\sigma_w^2 = \sigma_w^2 \begin{bmatrix} \frac{T^4}{4} & \frac{T^3}{2} \\ \frac{T^3}{2} & T^2 \end{bmatrix} \tag{25}$$

Equating the (1,2) and (2,2) elements of (22) gives expressions for p_{12} and p_{22}. Substituting p_{12} and p_{22} into (21) gives

$$\Gamma^2 = \frac{T^4\sigma_w^2}{\sigma_v^2} = \frac{\beta^2}{1 - \alpha - \beta\frac{\Delta t}{T}} \tag{26}$$

where Γ is the tracking or maneuvering index. Using (26) to eliminate σ_w^2 in the expressions of p_{12} and p_{22} gives

$$p_{12} = \frac{\beta\sigma_v^2}{T\left(1-\alpha-\beta\frac{\Delta t}{T}\right)}\left[1-\alpha-\left(\frac{2\alpha+\beta}{2}\right)\frac{\Delta t}{T}\right] \tag{27}$$

$$p_{22} = \frac{\beta\sigma_v^2(2\alpha-\beta)}{2T^2\left(1-\alpha-\beta\frac{\Delta t}{T}\right)} \tag{28}$$

Substituting p_{12} into (20) gives

$$p_{11} = \alpha\sigma_v^2 - \frac{\beta\sigma_v^2}{\left(1-\alpha-\beta\frac{\Delta t}{T}\right)}\left[1-\alpha-\left(\frac{2\alpha+\beta}{2}\right)\frac{\Delta t}{T}\right]\frac{\Delta t}{T} \tag{29}$$

The steady-state error covariance is then given by

$$P_{k|k} = \sigma_v^2\begin{bmatrix} \alpha - \frac{\beta}{\left(1-\alpha-\beta\frac{\Delta t}{T}\right)}\left[1-\alpha-\left(\frac{2\alpha+\beta}{2}\right)\frac{\Delta t}{T}\right]\frac{\Delta t}{T} & \frac{\beta}{T\left(1-\alpha-\beta\frac{\Delta t}{T}\right)}\left[1-\alpha-\left(\frac{2\alpha+\beta}{2}\right)\frac{\Delta t}{T}\right] \\ \frac{\beta}{T\left(1-\alpha-\beta\frac{\Delta t}{T}\right)}\left[1-\alpha-\left(\frac{2\alpha+\beta}{2}\right)\frac{\Delta t}{T}\right] & \frac{\beta(2\alpha-\beta)}{2T^2\left(1-\alpha-\beta\frac{\Delta t}{T}\right)} \end{bmatrix} \tag{30}$$

Equating the (1,1) elements of (22) and using (27) through (29) gives

$$a_3\beta^3 + a_2\beta^2 + a_1\beta + a_0 = 0 \tag{31}$$

where

$$a_3 = -\left(\frac{\Delta t}{T}\right)^2 - \frac{\Delta t}{4T} \tag{32}$$

$$a_2 = -2\alpha\left(\frac{\Delta t}{T}\right)^2 - 2\alpha\frac{\Delta t}{T} + 3\frac{\Delta t}{T} + \frac{1-\alpha}{4} \tag{33}$$

$$a_1 = -3\alpha^2\frac{\Delta t}{T} - \alpha^2 + 2\alpha\frac{\Delta t}{T} + 3\alpha - 2 \tag{34}$$

$$a_0 = \alpha^2 - \alpha^3 \tag{35}$$

The valid solutions of (31) for β are given by

$$\beta_\pm = \frac{2}{\left(1+4\frac{\Delta t}{T}\right)}\left(-\alpha\left(1+2\frac{\Delta t}{T}\right) + 2 \pm 2\sqrt{\left(1-\alpha\frac{\Delta t}{T}\right)^2 - \alpha}\right) \tag{36}$$

For $\frac{\Delta t}{T} > 0$, both solutions of (36) are valid for β depending on the selection of Γ and $\frac{\Delta t}{T}$. The β_- (i.e., minus sign in the front of the radical) is used for β with increasing α until the maximum α is reached, which is given by

$$\alpha_{max} = \frac{\frac{2\Delta t}{T} + 1 - \sqrt{\frac{4\Delta t}{T} + 1}}{2\left(\frac{\Delta t}{T}\right)^2} \tag{37}$$

Then β_+ (i.e., plus sign in the front of the radical) is used for β from α_{max} with decreasing α and it is valid as long as $1 - \alpha - \beta_+ \frac{\Delta t}{T} > 0$; that is, Γ in (26) is a real number. For $\frac{\Delta t}{T} \leq 0$, β_- is the only solution for β. If $\frac{\Delta t}{T} = -\frac{1}{4}$, (31) becomes a quadratic equation given by

$$b_2\beta^2 + b_1\beta + b_0 = 0 \tag{38}$$

where

$$b_2 = 0.125\alpha - 0.5 \tag{39}$$

$$b_1 = -0.25\alpha^2 + 2.5\alpha - 2 \tag{40}$$

$$b_0 = \alpha^2 - \alpha^3 \tag{41}$$

If there is no range-Doppler coupling (i.e., $\frac{\Delta t}{T} = 0$), (30), (26) and β_- of (36) give

$$P_{k|k} = \sigma_v^2 \begin{bmatrix} \alpha & \frac{\beta}{T} \\ \frac{\beta}{T} & \frac{\beta^2(2\alpha - \beta)}{2(1-\alpha)T^2} \end{bmatrix} \tag{42}$$

$$\Gamma^2 = \frac{T^4\sigma_w^2}{\sigma_v^2} = \frac{\beta^2}{1-\alpha} \tag{43}$$

$$\beta = 2(2 - \alpha) - 4\sqrt{1-\alpha} \tag{44}$$

These results of (42) through (44) agree with that derived from the Appendix of [1] and Kalata's papers [3,4]. Inserting (26) into (31) to eliminate α and expressing a polynomial equation of β in terms of Γ, Δt and T gives

$$\beta^4 - \Gamma^2\beta^3 + \left[\frac{\Gamma^4}{4} - \left(\frac{\Delta t}{T}\right)^2\Gamma^4 - 2\Gamma^2\right]\beta^2 - \Gamma^4\beta + \Gamma^4 = 0 \tag{45}$$

Note that (45) does not depend on the sign of Δt. Newton's method with a good initial guess of β can be used to find a zero of (45) when Γ and $\frac{\Delta t}{T}$ are given. A good initial guess of β is given by the case of $\Delta t = 0$, where the initial β is computed with (44) and

$$\alpha = -0.125\left(\Gamma^2 + 8\Gamma - (\Gamma + 4)\sqrt{\Gamma^2 + 8\Gamma}\right) \tag{46}$$

After β is found by utilizing Newton's method, the steady-state gain, α and the error covariance are then calculated for the given Γ and $\frac{\Delta t}{T}$ using (26) and (30).

Various results for the α, β filter are shown in Figures 1 through 6 and the results were comfirmed by iterating the Kalman filtering algorithm until the steady-state conditions are achieved. Figure 1 shows that the variance of range estimate decreases with increasing Δt for a given Γ. Figure 2 shows that the correlation coefficients for range and range rate estimates are between zero and one. Note that as Δt becomes more positive, the correlation coefficient for range and range rate goes to zero at higher Γ. This means that the range and range rate estimates are less correlated to each other at higher Γ. Thus, the predicted measurements will be more accurate at positive Δt. Figure 3 shows that the variance of range rate decreases with increasing Δt. Figure 4 shows α decreases with increasing Δt. Figure 5 shows that β is maximized for no range-Doppler coupling (i.e., $\Delta t = 0$) and β does not depend on the sign of Δt as indicated by (45). In Figure 6, note that there may be two solutions of β for a given α when $\Delta t > 0$, and there is only one solution of β for a given α when $\Delta t \leq 0$.

INITIALIZATION GAINS

Least-squares estimation can be used to derive the gains for initializing an α, β filter. For linear least-squares estimation, an equation formulating the measurement vector Z as a linear function of the parameter vector X to be estimated is given by

$$Z = WX + V \tag{47}$$

where $E[V] = 0$ and $E[VV^T] = \sigma^2 I_N$ for N measurements with I_N denoting the N x N identitiy matrix. The least-squares estimate $\widehat{X}$ [5] is given

$$\widehat{X} = (W^T W)^{-1} W^T Z \tag{48}$$

with error covariance

$$P_N = COV[\widehat{X}] = \sigma_v^2 (W^T W)^{-1} \tag{49}$$

A current state estimate of X denoted by $\widehat{X}_0 = [r_0 \quad \dot{r}_0]$ can be obtained from the current measurement plus the N previous measurements as

$$Z_N = W_N X_0 + V_N \tag{50}$$

where

$$Z_N = [y_{-N} \quad y_{-N+1} \quad \ldots \quad y_{-1} \quad y_0] \tag{51}$$

$$V_N = [v_{-N} \quad v_{-N+1} \quad \ldots \quad v_{-1} \quad v_0] \tag{52}$$

$$W_N = \begin{bmatrix} 1 & 1 & \ldots & 1 & 1 \\ \Delta t - NT & \Delta t + (-N+1)T & \ldots & \Delta t - T & \Delta t \end{bmatrix}^T \tag{53}$$

where $E[V_N] = 0$, $E[V_N V_N^T] = \sigma_v^2 I_N$, and Δt is the range-Doppler coefficient in (14). The error covariance of the least-squares state estimate $\widehat{X}_0$ with an LFM waveform is given by

$$COV[\widehat{X}_0] = P_N = \sigma_v^2 (W_N^T W_N)^{-1} \tag{54}$$

where

$$(W_N^T W_N) = (N+1) \begin{bmatrix} 1 & \Delta t - N\frac{T}{2} \\ \Delta t - N\frac{T}{2} & (\Delta t)^2 - \Delta t NT + N(2N+1)\frac{T^2}{6} \end{bmatrix} \tag{55}$$

Then

$$COV[\widehat{X}_0] = P_N = \frac{2\sigma_v^2}{(N+1)(N+2)} \begin{bmatrix} 2N+1-6\frac{\Delta t}{T} + \frac{6}{N}\left(\frac{\Delta t}{T}\right)^2 & \frac{3}{T}(1-\frac{2\Delta t}{NT}) \\ \frac{3}{T}(1-\frac{2\Delta t}{NT}) & \frac{6}{NT^2} \end{bmatrix} \tag{56}$$

Note that Δt cannot be selected to minimize the determinant of P_N, $|P_N|$, because $|P_N|$ is not a function of Δt. Also note that for $\frac{\Delta t}{T} = \frac{N}{2}$, the variance of range is minimized and the range and range rate estimates are uncorrelated.

Let the scheduled gains for initialization for the α, β filter be denoted by

$$K_k = \begin{bmatrix} \alpha_k & \frac{\beta_k}{T} \end{bmatrix}^T \tag{57}$$

where k denotes the gains for processing the $k+1^{st}$ measurement.

Letting $P_{k|k} = P_k$ of (56) in (8) provides a simple gain scheduling procedure for α and β during initialization that is given by

$$\alpha_k = max\left\{\frac{2(2k+1) - 6\frac{\Delta t}{T}}{(k+1)(k+2)}, \alpha\right\} \tag{58}$$

$$\beta_k = max\left\{\frac{6}{(k+1)(k+2)}, \beta\right\} \tag{59}$$

with $X_{0|-1} = [0 \quad 0]^T$. Note that as k approaches infinity, the functions of k for α_k, and β_k go to zero. This is because the least-squares estimation assumes there is no process noise. However, the steady-state gains, α and β are nonzero in Kalman filter, which takes process noise into consideration. Using the range measurement at $t = 0$, y_0, and the range measurement at $t = T$, y_1, the initial state estimate and error covariance based on two measurements with an LFM waveform are given by

$$\widehat{X}_{1|1} = \begin{bmatrix} y_1 - \frac{\Delta t}{T}(y_1 - y_0) \\ \frac{y_1 - y_0}{T} \end{bmatrix} \tag{60}$$

$$P_{1|1} = \sigma_v^2 \begin{bmatrix} \left(\frac{\Delta t}{T} - 1\right)^2 + \left(\frac{\Delta t}{T}\right)^2 & \frac{1}{T}\left(1 - 2\frac{\Delta t}{T}\right) \\ \frac{1}{T}\left(1 - 2\frac{\Delta t}{T}\right) & \frac{2}{T^2} \end{bmatrix} \tag{61}$$

The $X_{1|1}$ and $P_{1|1}$ are the result of the least-squares estimation with the first two measurements.

CONCLUDING REMARKS

The results for the α, β filter generated by using (36) and (45) are confirmed with the Kalman filtering equations. The steady-state gains and error covariance are presented as a simple function of $\alpha, \beta, \Delta t$, T and σ_v^2. The initialization equations of (60) and (61) assume two identical LFM waveforms at $t = 0$ and $t = T$. However, in a phased array radar, the confirmation dwell may include a LFM waveform with up-chirp and down-chirp to achieve range and range rate measurements from a single dwell.

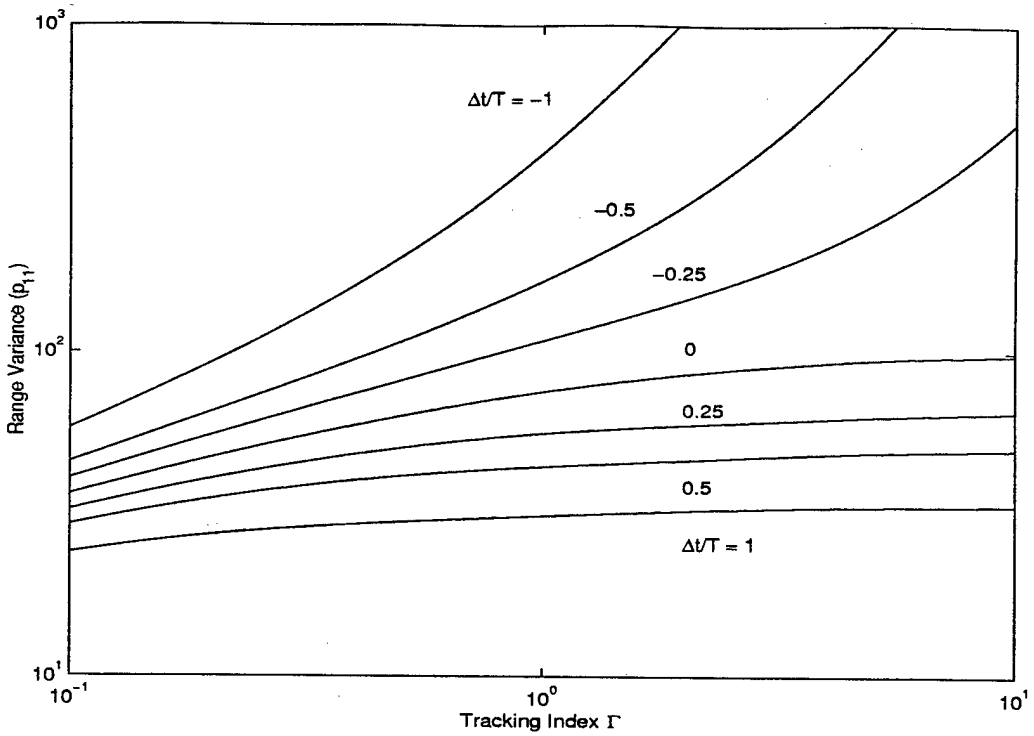

Figure 1. Range Variance Versus Γ with $T = 1$ s and $\sigma_v = 10$ m

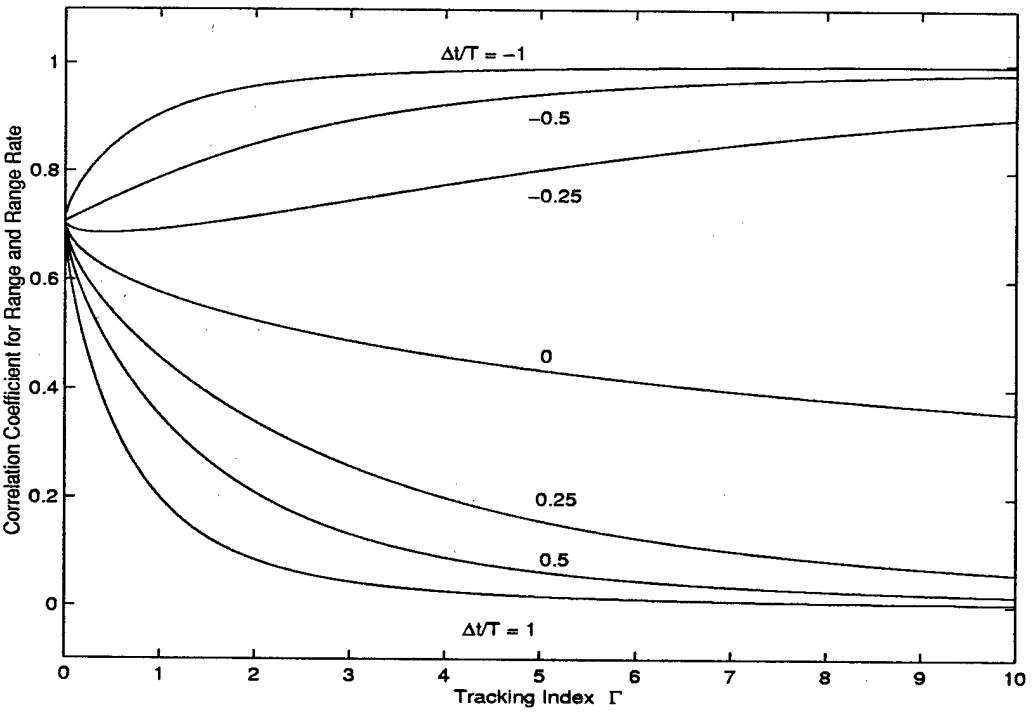

Figure 2. Correlation Coefficient for Range and Range Rate Versus Γ with $T = 1$ s and $\sigma_v = 10$ m

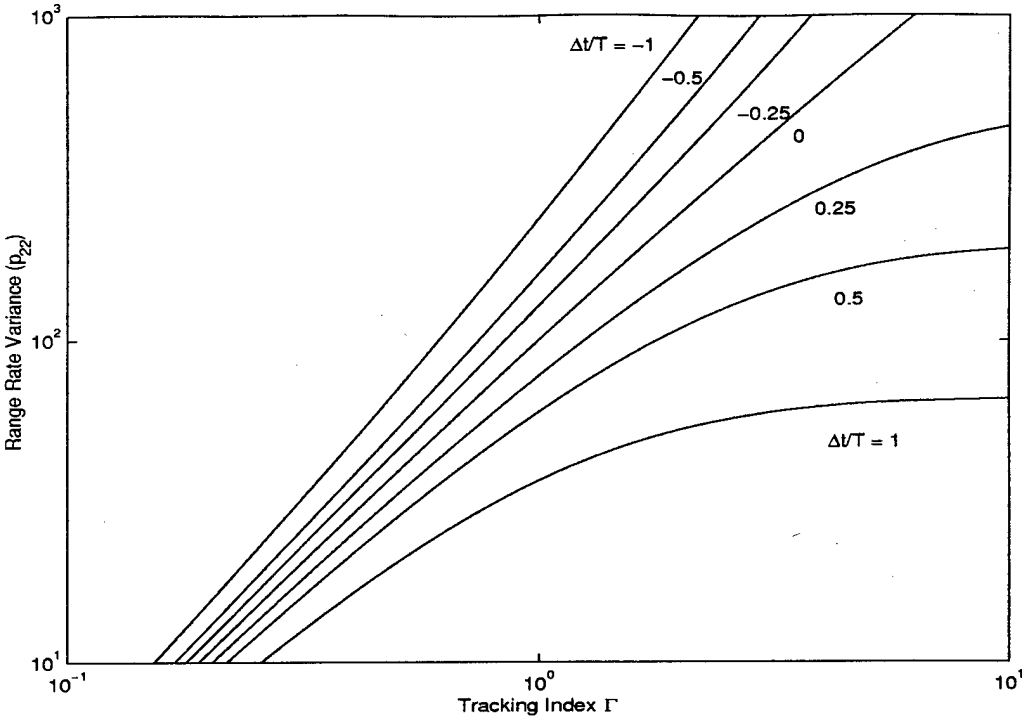

Figure 3. Range Rate Variance Versus Γ with $T = 1$ s and $\sigma_v = 10$ m

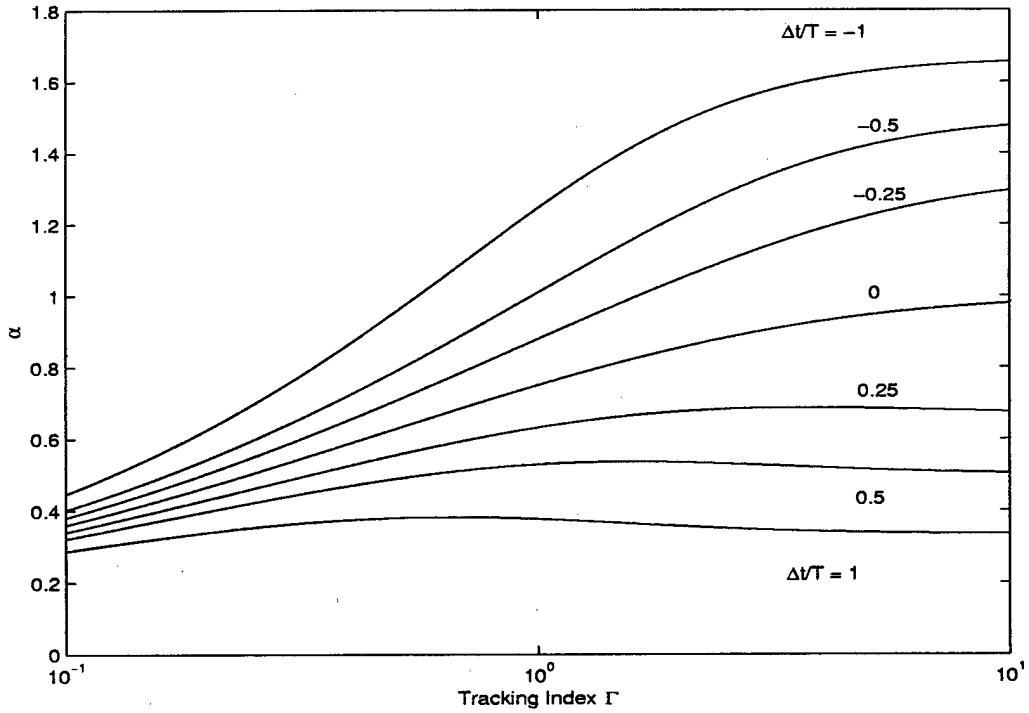

Figure 4. α Versus Γ with $T = 1$ s and $\sigma_v = 10$ m

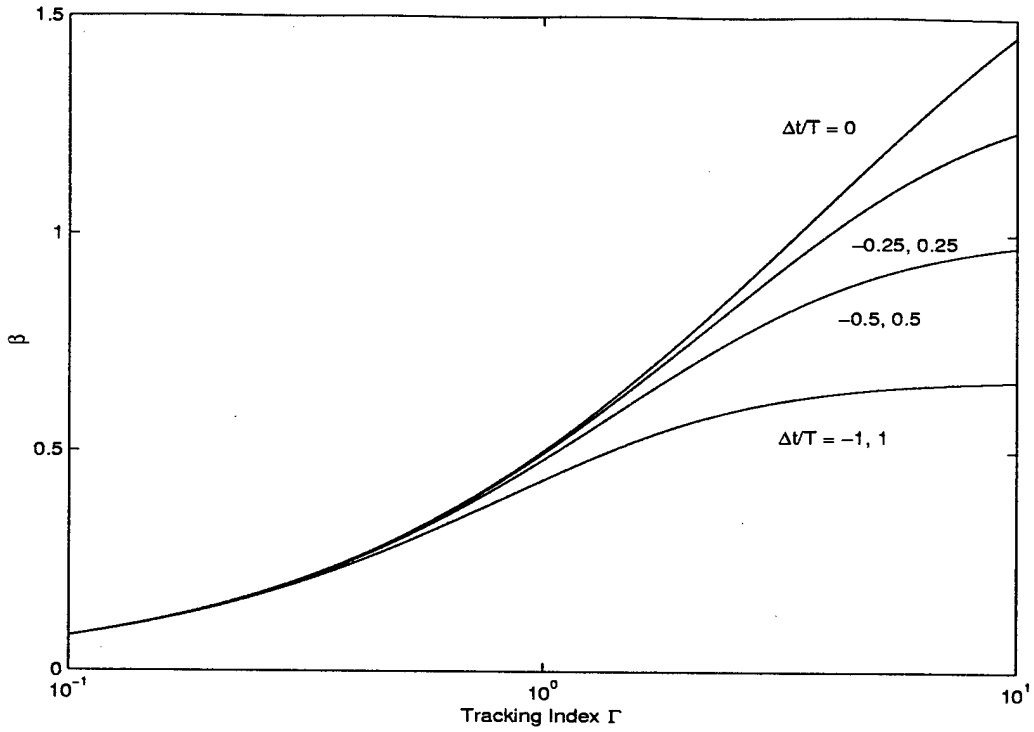

Figure 5. β Versus Γ with $T = 1$ s and $\sigma_v = 10$ m

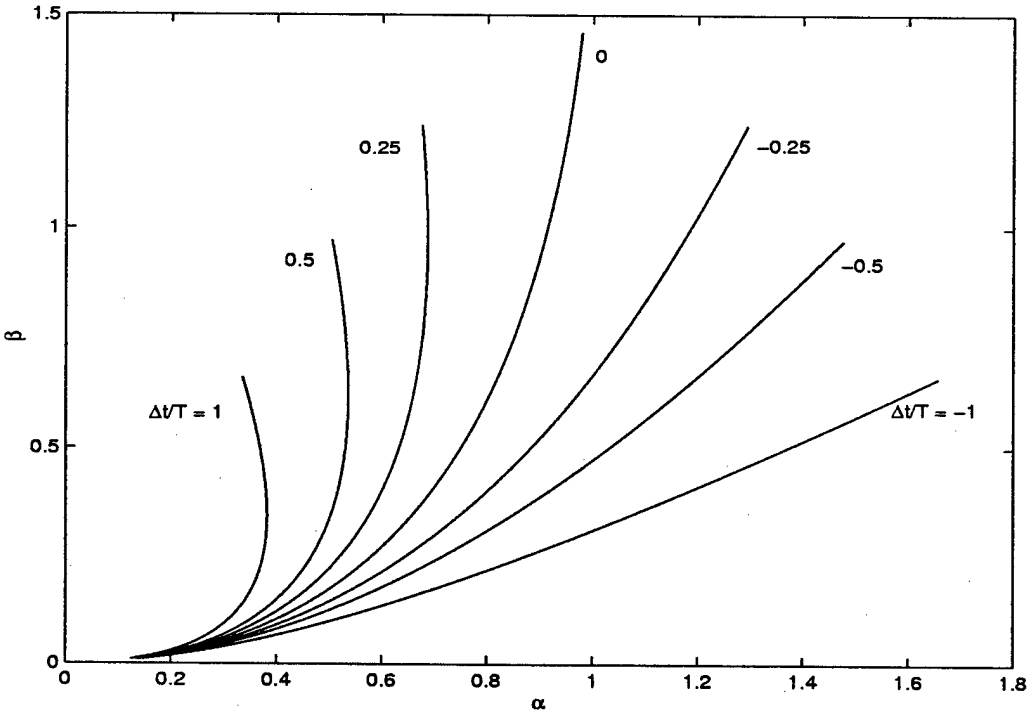

Figure 6. β Versus α with $T = 1$ s and $\sigma_v = 10$ m

REFERENCES

1. Blair, W.D., *Fixed-Gain, Two-Stage Estimators for Tracking maneuvering targets,* Naval Surface Warfare Center, Dahlgren Divison, Dahlgren, Virginia 22448-5000, July 1992.
2. Fitzgerald, F.J., "Effects of Range-Doppler Coupling on Chirp Radar Tracking Accuracy," *IEEE Transactions on Aerospace and Electronic Systems,* July 1974, pp.528-532.
3. Kalata, P.R., "$\alpha - \beta$ Target Tracking Systems: A Survey," 1992 ACC, 832-836.
4. Kalata, P.R., "The Tracking Index: A Generalized Parameter for $\alpha - \beta$ and $\alpha - \beta - \gamma$ Target Trackers," *IEEE Transactions on Aerospace and Electronic Systems,* Vol. AES-20, March 1984, pp. 174-182. Corrections: vol. AES-20, Nov. 1984, pp. 845.
5. Bar-Shalom, Y., and Li, X.R., *Estimation and Tracking: Principles, Techniques and Software,* Dedham, MA: Artech Hourse, 1993.

REPORT DOCUMENTATION PAGE

Form Approved
OMB No. 0704-0188

1. AGENCY USE ONLY (*Leave blank*)	2. REPORT DATE	3. REPORT TYPE AND DATES COVERED
	October 14, 1999	Annual Report, Oct. 1998 – Sept. 1999

4. TITLE AND SUBTITLE
Information-Based Multisensor Detection:
Progress Report for October 1998 through September 1999

5. FUNDING NUMBERS
Grant
N00014-99-1-0084

6. AUTHOR(S)
William Dale Blair

7. PERFORMING ORGANIZATION NAME(S) AND ADDRESS(ES)
Georgia Institute of Technology
Georgia Tech Research Institute
Atlanta, GA 30332-0800

8. PERFORMING ORGANIZATION REPORT NUMBER
Annual Report
GTRI A-5858 (1)

9. SPONSORING/MONITORING AGENCY NAME(S) AND ADDRESS(ES)
Office of Naval Research
800 North Quincy Street
Arlington, Virginia 22217-5660

10. SPONSORING/MONITORING AGENCY REPORT NUMBER

11. SUPPLEMENTARY NOTES

12a. DISTRIBUTION/AVAILABILITY STATEMENT
Approved for Public Release

12b. DISTRIBUTION CODE

13. ABSTRACT (*Maximum 200 words*)

This program addresses the Navy need for extended firm track range for low altitude cruise missiles through the integration of multiple sensors. Track-Before-Declare (TBD) techniques that utilize signal features are proposed for the synergistic integration of an Electronically Scanned Array (ESA) radar with other sensors for the detection of weak targets. The computer simulation models of the sensors will include the effects of many issues such as finite sensor resolution, limitations on the sensor resources, atmospheric refraction, sensor pointing errors, sea-surface induced multipath, nonhomogeneous clutter, sea clutter, etc. that are omitted in most of the legacy simulations. The two primary accomplishments for the first year of this program were the development of a phased array radar model with search and track management functions for multiple targets as well as the development of a sea-clutter model with moving target indictor (MTI) waveform designs.

14. SUBJECT TERMS
Target Tracking, Radar Systems, Modeling and Simulation,
Sea Clutter Modeling, Multisensor Integration

15. NUMBER OF PAGES
80

16. PRICE CODE

17. SECURITY CLASSIFICATION OF REPORT	18. SECURITY CLASSIFICATION OF THIS PAGE	19. SECURITY CLASSIFICATION OF ABSTRACT	20. LIMITATION OF ABSTRACT
Unclassified	Unclassified	Unclassified	UL